Dissertation zur Erlangung des
Doktorgrades der Fakultät für Chemie
und Pharmazie der
Ludwig-Maximilians-Universität
München

Ultrastructural Study of Axon Branching

Hana Nedozrálová

aus

Brno, Czech Republic

2021

Erklärung

Diese Dissertation wurde im Sinne von § 7 der Promotionsordnung vom 28 November 2011 von Frau Prof. Elena Conti betreut.

Eidesstattliche Versicherung:

Diese Dissertation wurde selbstständig, ohne unerlaubte Hilfe erarbeitet.

Brno den 1.7.2021

Hana Nedozrálová

Dissertation eingereicht am: 6.7.2021

1. Gutachterin / 1. Gutachter: Prof. Dr. Elena Conti

2. Gutachterin / 2. Gutachter: Prof. Dr. Frank Bradke

Mündliche Prüfung am: 16.9.2021

Contents

Summary 7

List of publication 11

Preface 13

1. Introduction 15
  1.1 Neuron 15
    1.1.1 Neuronal ultrastructure 16
    1.1.2 Neuronal development 17
  1.2 Axon branching 20
    1.2.1 Topology of axon branching 20
    1.2.2 Axon branching in CNS 21
  1.3 Regulation of axon branching 21
    1.3.1 Extracellular cues 21
    1.3.2 Signaling for branching 24
  1.4 Cytoskeleton organization and dynamics at the axon branch 26
    1.4.1 Actin remodeling 26
    1.4.2 Microtubule remodeling 27
  1.5 Organelle interplay within the neuronal branch 29
    1.5.1 Mitochondria 29
    1.5.2 Endoplasmic reticulum 30
    1.5.3 Golgi complex 32
  1.6 Membrane remodeling at axon branches 33
    1.6.1 Membrane expansion via fusion with synaptic vesicles 33
    1.6.2 Membrane expansion via ER contacts 34
    1.6.3 Membrane retraction 34
  1.7 Local translation in neurons 35
    1.7.1 Ribosomes 35
    1.7.2 Local translation and axon branching 36

Aim of thesis 39

2. Results 41
  2.1 Local orchestration of cellular machineries at axon branch by in-situ cryo-ET 41

2.2 Direct induction of microtubule branching by microtubule nucleation factor SSNA1 . . . 75

3. Discussion . . . 101

3.1 Visualization of axon branch . . . 101

3.2 Cytoskeleton remodeling . . . 102

3.3 Role of ER . . . 103

4. Outlook and future perspectives . . . 105

List of figures . . . 108

References . . . 109

Acknowledgment . . . 125

Summary

The brain function depends on a vast number of intricate connections between neurons to process, transmit and store information. To fulfill these tasks, neuronal cells adapt a distinct polarized morphology during their development and must maintain the polarity over the life span of the organism to sustain the correct brain function. Neurons establish two main compartments, the somatodendritic and the axonal compartments, which are distinct in their morphology, molecular composition, and subcellular functions. At the early stages of development, several long protrusions or neurites extend from the main cell body (soma), where the nucleus is located. One of the neurites develops into the axon, while the remaining become dendrites [1]. Dendrites receive signals from axons of upstream cells via synaptic connections, whereas axons transmit signals to the dendrites of downstream cells. At the tip of a growing axon, an actin-rich growth cone probes the extracellular signaling molecules to find the synaptic target on dendrites of another neuron [2, 3]. Besides the outgrowth and path-finding, axons form additional branches to create multiple synaptic contacts which are crucial for the proper intertwining of neuronal circuits [4].

Reflecting the specialized function of axons, their molecular organization is also unique in order to sustain the local developmental process. The cytoskeleton provides the structural supports needed to maintain the length of the axon shaft. Within the backbone of the axon, microtubules are parallelly forming bundles with their plus ends pointing towards the distal end of the axon whereas actin forms a ring-like lattice around the circumference of the axon [5, 6]. Actin is also accumulated at the areas undergoing dynamic changes, like growth cones and filopodia [7, 8, 9, 10]. Due to the long distance from the soma to the tip of an axon, neurons employ an intricate transport system delivering organelles, proteins, and other cell components into the distal regions, providing energy, synaptic vesicles, and new building material for growth and maintenance.

In addition to the cell-body based translation and transport of new proteins into distal regions of the axon, it has been suggested that neurons employ a regulatory system controlling the actions of molecules in local areas [11, 12, 13, 14]. This is advantageous to sustain the fast-changing local requirements at the areas far from the soma. Examples include localized translation and enrichment of protein, which are needed for the local axon development, regulation, and homeostasis. In particular, clusters of mRNAs are found in local areas within dendrites and axons [15, 13, 16, 17] giving an indication of local protein synthesis and the type of these mRNAs depends on the developmental stage and the location within a neuron [15]. Recent polysome profiling and ribosome footprinting

study revealed that neuronal ribosomes show local preferential translation by monosomes (single ribosomes engaged with an mRNA) and that these neuronal monosomes were in the process of active protein synthesis [18]. Local translation by monosomes has been suggested as a way to control protein expression when only a small amount of protein is locally needed [13]. Despite the critical role of local axon translation, details of the translation are not fully understood. While the evidence for the presence of ribosomes along the axons has been growing [19, 20, 21], the direct observation of ribosomes undergoing protein synthesis and the following effect on the cytoskeleton and organelle reorganization has remained to be a major challenge.

Axon branching is a major process during axon development and morphogenesis, which is necessary for the propagation of signals from one neuron to diverse regions within the nervous system [22, 23, 24]. The initiation of axon branching is regulated by extracellular cues, which activate signaling pathways affecting cytoskeleton dynamics. Local accumulation of actin leads to the formation of actin patch, which is applying force on axon shaft membrane forming short protrusion from the axon [25, 26, 27]. These protrusions, called filopodia, are filled with actin and they act as a structural precursor for the branch until microtubules are recruited to enter and stabilize the axon branch [28, 23, 29]. The enrichment of mRNA [30, 25] encoding proteins such as beta-actin has been reported at the axon branch point [31], suggesting that the proteins required to build up the branch are synthesized locally [32]. Interestingly, it has been reported that mitochondria are also enriched at axon branching points and that they are colocalizing with the mRNA [25]. The specific localization of mitochondria is suggested to generate necessary energy [33] and adjust Ca^{2+} concentration for establishing branch morphogenesis and signal transduction [34]. It was also reported that mitochondria along axons undergo fission and that the regulation of the mitochondria size coincided with terminal axon branching [35]. Curiously, very little is known about the role of the endoplasmic reticulum (ER) during axon branching, although ER is known to be present throughout the axon shaft and is suggested to influence microtubule stability through various interactions [36]. Nonetheless, the structural details of cytoskeleton and organelle orchestration and the organization of protein synthesis machineries at axon branches are largely unknown.

In this thesis, I aimed to directly visualize axon branching points using mouse primary neurons by in-situ cryo-electron tomography (cryo-ET), and to understand the structural organization of the key cellular machineries during axon branching. I compared the organization of the premature branch (filopodium before the microtubule invasion) and the mature branch (branch stabilized by microtubules). Small fragments of actin and small size mitochondria ($\sim$ 500 nm) were localized at axon branches. An intricate network of ER membranes was often found between microtubule bundles and mitochondria, and occasional interactions of the ER membrane to microtubules and mitochondria were visualized. In most cases ER was found only in mature branches together with microtubules, indicating that the migration of ER into the axon branch is guided by microtubules, raising a possible role of ER in branch maturation and stabilization. I further demonstrated the first direct observation of clusters of ribosomes selectively accumulated at axon branches. They were located in the cytoplasm as well as attached to planar ER membranes at places where ER tubes widen, spreading over the space made for the branching activity. Subtomogram-averaging and distance analysis of clustered ribosomes indicated that the ribosomes form polysomes, suggesting these ribosomes are active. Axon branches also contained isolated ribosomes, which agree with the report of monosomes, presumably synthesizing a small number of proteins. Our observation provides a comprehensive picture of the axon branching process utilizing the unique contextual advantage of in-situ cryo-ET.

List of publications

1. **Nedozralova H.**, Basnet N., Ibiricu I., Bodakuntla S., Biertuempfel Ch., Mizuno N., (2021). Local orchestration of cellular machineries at axon branch by in-situ cryo-ET observation. Submitted –Research article–
2. Basnet N., **Nedozralova H**., Crevenna A.H., Bodakuntla S., Schlichthaerle T., Taschner M., Cardone G., Janke C., Jungmann R., Magiera M.M., Biertuempfel Ch., Mizuno N., (2018). Direct induction of microtubule branching by microtubule nucleation factor SSNA1. *Nature Cell Biology* 20, 1172–1180. –Research article–
3. Bodakuntla S., **Nedozralova H.**, Basnet N., Mizuno N, (2021). Cytoskeleton and membrane organization at axon branches. *Frontiers in Cell and Developmental Biology*. Submitted. –Review article–

Preface

The work presented in this thesis was performed at the laboratory of Dr. Naoko Mizuno at Max Planck Institute of Biochemistry, Martinsried, Germany, and at National Heart Lung and Blood Institute, Bethesda, Maryland, United States. The thesis mainly comprises two research topics: 1) “In-situ survey of local reorganization of cellular machineries at axon branch”, and 2) “Direct induction of microtubule branching by microtubule nucleation factor SSNA1”. Therefore, this thesis is presented in a cumulative manner.

Chapter 1 includes the general introduction into the specialized polarized morphology of neurons, their ultrastructure, and the stages of neuronal development. The introduction then focuses on axon branching as an important event during neuronal development. The different topologies of axon branching are discussed and examples of axon branching in CNS are presented. The following sub-chapters are dedicated to different aspects of axon branching: regulation, cytoskeleton remodeling, organelle interplay, membrane remodeling, and local translation. Some of these topics are also covered in our review publication ”Cytoskeleton and membrane organization at axon branches” and thus the review is not presented separately in this thesis.

Chapter 2 presents the result section which consists of the research articles divided into two sub-chapters. The first sub-chapter 2.1 presents the research article’s first topic: “In-situ survey of local reorganization of cellular machineries at axon branch” followed by second sub-chapter 2.2 which includes the research article: “Direct induction of microtubule branching by microtubule nucleation factor SSNA1”.

Finally, chapter 3 includes an extended discussion and the last chapter 4 includes the outlook and future directions of the first topic.

1. Introduction

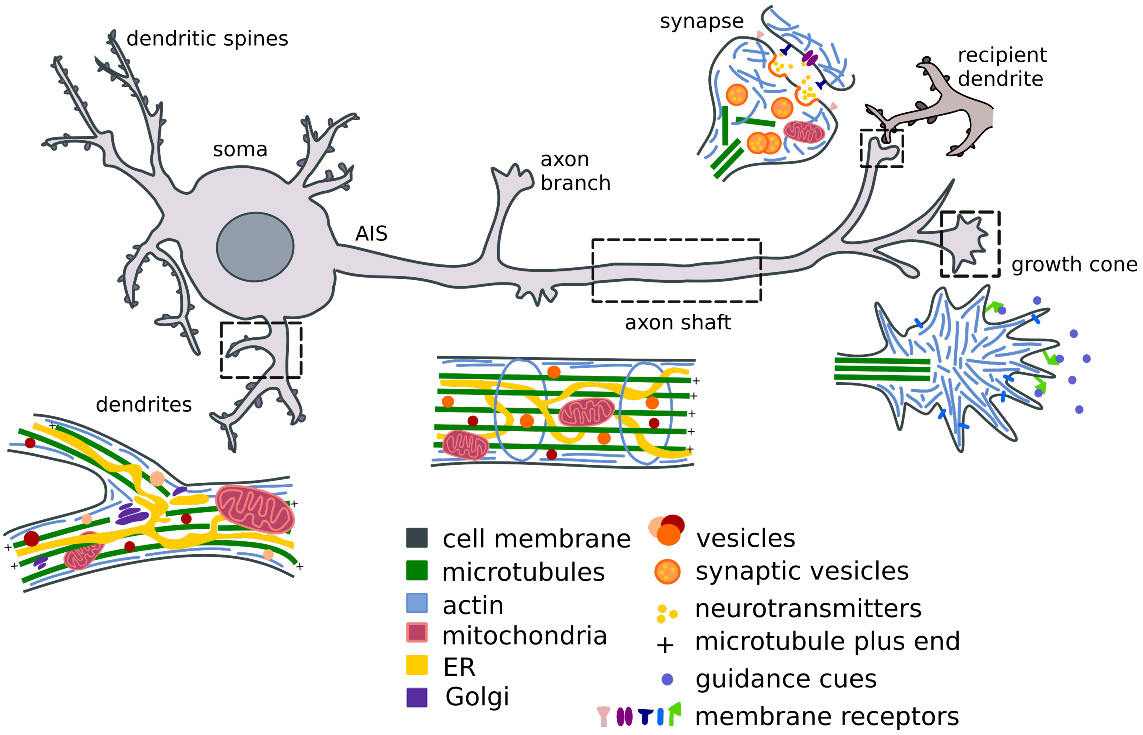
dendritic spines
soma
synapse
recipient dendrite
axon branch
AIS
axon shaft
growth cone
dendrites
cell membrane
microtubules
actin
mitochondria
ER
Golgi
vesicles
synaptic vesicles
neurotransmitters
microtubule plus end
guidance cues
membrane receptors

Figure 1: **Morphology and ultrastructure of neuron cell.** The scheme represents main neuronal compartments: soma, dendrites with spines, axon shaft and branches, axonal initial segment (AIS), growth cone and synaptic terminal. The cutouts are highlighting the distinct ultrastructure of the given segment. The color code for cell elements is depicted in the legend.

1.1 Neuron

Neurons are one of the most specialized cells with distinct highly polarized morphology which is directly linked to their function. The brain function is derived from neurons organized into a complex network. The processing and transmission of information depend on a vast number of intricate connections between neurons. The correct wiring of the neuronal network facilitates the development of cognitive functions and storage of memory. To fulfill the scale and complexity of its functions, it is crucial for neurons to develop properly and maintain neuronal homeostasis over the life span of the organism. Neurons are comprised of two main compartments, the somatodendritic and the axonal compartment, which are distinct in their morphology, molecular composition, and subcellular functions[1]. Axon is a single long neurite transferring signal over long distances to pass it to the downstream cells and dendrites are multiple shorter neurites protruding from the cell body whose task is to receive the incoming signal from other cells. The contacts between neurons occur at specialized junctions called synapses formed between axon terminals or boutons of the presynaptic neurons and dendritic spines of the postsynaptic neuron. Axonal boutons contain synaptic vesicles filled with neurotransmitters as well as cytoskeleton scaffolding, regulatory molecules, and organelles that organize, promote, and regulate the release of neurotransmitters [2, 3]. Synapses are established during the maturation of neuron, in earlier stages, during the growth phase, the distal tips of extending neurites are finished by a growth cone, which is seeking their synaptic target by following guidance cues [23]. The morphology of neuron is illustrated in Figure 1.

1.1.1 Neuronal ultrastructure

The inner organization of the neuron follows its polarized morphology. The cell body is small and contains the usual organelles present in every cell whereas dendrites and axons, thin and long membranous protrusions filled with cytoplasm, are mainly occupied by a cytoskeleton which provides scaffolding and stability to these protrusions. Composition of the cytoskeleton microtubules, actin, and neurofilaments differ between dendrites and axons. Both dendrites and axons have bundled arrays of parallel microtubule filaments crosslinked by various microtubule-associated proteins (MAP) [37], but axonal microtubules are oriented with their plus tip facing towards the distal end of the axon, whereas dendritic microtubule filaments have mixed polarity [37, 38]. Actin is mainly present in areas undergoing remodeling, like filopodia, growth cones, or dendritic spines, and as additional support along the length of neurites [38]. The growth cone is a large dynamic cytoskeleton-supported extension at neurite tip with motile function. The steering and mobility are maintained by constant building and rebuilding of the F-actin cytoskeleton, rising into filopodia and lamellipodia, dynamically reacting to the external stimuli via numerous membrane receptors present in the growth cone [23]. Actin also forms a lattice of ring-like patches around the length of the axon shaft, spaced out by spectrin dimers, supporting the axonal scaffold and increasing its elasticity [6, 39]. Neurofilaments are arranged along the axons between the microtubule bundles and membrane, they form an array of parallel filaments providing structural support and were suggested to control axon diameter [38].

Another structurally distinct compartment of the neuron is the axonal initial segment (AIS) which separates the somatodendritic region from the axon. AIS is positioned at the beginning of the axon adjacent to the soma and has two main functions, first, to maintain cell polarity by sorting the cellular elements which can enter into the axon, and second, to integrate synaptic inputs and generate an action potential. The function is carried by the distinct organization into three layers; plasma membrane, submembrane cytoskeleton, and inner AIS shaft. These layers are integrated by a multidomain scaffolding protein ankyrin G (AnkG) that functions as a master organizer of the AIS [40].

Organelles, synaptic vesicles, proteins, lipids, and other cell material are actively transported into the peripheries of neurons via motor proteins. The vesicle trafficking is bidirectional; anterograde transport is carried out by kinesins and retrograde transport is mediated by dyneins. Mitochondria transport into dendrites and axons is crucial to provide energy at the regions far from the cell body. Synaptic vesicles containing neurotransmitters are transported to axonal terminals. Various other vesicles travel between soma, dendrites, and axons [41]. The endoplasmic reticulum is present through the whole neuron whereas the Golgi apparatus is mainly located in soma, with outposts and satellites in dendrites [42]. Proteins are synthesized centrally in the soma and distributed throughout the length of the neuron. However, in recent years it was reported that part of translation is carried out locally at axons and dendrites [13]. Local translation serves as a unique solution to produce, maintain and modify the proteins that are required for the correct development, function, and plasticity of the nervous system.

The above description of neuron ultrastructure is only a brief summary of the topic. A more in-depth description of axonal ultrastructure will be discussed in later chapters. Visual representation of the summary in Figure 1.

1.1.2 Neuronal development

Neurons undergo multiple stages of development from unpolarized embryonic neurons to differentiated neurons with mature synapses. First, the polarity of the neuron is established and the axon starts to elongate, then collateral branches and terminal arbors are formed to facilitate the correct wiring of the neural network, finally, the maturation of the neuron is complete when synapses are formed.

The process of polarization and neuronal development was first described in cultured hippocampal neurons [43] and comprises 5 well-defined steps (Figure 2). At stage 1, soon after seeding, round neurons form a lamellipodium while they attach to their substrate. Stage 2 starts within few hours when undifferentiated neurites begin to sprout. The neurites are cylindrical protrusions that contain a growth cone, the expanded motile tip of growing protrusion. They lack molecular and structural characteristics of mature axonal or dendritic processes. At this stage, multiple neurites can extend and retract without significant elongation. At stage 3, usually one day after seeding, one of the neurites with an enlarged growth cone starts to elongate rapidly without retraction to form an axon while the other neurites pause. Within a week at stage 4, the remaining neurites continue to grow and branch to form multiple dendrites. Later at the final step, the axon and dendrites continue to develop further, axon starts forming collateral and terminal branches along its shaft, and dendritic protrusions, or spines, appear. After two weeks, the maturation of the neuron is completed by synapse formation allowing for electrical activity throughout the neuronal network [43, 44, 45, 46].

The polarization process begins between stage 2 and 3 of neuron development when one of the neurites start to elongate to become the axon. Further polarization occurs during the following days of development when axon and dendrites become increasingly different, adopting their specialized shape and function. Neuronal wiring refers to the process of neuronal branching during which neurons start to form complex networks by diversifying their connections to multiple target cells. Both dendrites and axons can form branches, dendrites in form of branches with spines and axons as either collateral branches or terminal branches or arbors. Thus one axon can create a synaptic connection with multiple dendrites of target cells. The development of neurons as well as the maintenance of their homeostasis and plasticity during the whole life span is a complex task and requires perfect coordination between signaling, cytoskeleton remodeling, cellular transport, and protein synthesis, so all the components are at the right time at the right location.

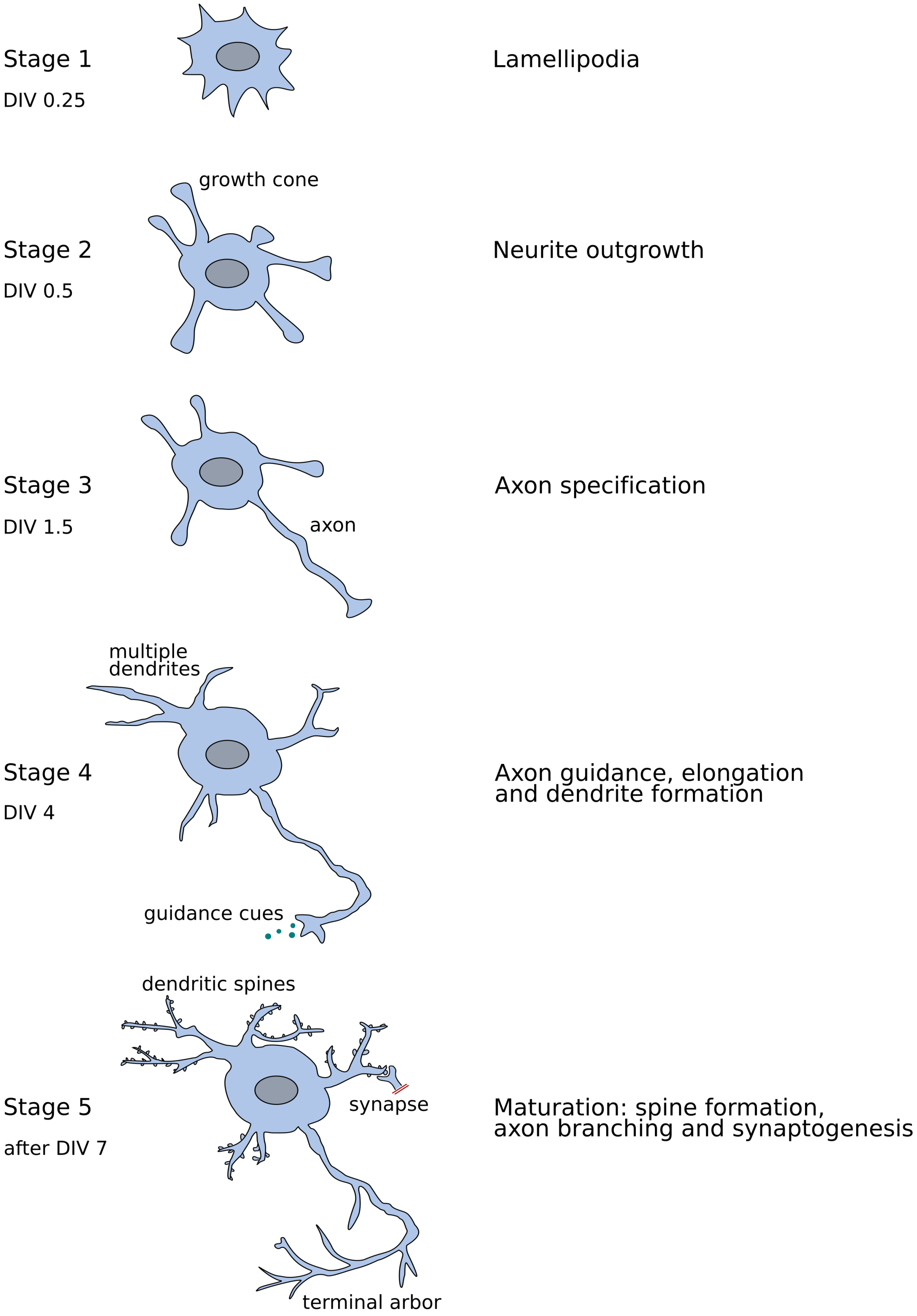
Stage 1
DIV 0.25
Lamellipodia
growth cone
Stage 2
DIV 0.5
Neurite outgrowth
Stage 3
DIV 1.5
axon
Axon specification
multiple dendrites
Stage 4
DIV 4
Axon guidance, elongation and dendrite formation
guidance cues
dendritic spines
Stage 5
after DIV 7
synapse
Maturation: spine formation, axon branching and synaptogenesis
terminal arbor

Figure 2: **Establishment of polarity and stages of neuronal development in hippocampal neurons in culture.** DIV (days in-vitro) refers to a time in culture.

1.2 Axon branching

During the establishment of the correct intra-neuronal connectivity between neurons and target cells, axon branches and even whole axons can be remodeled. To generate and specify their correct wiring into the neuronal network, developing axons sprout collateral and terminal branches with variable length, density, and complexity, allowing them to create synapse with multiple target cells simultaneously, with excess synapses being pruned at later stages [24].

1.2.1 Topology of axon branching

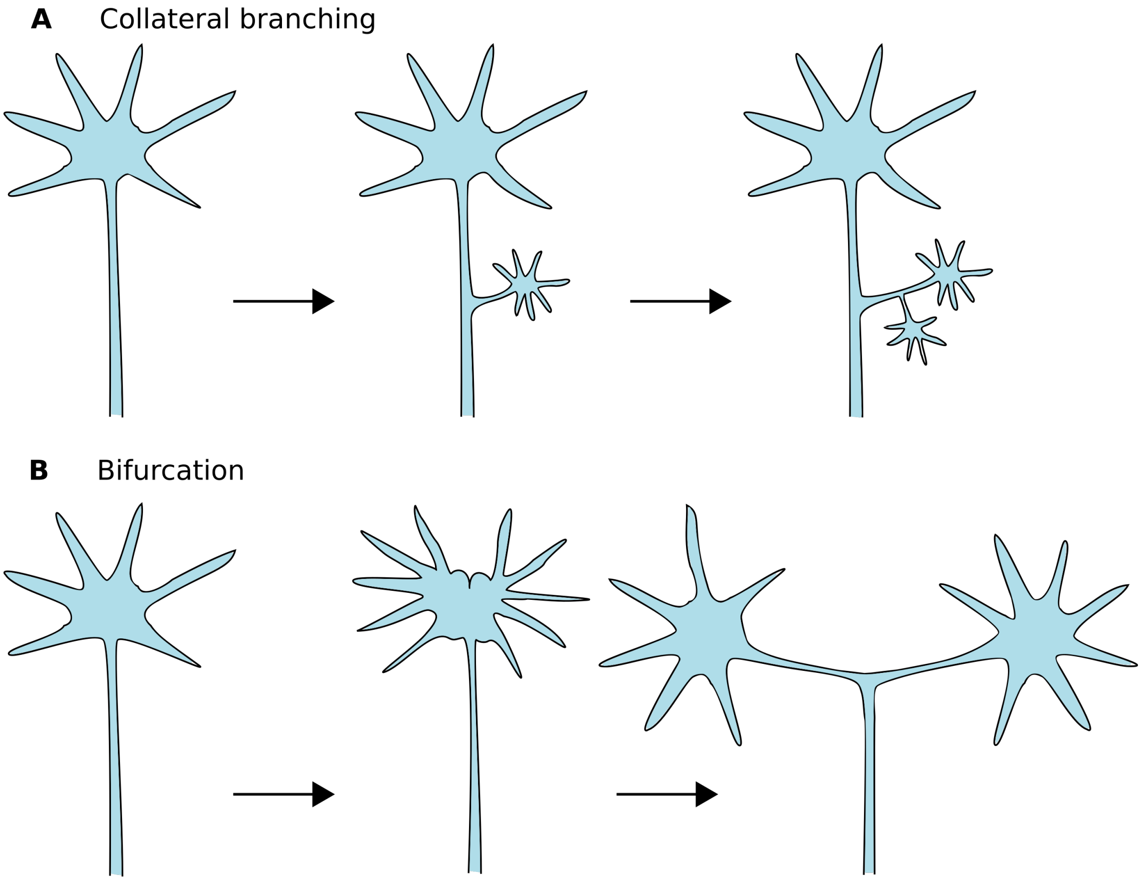

Figure 3: **Axon binding topology.** A) Collateral branching. New branch emerges along the length of the axon shaft. B) Bifurcation. The tip of the growth cone splits into two equal branches.

Even though growth cones lead the elongation of axons towards their target location following the pathways marked by the extracellular guidance cues [47], in the vertebrate CNS, axonal growth cones themselves do not typically enter all the way into their target region. Instead, axons form synaptic connections with their target through growth cone-tipped collateral branches that emerge from the axon shaft, which further re-branch from the collateral branches into terminal arbors [22]. This collateral or interstitial type of branching is the most common (Figure 3A) [48], nevertheless, the second type of branching can occur in certain circumstances [49]. Branches can arise by bifurcation (Figure 3B), a splitting of the terminal growth cone [50], such as at the mouse dorsal root entry zone, where the growth cones of dorsal root ganglion (DRG) axons split to form two daughter branches that arborize in the spinal cord [51, 52].

1.2.2 Axon branching in CNS

In the mammalian CNS, axon branches typically extend collaterally from the axon shaft behind the terminal growth cone. This branching typically occurs after the main axon growth cone has bypassed the target region [48]. Cortical axons in rodents initially bypass the basilar pons [53], but after a delay, they form filopodia, which can develop into stable branches that arborize in the pons [54] (Figure 4A). Developing corticospinal axons also bypass spinal targets and later form interstitial branches that arborize once they have entered topographically appropriate target sites in the spine [55] (Figure 4A). Segments of the axons distal to the target are later eliminated [48, 56]. Callosal axons, which connect the two cerebral hemispheres, also undergo delayed interstitial branchin [57] beneath their cortical targets and developing thalamocortical axons in vivo form layer-specific lower and upper tiers of terminal arbors in the barrel field, which together form a spatial map of the facial vibrissae in the rodent somatosensory cortex [58] (Figure 4B). In the avian [59] and rodent [60] retinotectal systems, retinal ganglion cell axons initially overshoot their termination zone in the tectum and later emit collateral branches at correct tectal positions, which is followed by terminal arborization and regression of the distal axon [61, 62] (Figure 4C). However, in frogs and fish, growth cones of retinal axons form only terminal arbors [63]. Thus, the neuron wiring in the vertebrate CNS is mediated via collateral axon branching and terminal arborization.

1.3 Regulation of axon branching

The process of axon branching must be tightly controlled and regulated. The length of the axon shaft must maintain its stability while at the selected site of new branch formation, dynamic remodeling of axon into branch takes place.

1.3.1 Extracellular cues

Axon branching occurs at localized regions of the axon and is regulated by target-derived molecular cues. Families of extracellular axon guidance cues, growth factors, and morphogens can regulate axon branching by determining the correct position of branches or by shaping terminal arbors [64, 24, 22].

Netrins, such as netrin-1, are diffusible guidance cues with attractive effect [65]. They guide axon path and induce axon branching [66, 67]. Focal application of netrin-1 can induce localized filopodial protrusions de novo along the axon shaft and increase branch length without increasing the extension of the primary axon [66, 26]. Netrin-1 also increases the total number of terminal arbor branches in the frog optic tectum [68].

Ephrins are membrane-bound repulsive cues [69, 70], they have a role in specifying the

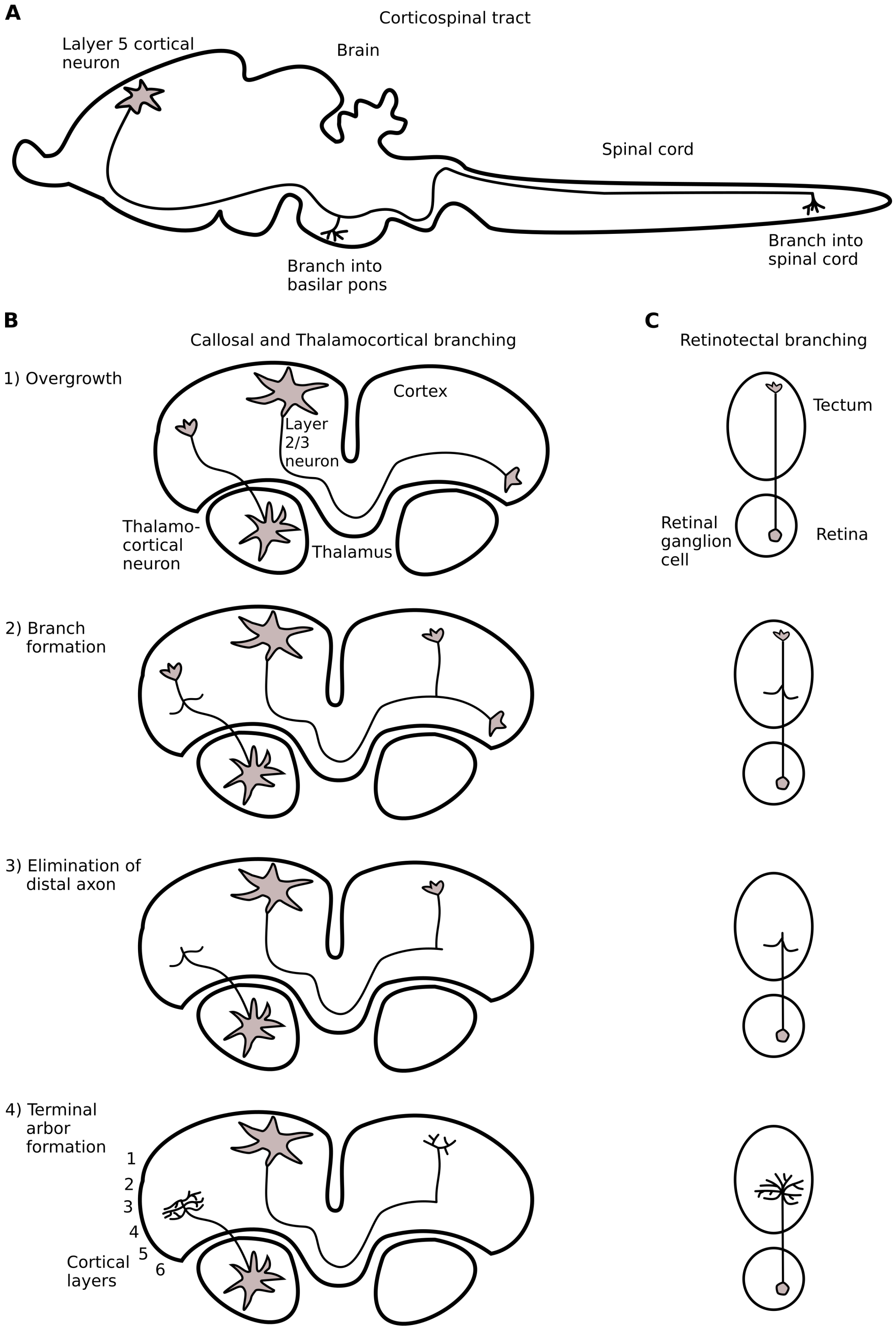
A
Corticospinal tract
Lalyer 5 cortical neuron
Brain
Spinal cord
Branch into spinal cord
Branch into basilar pons
B
Callosal and Thalamocortical branching
C
Retinotectal branching
1) Overgrowth
Cortex
Layer 2/3 neuron
Thalamo-cortical neuron
Thalamus
Tectum
Retinal ganglion cell
Retina
2) Branch formation
3) Elimination of distal axon
4) Terminal arbor formation
1
2
3
4
5
6
Cortical layers

Figure 4: **Axon branching in developing CNS.** A) Sensorimotor cortical axon forms branches into the pons and spinal cord. B) In corpus callosum and thalamocortical axons initially extend past their eventual terminal regions (1). After a delay, branches extend from the axon shaft (2) and the distal axons are eliminated (3). Finally, terminal arbors are formed in target regions (4). C) Retinotectal terminal branching [22].

locations of axon branches. Ephrin-A5 and its receptor (EPHA5) can both promote or repress the branching of various cortical axons by growing on membranes from specific cortical layers [71]. Ephrin-As can both stimulate the branching of one type of axons while repelling axons from other regions that do not innervate the same brain area [22]. In some cases, EPHAs act both as receptors activated by ephrin ligands (forward signaling) and as ligands that activate ephrins (reverse signaling) [61, 72]. Their activity also cooperates with the other branch-promoting molecules such as brain-derived neurotrophic factor (BDNF) [73]. Axon branching is repressed while extending axon is traversing the non-target regions until reaching the area with enriched positive cues which signal the arrival to the correct target region where axon branching is evoked.

Semaphorins (SEMA) are repellent axon guidance cues that function in the assembly of neuronal circuits [74]. For example, in primary cortical neurons, SEMA3A repels axons, inhibits axon branching, and decreases branch length without affecting the length of the primary axon [66, 68]. SEMA3D has been also shown to selectively affect branches depending on their position along the axon. Central branches were not affected while the branching at the peripheral areas was induced [75]. However, SEMA3A can also positively influence axon branching. Recently, SEMA3A was shown to promote branching by cerebellar basket cell axons onto Purkinje cells in the cerebellar cortex [76].

Like semaphorins, SLITs, which act on ROBO (Roundabout) receptors, are repulsive cues and they can also both promote and inhibit branching. For example, SLITs can promote the collateral axon branching of mammalian sensory DRG axons in-vitro [27] but also inhibit arborization of retinal ganglion cell axons in the zebrafish optic tectum [77]. It seems that both SLITs and semaphorins manifest context-dependent repression or promotion of axon branching, depending on the particular population of neurons.

Growth factors, such as fibroblast growth factor (FGF), and neurotrophins, such as nerve growth factor (NGF) and brain-derived neurotrophic factor (BDNF), can also promote axon branching and terminal arbor formation. For example, NGF increases DRG axon branching [78, 79], BDNF induces filopodial and lamellipodial protrusions along frog spinal axons [80], and FGF-2 and BDNF stimulate branching in cortical axons [81, 50]. BDNF has been also shown to induces rapid extension of new terminal branches on frog retinal axons [82]. Interestingly, although both BDNF and netrin-1 increase the arbor complexity of retinal arbors, their mode of action seems to be different [68]. BDNF promotes the addition and stability of axon branches whereas netrin-1 induces new branch growth but not branch stabilization. This example shows that different guidance cues can, therefore, have a similar effect on final arbor morphology by different dynamic strategies [22].

WNTs comprise a diverse family of secreted morphogens that shape embryonic development. Several WNTs also function as axon guidance cues [83, 84], enhances axon extension [85], or regulate axon branching [86, 87]. For example, WNT7A, secreted by cerebellar granule cells, induces remodeling of pontine mossy fiber axons by inhibiting their elongation and enlarging their growth cones causing an increase in axon branching [88]. WNT3A, secreted by motor neurons, induces axon branching by regulating presynaptic terminal arborization of spinal sensory neurons [86, 87], whereas WNT5A, a repulsive axon guidance cue for cortical axons in-vivo [89], induced the elongation of axons and branches [85] but did not increase the numbers of axon branches itself [90].

Together these findings indicate that extracellular cues can selectively promote or repress only axon branching without affecting the growth and guidance of the parent axon. The explanation, why the same guidance molecules can have a distinct effect on axon guidance, elongation, and branching, could be in the differences between local signaling and cytoskeleton remodeling mechanisms at the growth cone versus along the axon shaft.

1.3.2 Signaling for branching

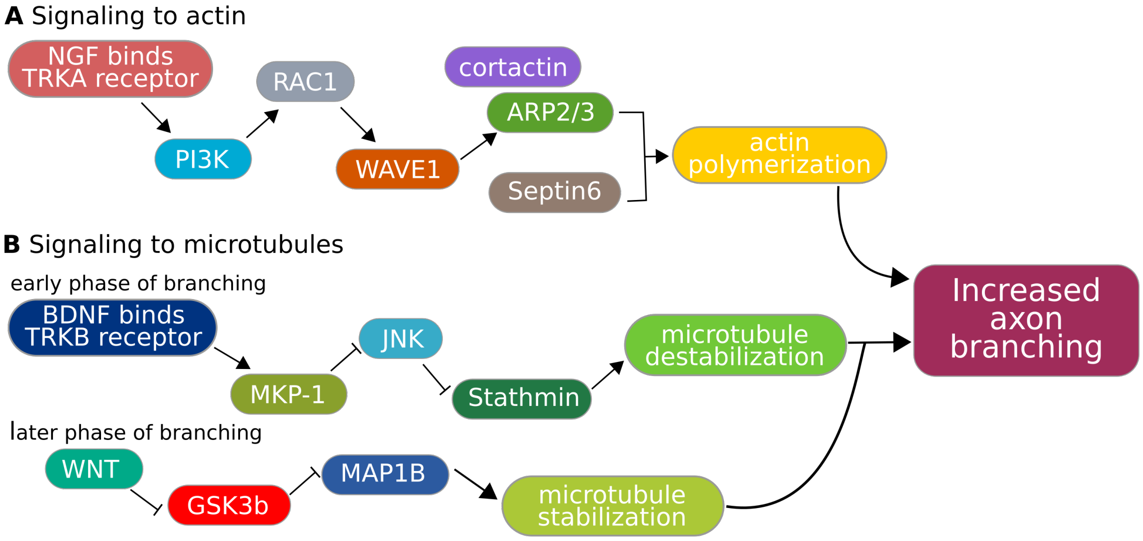
A Signaling to actin
NGF binds TRKA receptor
PI3K
RAC1
WAVE1
cortactin
ARP2/3
Septin6
actin polymerization
B Signaling to microtubules
early phase of branching
BDNF binds TRKB receptor
MKP-1
JNK
Stathmin
microtubule destabilization
later phase of branching
WNT
GSK3b
MAP1B
microtubule stabilization
Increased axon branching

Figure 5: **Signaling pathways promoting axon branching.** A) Signaling promoting actin polymerization. NGF-induced TRKA signaling promotes axon branching by activating PI3K and, in turn, RAC1, which activates actin-associated proteins to increase actin polymerization and the formation of actin patches. Cortactin, recruited by Septin6, promotes the emergence of filopodia from actin patches. B) Signaling promoting microtubule destabilization at early branching stages (top) and microtubule stabilization at later branching stage (bottom). Both pathways promote axon branching each by opposing effects on microtubule stability. BDNF-induced TRKB signaling activates MKP-1 and, in turn, inactivates JNK, resulting in microtubule destabilization caused by increased tyrosination of Stathmin. WNT induced GSK3beta inhibition decreases MAP1B phosphorylation leading to an increase in microtubule stability [22].

The numerous guidance cues described in the previous chapter are affecting axon branching via the activation of multiple signal transduction pathways. So far signaling through RhoGTPases [91] and the protein kinase glycogen synthase kinase 3 beta (GSK3beta) [92] have emerged as a transduction node for the signal from the multiple extracellular cues onto cytoskeletal effectors resulting in changes of actin and microtubule dynamics. Although no single pathway from receptor to the cytoskeleton has been completely defined yet, several examples of signaling pathways regulating axon branching have been described already [22].

NGF promotes the formation of filopodia and branches in chick sensory axons [78] by affecting the rate of actin patch formation [93] (Figure 5A). In particular, NGF binds TRKA (Tropomyosin receptor kinase A) receptor, activating PI3K (phosphoinositide-3-kinase), resulting in activation of RAC1 (Ras-related C3 botulinum toxin substrate1) GTPase, which drives the activity of the ARP2/3 (actin-related protein 2/3) activator WAVE1 (WASP-family verprolin homologous protein 1). WAVE1 promotes ARP2/3 dependent actin patch initiation and subsequent axon branch formation [94, 30].

The actin-associated protein cortactin influences axon branching by promoting actin polymerization and the membrane protrusion by the emergence of filopodia [95, 96]. Proteolysis of cortactin by caplain represses actin polymerization and keeps axon shafts in a consolidated state. The effect of calpain can be negated by factors such as netrin-1 and BDNF to initiate branching. These examples illustrate the part of the axon branching signaling pathway responsible for the remodeling of actin.

Multiple pathways regulating the remodeling of microtubule cytoskeleton have been described so far. The BDNF has been shown to induce axon branching of mouse cortical neurons by microtubule destabilization through binding to TRKB (Tropomyosin receptor kinase B) receptor [81], whereas WNT has been reported to promote axon branching by having stabilizing effect on microtubules through GSK3beta signaling [88] (Figure 5B). The seemingly contradictory effects of BDNF and WNT on microtubules have been explained by discovering that microtubule destabilization occurs during the early phase of branching whereas the destabilization comes into play in the later phase of branch maturation when stable neurons enter the nascent branch.

BDNF binds TRKB receptor, inducing MPK-1 phosphates (mitogen-activated protein kinase phosphates) which then inactivates JNK (MAPK c-jun N-terminal kinase) by dephosphorylation, which in turn reduces the phosphorylation of the JNK substrate stathmin-1 (STMN1), thereby activating STMN1 leading to increased microtubule tyrosination and their consequent destabilization resulting in increased cortical axon branching [81, 37].

WNT inhibits GSK3beta activity [84, 88], which normally phosphorylates MAPs (microtubule associated proteins) such as tau, APC (Adenomatous polyposis coli protein), and MAP1B. Phosphorylated MAP1B maintains microtubules in a dynamic state [97], therefore the activation of the WNT pathway decreases MAPs phosphorylation and in turn increases microtubule stability leading to axon branching [81].

BDNF and netrins have been shown to specifically promote terminal axon branching in frog retinotectal axons [68, 82]. In this signaling pathway, NEDD4 (E3 ubiquitin-protein ligase) ubiquitinates PTEN (Phosphatidylinositol 3,4,5-trisphosphate 3-phosphatase and dual-specificity protein phosphatase) and PTEN degradation increases terminal arborization by promoting PI3K, which is known to regulate cytoskeletal dynamics [98]. On the other hand, inhibition of NEDD4 caused an increase in PTEN levels and subsequent inhibition of axon branching.

1.4 Cytoskeleton organization and dynamics at the axon branch

The extensive reorganization of the cytoskeleton is an important part of the axon branch formation [23]. First, actin-filled filopodium emerges to form a premature branch which is later stabilized by the insertion of microtubules into the mature branch (Figure 6).

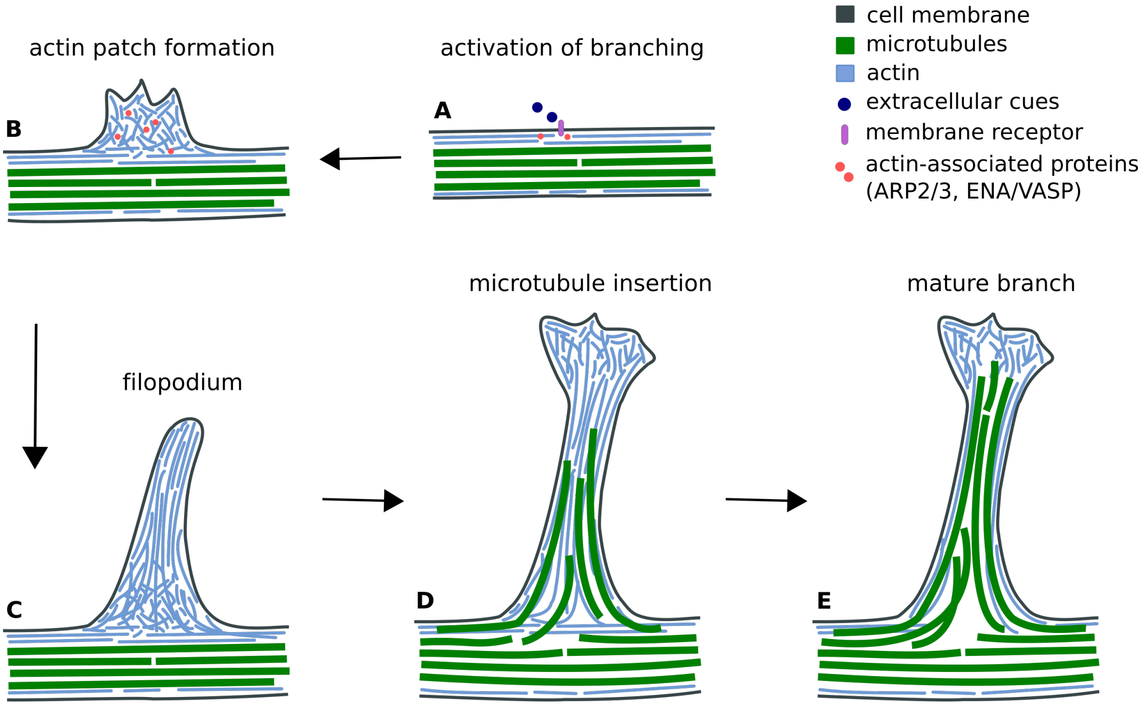
actin patch formation
activation of branching
cell membrane
microtubules
actin
extracellular cues
membrane receptor
actin-associated proteins (ARP2/3, ENA/VASP)
B
A
microtubule insertion
mature branch
filopodium
C
D
E

Figure 6: **Remodeling of the cytoskeleton during axon branching.** A) Extracellular cues activate signaling pathways that locally increase actin remodeling. B) Actin patch is formed by the pressure of accumulated actin on the outer membrane. C) Further extension of plasma membrane under the force of actin-based components leads to the formation of filopodium protrusions. D)-E) Microtubules start invading filopodium to stabilize the new branch and promote its maturation. The color code for cell elements is depicted in the legend.

1.4.1 Actin remodeling

The first step of axon branching is the formation of the actin patch (Figure 6B) when short pieces of actin accumulate along the axon shaft pushing at the plasma membrane to protrude outwards [94]. Further extension of plasma membrane under the force of actin-based components leads to the formation of protrusions (Figure 6C), either finger-like filopodia or sheet-like lamellipodia. Actin in the axon branch is nucleated and remodeled via several actin-associated proteins such as a nucleator complex ARP2/3 (actin-related protein 2/3) and remodeling protein ENA/VASP (enabled/vasodilator-stimulated phosphoprotein) [99]. These proteins are directly linked to the formation of filopodia, the deletion of ARP2/3 in hippocampal neurons reduced the frequency of filopodia and the reduction of ENA/VASP proteins in the retinal ganglion neurons led to diminished filopodia formation and axon branching [100]. ARP2/3 is also required for NGF (nerve growth factor) induced branching of sensory neurons [94, 30, 101].

The formation of the actin patch is also regulated by cortactin which stabilizes the ARP2/3 complex. Cortactin also positively regulates actin patch duration and contributes to the probability of the emergence of a filopodium from the patch [30]. The duration and frequency of filopodia formation have been shown to influence the number of axon branches [102]. Together, these studies demonstrated the importance of the actin cytoskeleton remodeling for the initiation of axon branch formation. However, due to the dynamic nature of actin, actin-filled filopodium alone is not sufficient for the maturation of the axon branch. Hence the extending protrusions in this stage are referred to as premature branches.

1.4.2 Microtubule remodeling

The premature branches are thought to be stabilized by the insertion of microtubules into the emerging protrusion (Figure 6D), as the disruption of microtubules causes a reduction in axon branching [28]. However, the microtubule entry into a premature branch does not always result in the establishment of a matured branch with a new synapse. It has been shown that even longer axon branches containing microtubules can regress [103], presumably because of the dynamic instability of microtubules [104, 105] switching between phases of microtubule polymerization and depolymerization. Hence, additional stabilizing mechanisms likely play a role during the branch maturation.

It is thought that microtubules are stabilized by the interaction with pre-organized actin filaments in filopodium [28, 22, 106] (Figure 7). It has been shown that septins localize at actin patches during the initiation of axon branching. Septins control axon branching by regulation of the microtubule-actin interactions in filopodium [107]. The actin-binding protein drebrin also localizes at axon branching sites and was shown to promote the entry of microtubules into filopodia, resulting in the formation of mature branches [108]. Drebrin mechanism seems to be responsive to extracellular branch promoting signaling, since the treatment with NGF which promotes axon branching also increased the levels of axonal drebrin [101]. The interplay of microtubule and actin cytoskeleton has a key role in the axonal branch formation process, nevertheless, a more detailed understanding of these mechanisms as well as their exact spatiotemporal coordination at the axon branch region are to be explored.

Besides the promotion of branch maturation via stabilizing microtubule-actin interactions, several neuronal microtubule-associated proteins (MAPs) contribute by promoting microtubule polymerization and stability [22] (Figure 7). For example, MAP7 (ensconsin or E-MAP-115) promotes microtubule polymerization in-vitro and it has been shown to accumulate at the newly forming axon branches and increase the number of axon branches [109]. Similarly, SSNA1 (NA14) also accumulates at axon branching sites [110] and its overexpression induces axon branching [111]. Interestingly SSNA1 has been shown to induce not only microtubule nucleation but also a unique microtubule branching in-vitro [110].

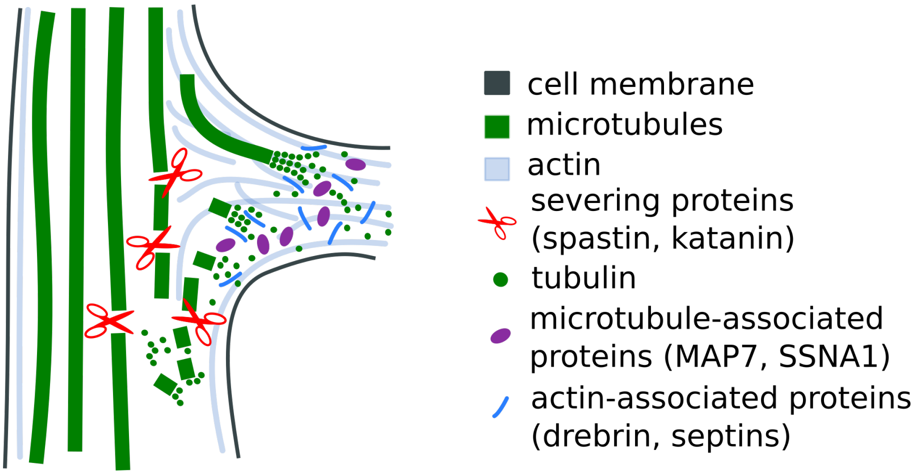
cell membrane
microtubules
actin
severing proteins (spastin, katanin)
tubulin
microtubule-associated proteins (MAP7, SSNA1)
actin-associated proteins (drebrin, septins)

Figure 7: **Remodeling of cytoskeleton facilitating the branch growth.** Bundled microtubule arrays in the axon are fragmented with the help of microtubule severing enzymes such as spastin and katanin to increase microtubule mass available for polymerization. Different microtubule-associated proteins (e.g. MAP7 and SSNA1) that promote and stabilize the microtubule growth are reported to localize at the axonal branch. In addition, other cytoskeletal proteins like drebins and septins were suggested to promote the entry of microtubules into the actin-rich filopodia. The color code for cell elements is depicted in the legend.

The mechanism by which are tightly bundled microtubules in the axon shaft able to enter the new branch is suggested to rely on local microtubule destabilization and fragmentation [112, 22, 113]. These microtubule fragments would be then transported to the forming branch to serve as a nucleation template and the local increase of free tubulin pool would be available for new microtubule polymerization promoting the axon branch growth [114, 103] (Figure 7).

Microtubules are fragmented by microtubule severing enzymes spastin and katanin, their overexpression increases the local microtubule mass [115, 116]. Both spastin and katanin are expressed in neurons, overexpression of spastin dramatically enhances the formation of axon branches [117]. But interestingly overexpression of katanin increases branching only in tau depleted neurons, suggesting a branching regulation mechanism based on local changes in microtubule-associated protein interactions [117].

In agreement with the microtubule destabilization hypothesis, the increase of local calcium concentration along axon shaft was reported to promote collateral branching [118], whereas the exposure of neurons to taxol, microtubule-stabilizing drug, reduced the number of microtubules entering the new filopodia resulting in decreased branching [28, 2].

Another mechanism regulating microtubule stability and dynamics with reported influence on axon branching is the post-translational modifications of tubulin including acetylation and polyglutamylation [119]. Particularly, tubulin acetylation controls axonal branching by regulating microtubule dynamics [120].

Further, it was shown that the spatiotemporal coordination of microtubule dynamic behavior is critical for axon branching. As reported in the case of branch-specific destabilization of microtubules by the enzyme spastin at neuromuscular synapses, which resulted in the loss of branches instead of their induction [121]. Altogether, these observations highlight a key role of microtubule dynamics and the cooperation between actin and microtubule cytoskeleton in axon branching.

1.5 Organelle interplay within the neuronal branch

While the crucial structural role in the remodeling during branching belongs to the cytoskeleton, the other cellular organelles also play an important function during axon branch formation and maintenance.

1.5.1 Mitochondria

Mitochondria transport within the axon is crucial for the correct function of neurons. The malfunction of mitochondria transport has been linked to various neurodegenerative conditions as Alzheimer's disease, Huntington's disease, or amyotrophic lateral sclerosis (ALS) [122, 123, 124]. In healthy neurons, mitochondria undergo both anterograde and retrograde transport, delivering mitochondria to the synapses and back to the cell body. The transport and distribution of mitochondria is mediated via the motor proteins dynein and kinesin, mitochondria adapter proteins such as TRAKs/Milton, and the anchoring protein, syntaphilin [125]. Mitochondria are continuously transported throughout the axon but tend to accumulate at the sites which have a higher demand for energy supply like synaptic terminals, growth cones, and axon branching points [33]. Mitochondria were reported to be actively transported into the new axon branches [126] and their stalling at the branching site is linked to branch maturation [25], suggesting their role during branch formation. Mitochondria were found together with translational machinery at the base of filopodia, linking the mitochondrial respiration to the sites of preferential local protein synthesis hot spots in the axon. The maturation of filopodia into branches was shown to depend on the mitochondria respiration [25]. The mitochondria colocalized with the mRNA coding for actin, providing new material for the elongation of the forming branch. Interestingly, the regulation of the microtubule cytoskeleton aspect of branching was not found to be dependent on mitochondria function [25].

However, stalling of mitochondria inside the axon shaft is not sufficient to induce new branch formation on its own, as notably about 70% of mitochondria are stalled along axons at a given time [127]. It is only when mitochondria stall at the sites of emerging filopodia when the branching maturation effect takes place. Other evidence indicates the involvement of additional coordination of mitochondria by signaling and adapter proteins during the branching process. In cortical neurons, overexpression of liver kinase B1 (LKB1) or the anchoring protein syntaphilin increased the number of stalled mitochondria in axons and also the number of axon branches, whereas the depletion of these proteins caused a reduction in mitochondria stalling events and decrease in branching [128]. Similar effects were observed by manipulating adenosine monophosphate-activated protein kinase AMPK signaling [129] and the deletion of the mitochondria adaptor protein TRAK1 (trafficking kinesin-binding protein 1) lead to diminished axon growth and branching [130].

Further studies demonstrated that the fission and fusion of mitochondria may also play a role in axon branching. Especially Drp1 (dynamin-related protein 1) induced fission mediated via MFF (mitochondrial fission factor) was found to be specific for axons [35]. MFF has been shown to regulate the size of mitochondria in axons and coincided with terminal axon branching. The regulation of mitochondria size via MFF has been also linked to the calcium-controlled presynaptic release. The size of mitochondria presumably correlated with the calcium concentration homeostasis in the presynaptic site [35]. In sensory neurons, the fission of mitochondria was also observed to be induced by branching-promoting neurotrophins [131]. NGF has been shown to induce the activity of Drp1 via Mek-Erk signaling while also contributing to an actin-dependent aspect of fission via PI3K. In-vitro, Drp1-mediated fission was required for NGF-induced collateral branching while expression of dominant-negative Drp1 impaired the sensory axon branching in-vivo [131]. NGF-induced mitochondrial fission was also required for local translation of the actin regulatory protein cortactin, which was previously described in the NGF-dependent axon branching [131, 30, 25, 102]. Thus this study links mitochondria fission with the actin cytoskeleton remodeling events of axon branching described earlier.

Together these observations indicate that the fission-mediated control over the numbers of mitochondria and their size plays a significant role during the axon branching process (Figure 8A).

1.5.2 Endoplasmic reticulum

The endoplasmic reticulum (ER) forms an extensive continuous network spanning the whole cell. The ER membrane adopts two structurally and functionally distinctive forms, the ER cisternae, and tubules. In unpolarized cells, the sheets of ER cisternae are distributed around the nucleus and ER tubules are located at the cell periphery while connecting into a complex ER matrix [132]. In mature polarized neurons, ER extends along the whole axon shaft mostly in tubular form, while in dendrites both tubular and planar form have been reported [133]. Neuronal cell bodies contain both rough and smooth ER but the presence of rough ER in axons has been an open question. The presence of mRNAs coding for plasma membrane proteins and components of the secretory machinery gave the first indication of their existence and local translation in axons [134, 135]. More direct evidence was so far observed only by electron microscopic data which showed densities resembling rough ER at axonal tips [136].

The function of ER is diverse such as lipid synthesis, a platform for secretory protein synthesis, maintenance of calcium and glucose homeostasis, and redistribution of membrane-associated proteins [137]. ER interacts with microtubules, mitochondria, cytoplasmic membrane, and other organelles [25, 133, 36]. It was implicated that ER plays a role in establishing neuronal polarity and dendrite arborization [138]. More recently it was reported that the crosstalk between ER and axonal microtubules is decisive for the neuronal polarity [36]. It has been shown that an ER protein p180 (also known as ribosome binding protein 1 homolog 180-kDa, RRBP1) interacts with both ER and microtubules in axon specific manner, controlling neurite transformation into axon by inducing microtubule stabilization.

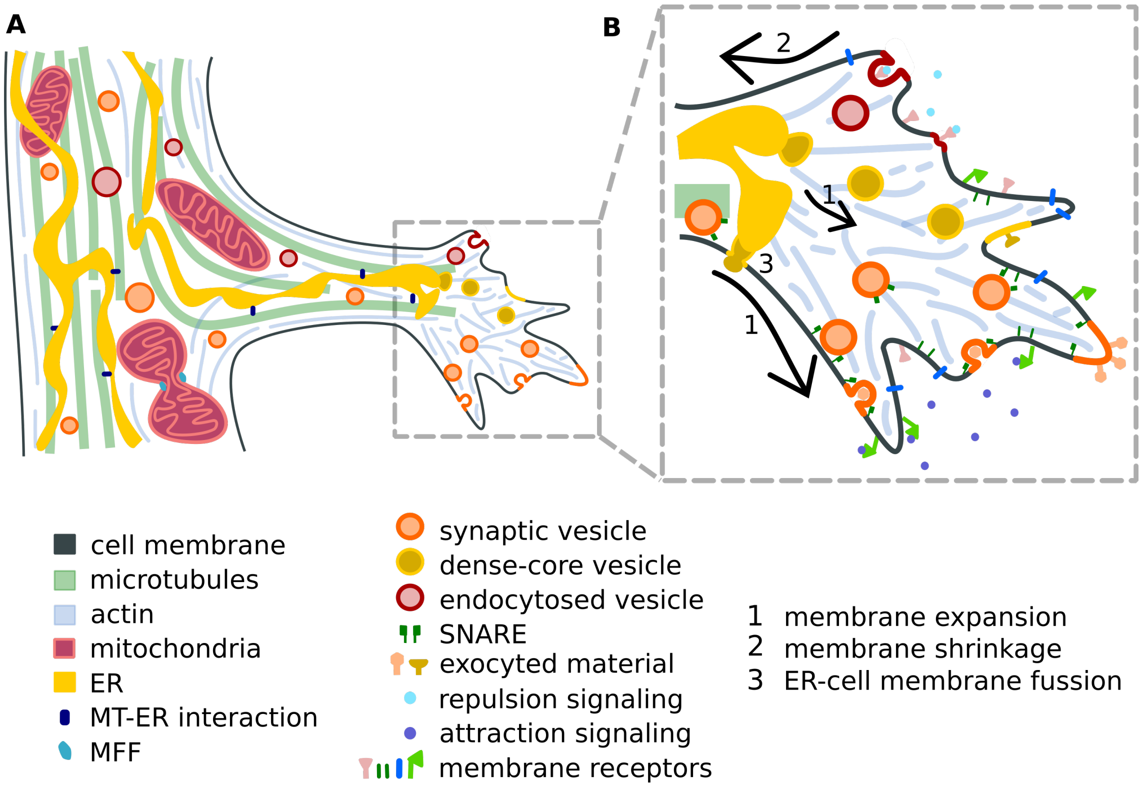
A
B
2
1
3
1
cell membrane
microtubules
actin
mitochondria
ER
MT-ER interaction
MFF
synaptic vesicle
dense-core vesicle
endocytosed vesicle
SNARE
exocyted material
repulsion signaling
attraction signaling
membrane receptors
1 membrane expansion
2 membrane shrinkage
3 ER-cell membrane fussion

Figure 8: **Organelle organization and remodeling of the plasma membrane at the axon branch.** A) Schematic representation of a growing matured branch. At the branching site, mitochondria increase in numbers through fission mediated by mitochondria fission factors. ER is suggested to stabilize microtubules via ER-MT interacting proteins. B) Magnified inset from panel A highlights the various mechanisms taking place to regulate membrane expansion and retraction. Membrane expansion in response to attraction guidance molecules is carried out using the fusion of synaptic vesicles to the plasma membrane or exocytosis using SNARE proteins. Retraction of membrane initiated by repulsion guidance molecules is achieved through endocytosis of membrane material. The color code for cell elements is depicted in the legend.

Other ER-associated proteins also interacting with microtubules include CLIMP63 (cytoskeleton linking protein 63), kinectin (KTN1) [139], and atlastin-1. Notably, enrichment of atlastin-1 in vesicular structures was found at the growth cones and at the branch points, while the depletion of atlastin-1 compromised the development of rat cortical neurons [140]. Atlastin-1 also regulates the number of mitochondria at dendritic branch points in sensory neurons [141], raising the question if atlastin-1 may have a similar role also at the axon branches. Even though these reports show the importance of ER during axon development, the role of ER in axon branching is not fully understood. Yet interestingly reports from other cell types demonstrated that ER facilitates mitochondria fission regulated by Drp1 by wrapping around mitochondria cleavage site [142]. Another report showed that ER-associated formin INF2 (inverted formin 2) is required for efficient mitochondria fission. It was suggested that INF2-induced actin filaments drive initial mitochondrial constriction, which allows Drp1-driven secondary constriction resulting in actin-mediated mitochondria division [143]. Thus these observations are raising the question of whether the ER-mediated mitochondria fission plays a role in axon branching as well.

Together this accumulating evidence supports the active role of ER as an important cellular organelle involved in the orchestration of axon branching event, regulating the cytoskeleton stability and possibly also the mitochondria fission (Figure 8A).

1.5.3 Golgi complex

In neurons, the Golgi apparatus facilitates forward trafficking of transmembrane and secreted proteins and performs posttranslational modification of proteins and lipids [144]. The membrane and secreted proteins are synthesized in the neuronal cell body progress through rough ER and Golgi complex, finally ending up in vesicles that are transported into the dendrites and axons [135].

In the cell body, the Golgi complex is composed of distinct compartments or cisternae [145], located adjacent to the endoplasmic reticulum. Different Golgi compartments have distinct functions for sorting proteins and conducting post-translational modifications [146, 147]. Endoplasmic reticulum-related structures referred to as ER exit sites (ERES) and ER-Golgi intermediate compartments (ERGICs) are distributed throughout the soma and dendritic compartment [148, 149]. A special Golgi satellite containing glycosylation machinery has been recently described in dendrites of pyramidal neurons [150]. These Golgi satellites are located between ERGIC and retromer and the Golgi satellite system allows for protein recycling and local processing of transmembrane proteins in dendrites [150]. Different discrete Golgi units referred to as Golgi outposts have been found in proximal dendrites of cultured hippocampal neurons and in apical dendrites of pyramidal neurons in-vivo [149]. The Golgi outposts have been shown to increase dendritic complexity [151] and were frequently found localized at dendritic branch points [152], suggesting their active role during dendrite branching.

While ultrastructural studies suggest that axons do not have Golgi apparatus or rough ER, mRNAs for transmembrane and secreted proteins have been found to localize to axons. Recent studies showed that axons contain ER and Golgi components needed for classical protein synthesis and secretion [135] suggesting an axon localized mechanism for protein secretion. Others described mix-identity organelles or endosomes in axons, trafficking proteins from ER to plasma membrane [42]. The evidence is rather still speculative, but it suggests that mixed-identity organelles may combine exocytic, lysosomal, and endocytic functions, determining the composition of ion channels and adhesion proteins at the axonal plasma membrane. Another suggested mechanism is via ER endosome contacts possibly facilitating the translocation of protein from ER to endosome followed by endosome fusion with the outer cell membrane [153, 42]. Golgi outposts, present in dendrite branch points, were only rarely found in axons [152], but it was suggested that Golgi satellites, also characterized in dendrites, may be present in axons, however, their existence needs to be still confirmed [42]. Even though the evidence of possible alternative organization of Golgi apparatus has been accumulating in recent years, the current understanding of the local axon secretory trafficking is still very limited.

Thus Golgi complex is undoubtedly an important organelle in neuron cells and its role in the soma and dendrites has been studied extensively. However, the role of Golgi or its functional equivalent in axons is still not clear and needs further investigation. Golgi outposts in dendrites were suggested to play a role during dendrite branching, but whether there is some equivalent Golgi-related structure involved in axon branching still needs to be explored.

1.6 Membrane remodeling at axon branches

The growth of axons is driven by the constant remodeling of the cell membrane. Especially at the actively remodeling areas of growth cones and axon branches, the membrane extension requires a variety of proteins and lipid components. These areas undergo expansion or retraction depending on the external guidance cues (Figure 8B).

1.6.1 Membrane expansion via fusion with synaptic vesicles

The main material supply for the extending cell membrane is the accumulation of synaptic vesicles, dense-core vesicles, and ER membranes [154]. Synaptic vesicles are reported to be present in high numbers along the axon shaft and at branching sites [154]. Synaptic vesicles deliver membrane materials to the expanding plasma membrane by fusion or exocytosis via SNARE (soluble N-ethylmaleimide-sensitive factor-attached protein receptor) complexes [155, 154]. The fusion-mediated supply of membrane and secretory materials is well studied at synapses of mature neurons, but the presence of clustered synaptic vesicles and accompanying exocytosis machinery has been also shown in developing axons even before synaptogenesis [156, 157]. Moreover, the number of branches was enhanced after the overexpression of these components in neurons [158, 82, 159]. The insight into the potential function of these vesicle accumulations has been further revealed by the fluorescent imaging of GFP-tagged synaptic vesicle components in neurons. Previous studies demonstrated that synaptobrevin II, a synaptic vesicle marker, is enriched at branching sites of retinal ganglion cells, and most of the observed branches emerged from GFP-labelled sites [82]. When neurons were exposed to brain-derived growth factor (BDNF), the axon branching was increased as well as the density of GFP-synaptobrevin at given branch points. Whereas the reduction of the NDNF levels by neutralizing antibodies resulted in the reduction of synaptobrevin and also depletion of axonal branches [160]. These observations are showing the direct response of synaptic vesicles to extracellular stimulation and they demonstrate the importance of the accumulation of synaptic vesicles prior to axon branching to create a source of new membrane material for the emerging branch. The use of synaptic vesicles makes the membrane expansion mechanism dynamically adaptable to the various physiological needs during the development, maintenance, and communication of neurons.

Similarly, Netrin-1, an extracellular signaling molecule with attractive properties, has been shown to increase the number of axon branches in cultured cortical neurons [66]. A study demonstrated that a high local concentration of Netrin-1 induced an increase in calcium transients in neurons [34], possibly causing the modulation of synaptic exocytosis and stimulated branch formation. A fusion of synaptic vesicles during the Netrin-1 increased branch formation in cortical neurons was also observed [161]. Another study used fluorescently labeled synaptic-vesicle protein synaptophysin in live-cell imaging in zebrafish and Xenopus retinotectal projections to investigate its role in axon branching. They showed that terminal branches emerge from sites displaying high fluorescence intensity whereas the branches emerging from only faintly labeled puncta retracted themselves, proposing that the maturation of axon branch needs a critical accumulation of synaptic vesicle components [163, 162]. Also, the overexpression of syntaxin1-binding protein Sec1, involved in the SNARE complex formation [164, 165], resulted in the increase in collateral axon branching in hippocampal neurons [166]. Together, these studies demonstrate how the synaptic vesicles accumulation and their fusion to the plasma membrane are important for the formation of axon branches.

1.6.2 Membrane expansion via ER contacts

The ER present in axons has been shown to form contacts with the plasma membrane. These contacts were suggested to provide new lipids for the expansion of cell membrane necessary for the growth and extension of axons [167]. At axon branches, ER is contributing to the membrane remodeling by regulating the pool of available synaptic vesicles and the membrane fusion via the action of ER-associated proteins. Changing the levels of atlastin, an ER-associated protein, affects the release of synaptic vesicles along axons in Drosophila motor neurons [168]. Whereas the overexpression of protrudin, an ER-resident protein, causes membrane deformation and the formation of long neurites [169]. This effect is likely mediated by the interaction with the GDP-form of Rab11 and Kinesin-1 since they are both involved in the regulation of the anterograde transport of recycling endosomes to the plasma membrane during the axon growth [169, 170, 153]. A similar protrudin mediated effect was observed in cultured cortical neurons and in injured optic nerve in-vivo [171]. Recently was reported that the interaction of protrudin with ER is mediated via PDZD8 (PDZ domain-containing protein 8), which was shown to have a lipid transferring activity at the contact sites between the ER and endosomes [172]. This finding is suggesting that protrudin might play a role as part of the lipid shuttling machinery which controls the membrane expansion and shrinkage.

1.6.3 Membrane retraction

While the expansion of membranes at the branching axon is mediated by exocytosis, the retraction of branched axons is controlled by the elimination of the membrane through endocytosis. The inhibition of endocytosis and related pathways which resulted in increased branching was observed across different types of neurons [173, 174], likely by preventing the pruning process [175]. In particular, the inhibition of endocytosis through fibroblast growth factor receptor (FGFR1) has been shown to increase the axon branching in dorsal root ganglion (DRG) neurons [174], and the knockdown of syndapin I and other proteins of F-BAR (FER/CIP4 Homology Bin-Amphiphysin-RVS) family increased axon branching. The F-BAR are membrane curvature forming proteins that are involved in endocytosis and so are considered to be negative regulators of axon branching [154]. Furthermore, GFP-labelled Rab5 vesicles, that mark early endosomes, were shown to accumulate at the axon branching site [176]. These experiments demonstrate that endocytosis itself negatively regulates axon branching, while exocytosis of synaptic vesicles positively correlates with increased axon branching

1.7 Local translation in neurons

Due to the complex polarized morphology of neuronal cells and their compartmentalized function, neurons are thought to employ a regulatory system controlling their local environments [11, 12, 13, 14]. This includes the differential expression of proteins and their enrichment, which is critical for the local development and regulation of axonal homeostasis and plasticity [13].

To facilitate the prompt adjustment of local requirements, specific areas of neurons are thought to have capacities to locally translate proteins. In particular, clusters of mRNAs are found in local areas within dendrites and axons [15, 13, 16, 17]. Recently 2,500 mRNAs localized at dendrites and axons of hippocampal pyramidal neurons were identified by in-depth RNA sequencing combined with FISH and Nanostring analysis [178] and more than 450 mRNA transcripts were localized in excitatory presynaptic nerve terminals of purified mouse synaptosomes [179]. The type of locally enriched mRNAs depends on the developmental stage and the location within a neuron [15]. During the growing phase, mRNAs coding for proteins of the synthesis machinery and cytoskeletal components are particularly found in the growth cones [180, 181], reflecting the necessity of producing those building blocks to grow longer. Such regulatory mechanisms have also been observed in distal axons during regeneration [182].

Another study reported RNA granules associated with endosomes along the axon of retinal ganglion cells. RNA-bearing Rab7a late endosomes were associate with ribosomes and were also identified as the sites of local protein synthesis. RNA-bearing late endosome was reported to interact with mitochondria and to translate proteins for mitochondrial function [183].

1.7.1 Ribosomes

The presence of ribosomes was first identified in dendrites [184, 185], but only recently ribosomes were also visualized along the axon shaft [19, 20, 21] and at the synapses [179, 186]. Ribosomes are thought to be sparsely scattered, only rarely grouped into polysomes (clusters of mRNA and two or more ribosomes). Even though some polysomes have been detected in dendritic spines and throughout the length of the dendrite [187, 188], data from polysome profiling and ribosome footprinting of microdissected synaptic regions in-vivo have shown local preferential translation by monosomes (single ribosomes engaged with an mRNA) [18]. Furthermore, the neuronal monosomes were in the process of active protein synthesis. Most mRNAs showed a similar translational status in the cell bodies and neurites, but some transcripts exhibited a preference for monosomes in the dendritic and axonal compartments [18]. These ribosomes are suggested to be involved in synthesizing proteins that are only locally needed [189, 13].

However, despite the critical role of locally focused translation in axons, the actions of the translations are not fully understood. Despite the growing evidence for the presence of mRNAs, ribosomes, and locally synthesized proteins, the direct observation of the protein synthesis accompanied by cytoskeleton and organelle re-organization has remained to be a major challenge. Understanding how the promotion of neuronal growth and the local reorganization is hampered by a lack of direct observations of local axonal environments at a molecular level.

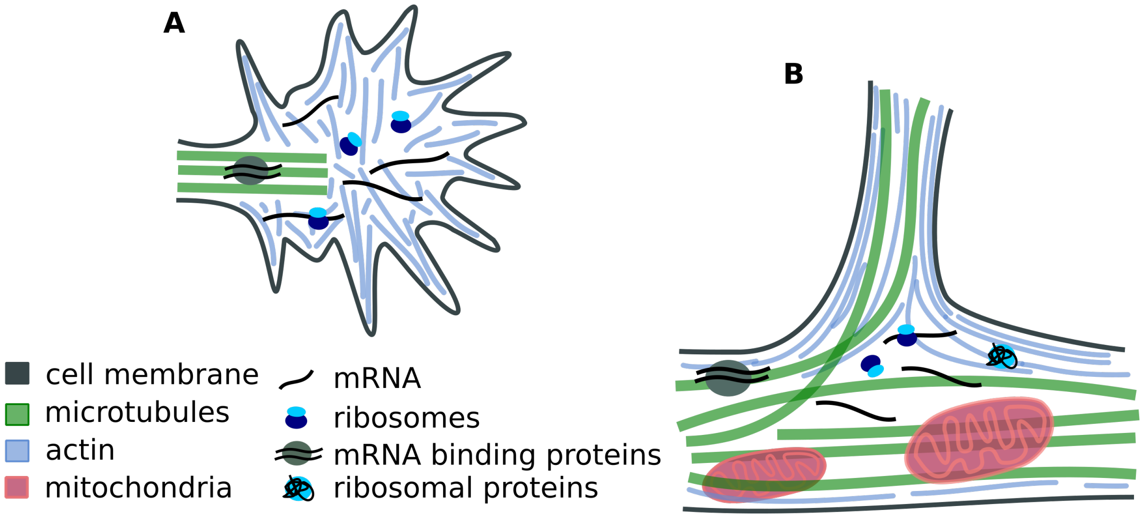

Figure 9: **Local translation at axon.** A) Schematic representation of suggested cellular components involved in local translation. mRNA transcripts are transported to distal regions of the axon via mRNA binding proteins. Once at the correct region, mRNA is then translated into new proteins. The translation along the axon is suggested to be performed by single ribosomes (monosomes). B) Locally synthesized beta-actin has been linked to the NGF mediated branching and locally synthesized ribosomal proteins were shown as essential for axon branching. The color code for cell elements is depicted in the legend.

1.7.2 Local translation and axon branching

The local translation is known to have a role in the branching of axons. At the axon branch point, an indication of the transnational machinery presence and the enrichment mRNA [25] encoding proteins such as beta-actin have been reported [31], presumably to synthesize required proteins to build up a branched axon [32]. In particular, data from chick embryonic sensory neurons suggest that NGF promoted axonal branching modulates the actin cytoskeleton by stimulation of local protein syntheses through phosphoinositide 3 kinase (PI3K) signaling detected as the accumulation of actin-related mRNA transcripts [25]. These axon branching sites were enriched with newly synthesized beta-actin important for axon arbor dynamics [31]. Furthermore, RNA granules were found to dock at the bases of newly formed branches and to invade into the stable branches as well [31].

Recently it was also reported that ribosomal protein mRNA is locally translated in axons and that these ribosomal proteins are then incorporated into existing ribosomes, possibly working to maintain the ribosome function [190], giving a possible scenario that ribosome itself may as well be locally remodeled. It was also shown that axonal ribosomal protein synthesis is essential for axon branching in-vivo [190]. Altogether these findings implicate that local synthesis plays an important role during axon branching (Figure 9).

Aim of thesis

Axon branching is an important event during neuron development and plasticity. Branching of axon allows to establish synaptic connections of one neuron cell with multiple targets, thus creating a more complex network of interneuronal connections and the topology of these connections allows the development of cognitive functions in the brain. Understanding the process of axon branching is a challenging task as several pathways have to work together in a highly coordinated fashion on an intracellular as well as intercellular level. The branching event is regulated by the binding of extracellular cues, presented by target neurons, to the membrane receptor in the axon shaft. Binding event triggers signaling pathways resulting in the activation of local protein synthesis, the remodeling of cytoskeleton and cell membrane, and the reorganization of organelles, all working together to raise and stabilize the new branch.

So far, research has been focusing on the different aspects of axon branching providing in-depth information about the individual events of cellular reorganization but lacking the ability to see them in full context within the cell. Due to the neuronal cells being extremely sensitive to stress and environmental cues, it has been difficult to apply many biological and biochemical approaches used in other cell types, but thanks to the development of in-situ cryo-electron tomography (cryo-ET) techniques in recent years it starts to be possible to observe the event of axon branching in a cellular context.

The aim of this thesis and my doctoral research is to provide a real view of the whole axon branching event by using in-situ cryo-ET to visualize the axon branches of primary mice neurons. My goal is to answer how the axon branch looks like, how are the cytoskeleton, organelles, and other components organized. Describe the structural difference between premature and mature axon branches. Elucidated the presence of translational machinery in axon branch, analyze how many ribosomes there are there and if they are present as polysomes or monosomes. Try to visualize the interaction between actin and microtubule cytoskeleton and the way how are microtubules entering the filopodia.

2. Results

2.1 Local orchestration of cellular machineries at axon branch by in-situ cryo-ET

Nedozralova H., Basnet N., Ibiricu I., Bodakuntla S., Biertuempfel Ch., Mizuno N., (2021). *Submitted*

This study presents a direct visualization of premature and mature axon branches of primary mouse neurons. The use of in-situ cellular cryo-ET allowed us to uncover the orchestration of the remodeling of organelles and the cytoskeleton at axon branch points. In the premature branch, filopodia protrusions were filled with aligned actin filaments while short pieces of unaligned actin filaments accumulated at the base of the filopodia. Upon maturation, microtubules and ER co-migrated into the preformed branch replacing actin and supporting its outgrowth, while the short actin filaments remained as membrane support. In both, premature and mature branches, mitochondria localized at the root of branches together with clusters of ribosomes, which are typically not present along axons. The visualization of ribosomes is the first direct evidence of local translation selectively taking place at axon branches, making them local regulation centers for axon development.

This study was conducted under the supervision of Dr. Naoko Mizuno within my doctoral project in which I was focusing on learning and establishing the in-vitro cryo-ET and primary neuron preparation techniques in our laboratory. For this study, I prepared the neuronal samples for cryo-ET including brain dissection, cell cultures, and vitrification. I collected and reconstructed tomograms and performed segmentation and data analysis together with my colleagues. Detailed author contributions are included in the attached article.

In situ cryo-electron tomography reveals local cellular machineries for axon branch development

Authors: Hana Nedozralova[1,2*], Nirakar Basnet[2*], Iosune Ibiricu[1], Satish Bodakuntla[2], Christian Biertümpfel[2], Naoko Mizuno[2,3**]

Affiliations:

[1] Department of Structural Cell Biology, Max Planck Institute of Biochemistry, Am Klopferspitz 18, D-82152 Martinsried, Germany

[2] Laboratory of Structural Cell Biology, National Heart, Lung, and Blood Institute, National Institutes of Health, 50 South Dr., Bethesda, MD, 20892, USA

[3] National Institute of Arthritis and Musculoskeletal and Skin Diseases, National Institutes of Health, 50 South Dr., Bethesda, MD, 20892, USA

*Equal contribution

**Correspondence and lead contact: naoko.mizuno@nih.gov

Abstract

Neurons are highly polarized cells forming an intricate network of dendrites and axons. They are shaped by the dynamic reorganization of cytoskeleton components and cellular organelles. Axon branching allows to form new paths and increases circuit complexity. However, our understanding of branch formation is sparse due to technical limitations. Using *in situ* cellular cryo-electron tomography on primary mouse neurons, we directly visualized the remodeling of organelles and cytoskeleton structures at axon branches. Strikingly, branched areas functioned as hotspots concentrating organelles to support dynamic activities. Unaligned actin filaments assembled at the base of premature branches and remained while filopodia diminished. Microtubules and ER co-migrated into preformed branches to support outgrowth together with accumulating compact ~500 nm mitochondria and locally clustered ribosomes. We obtained a roadmap of events and present the first direct evidence of local protein synthesis selectively taking place at axon branches, allowing to serve as unique control hubs for axon development and downstream neural network formation.

Introduction

The development of neurons with their extremely polarized structure and function is unique. Several long protrusions or neurites extend from the main cell body, the soma, where the nucleus is located. One of the protrusions develops into the axon, while the remaining protrusions develop into dendrites(Barnes and Polleux, 2009). Axons are functionally distinct from dendrites; dendrites receive signals from the axons of upstream cells via synaptic connections, whereas axons transmit signals to the dendrites of downstream cells. The molecular organization of the axon is uniquely suited to support local developmental processes, reflecting its specialized function. Within the backbone of the axon, microtubules form parallel bundles with their plus ends oriented towards the distal end of the axon(Baas et al., 1988; Baas and Lin, 2011; Stepanova et al., 2003; van Beuningen and Hoogenraad, 2016). An actin-rich growth cone at the tip of a growing axon probes extracellular signalling molecules to identify the synaptic target on dendrites of an adjacent neuron (Dent and Gertler, 2003; Lowery and Van Vactor, 2009).

The long distance from the soma to the tip of an axon indicates that there is a regulatory system controlling local molecules(Dalla Costa et al., 2021; Goldberg, 2003; Holt et al., 2019; Stiess et al., 2010). This regulatory system includes differential expression of and enrichment for proteins that are critical for the local development and regulation of axonal homeostasis. In particular, clusters of mRNAs localized within dendrites and axons(Cioni et al., 2018; Holt et al., 2019; Poon et al., 2006; Taylor et al., 2009) indicate local protein synthesis. The types of locally enriched mRNAs depend on the developmental stage and their location within a neuron(Cioni et al., 2018). During the growth phase, mRNAs coding for proteins of the synthesis machinery such as ribosome and for cytoskeletal components, which are needed to extend the cell, are found predominantly in the growth cones(Bassell et al., 1998; Zivraj et al., 2010). This type of regulation has also been observed in distal axons during regeneration(Gumy et al., 2010). However, despite the critical role of local translation in axons, actions of the translation process is not well understood. While there has been growing evidence for the presence of ribosomes along the axons (Koenig et al., 2000; Noma et al., 2017; Tcherkezian et al., 2010), there is no direct observation for protein synthesis that is accompanied by cytoskeleton and organelle re-organization and this has been a major challenge. Direct observations of the local axonal environment at a molecular level would aid in our understanding of neuronal growth and local reorganization.

During the development of the nervous system, axon branching serves to propagate signals to diverse regions of the nervous system(Kalil and Dent, 2014). Axon branching begins with the formation of actin-rich filopodia, short cellular protrusions, resulting from a signaling pathway that is induced by extracellular cues (Spillane et al., 2013; Tang and Kalil, 2005; Wang et al., 1999). Filopodia are the structural precursors of axon branches, and they develop to mature branches by the action of microtubules recruitment to the filopodia(Dent and Kalil, 2001; Gallo, 2011; Gallo, 2013). At the axon branch point, there is an enrichment of mRNAs(Spillane et al., 2013) encoding proteins such as beta-actin(Wong et al., 2017) that may be required to form the initial premature branched axon(Donnelly et al., 2013). Interestingly, it has also been reported that mitochondria are enriched at axon branching points(Spillane et al., 2013), which may provide energy (Sheng, 2017) and may adjust the Ca^{2+} concentration for signal transduction and branch morphogenesis(Hutchins and Kalil, 2008). While the information for those individual components are available, the orchestration that control the organized assembly of the protein synthesis machinery, organelles, and the cytoskeleton at axon branches are largely unknown.

To understand the organization of the key players for axon branching, we directly visualized the molecular organization of both premature and mature axon branching sites of mouse primary neurons by cryo-electron tomography (cryo-ET). We show the localization of small, ~500 nm mitochondria and short actin fragments at the branches. An intricate network of endoplasmic reticulum (ER) membranes was often found between microtubule bundles and mitochondria, with occasional interactions of the ER membrane with microtubules and mitochondria. The ER was generally accompanied by microtubules at the mature axon branch, indicating that ER migration is guided exclusively by microtubules. We further demonstrate the first direct observation of clusters of ribosomes accumulated preferentially at axon branches. In some cases, the ribosome clusters attached to meshed-planar ER membranes as ER tubes widened, spreading into the space made for the branching activity. Subtomogram-averaging and distance analysis indicated that the clustered ribosomes formed active polysomes. Isolated ribosomes, possibly monosomes (Su et al., 2016) synthesizing a small number of proteins, were also seen but only sparsely. This is in stark contrast to ribosomes found at synapses, where the majority of ribosome formed monosomes (Biever et al., 2020), highlighting the requirement for different types and amounts of newly synthesized proteins at various local environments within an axon. Our observations provide a comprehensive picture of the axon branching process.

Results

Structural analysis of branching axons

To visualize the molecular organization of axons and axon branches, we prepared primary neuronal cell cultures from hippocampus and thalamus explants of mouse embryos at stage E15.5. We observed 117 tomographic reconstructions of axons (Table 1) corresponding to ~260 µm in total length. Among these reconstructions, 43 axon branches contained microtubules in the branch site, indicating mature axon branches (a representative tomogram in Fig. 1, Fig. 2G, 2H, movie 1), and 20 nascent branch points had membrane protrusions made of actin-containing filopodia but lacked microtubule-reinforcements, indicating premature axon branches (representative tomogram in Fig. 2, movie 2). At mature branches, microtubules were tightly packed along the axon (Fig. 1B and C, arrows, also Fig. S6C, S6D [axon shaft]) but were looser at the branch points where sections of microtubules spread apart to enter the branch. In mature branches, short unorganized fragments of actin appeared to fill the space (Fig. 1C, light blue), which lacked other large organelles. In contrast, in premature branches, a dense parallel actin network formed filipodia perpendicular to the axis of the axon, followed by accumulation of short fragments of actins at the connection to the axon, while microtubules ran along the axon (Fig. 2C).

Organelle organization within axon branches

In addition to the unique organization of the cytoskeleton, branching sites showed localization of mitochondria. Out of the surveyed areas including 63 branches (43 mature and 20 premature) and 54 unbranched areas (44 axon shafts, 10 growth cones), we found 44 mitochondria among 23 mature and premature branches, with only 9 mitochondria along axon shafts, indicating a strong association of mitochondria with axon branches. Axon branch mitochondria had a median size of 500 nm (N=44) (Fig. 3A, 3B) This is in accordance with previous studies showing that axonal mitochondria are significantly smaller than dendritic mitochondria, which are about 4–13 µm (Delgado et al., 2019; Lewis et al., 2018; Popov et al., 2005). Mitochondrial size may be related to the local Ca^{2+} concentration or to presynaptic neurotransmitter release (Lewis et al., 2018), which then eventually lead to terminal axon branch formation. Branching axons accumulated several adjacent ~500 nm mitochondria and mitochondria undergoing fission instead of a single large mitochondrion (Fig. 3A, 1D, S1,).

The small mitochondria were often next to the ER network, and tubular ER was occasionally wrapped around the mitochondria, either loosely (Fig. 1D), or more tightly contacting to the wide surfaces of their membranes (Fig. 2A, 2B, S1A). The wrapping of the mitochondrion by the ER likely represents a stage of ER-facilitated fission of mitochondria(Lewis et al., 2016; Wu et al., 2017), but it appears the fission of mitochondria may not require wrapping by the ER (Fig. S1B, S1D). The ER at branching sites took on a planar mesh-like spreading form (Fig. 3B, 3D), while along the axon shaft it adopted a thin, tightly-packed tubular structure. The size of the ER ranged from thin tubes as small as 4 nm (Fig. S2A, S2D) to wide flat areas over 200 nm in width (Fig. 1F, 3D-G, 5G). ER membranes were often intertwined with microtubules (Fig. 1E and F, S2B) or occasionally tethered to the walls of microtubules (Fig. 3F, 3G, S2C). We found no density bridging microtubules and ER membranes, presumably due to the low signal-to-noise ratio, though ER-microtubule connections can be made by molecules like p180, CLIMP63, and kinectin(Cui-Wang et al., 2012; Farias et al., 2019; Shibata et al., 2010). Interestingly, we found that the ER propagation to axon branches (Fig. S3) occurred for 41 mature branches out of 43, but for only 3 out of 20 premature branches (Fig. 3C), indicating that the ER and microtubules co-migrated to the branching axon.

Ribosomes are in action at axon branch sites but not along the stable axon shaft

It is critical that neurons control their local environment due to their polarized and compartmentalized morphologies. To react rapidly to local requirements, specific areas of neurons may locally translate proteins(Holt et al., 2019); however, direct observation of localized protein synthesis is challenging. Our tomographic observations of axons provide direct evidence of ribosomes (Fig. 1, 2, 4, S4), particularly at axon branching sites where we found clusters of ribosomes in 29 of 63 axon branches. Ribosome clusters were found in 65% of premature axons and 37% of mature axons, indicating that ribosome clusters localized to developing axon branches. Ribosomes were also found in the filopodia at the growth cone (Fig. S6A, S6B). In contrast, we did not observe ribosomes along the tightly packed axon shafts. The visualization of ribosomes provides direct evidence that proteins are synthesized locally in the distal area of the axon, the site of dynamic cellular activities. The clustered, closely-packed ribosomes were close each other with a distance of 29.5 nm ± 3.4 nm (Fig. 4F, 4G), similar to the distance between adjacent ribosomes in a polysome (25–35 nm)(Brandt et al., 2010; Brandt et al., 2009; Mahamid et al., 2016). Therefore, clustered ribosomes likely represent a polysome in which ribosomes are arranged along a strand of mRNA, sequentially synthesizing protein. Short distances between ribosomes were observed consistently in axon branches with 70% of ribosomes falling within this short distance range (Fig. 4H, S4). This suggests that most of the ribosomes (in polysomes) in the branching axons were engaged actively in the polysome based translation, synthesizing the same types of proteins. However, 13 % of ribosomes were more than 50 nm from the nearest ribosome, too far to be considered a polysome. Although our observation does not offer to exclude if these ribosomes are in the resting state, not engaged in protein synthesis, it agrees with the notion that isolated ribosomes, termed monosomes, may be active in neurons, especially in synthesizing proteins that are only needed locally(Heyer and Moore, 2016; Holt et al., 2019). In contrast, the majority of ribosomes found at synapses are reported to form monosomes (Biever et al., 2020).

To understand the molecular topology of ribosomes in axon branches, we computationally extracted 1614 ribosomes and performed subtomogram averaging to 38.4 nm resolution (Fig. 5A, 5B, S7). The parameters of the orientation of the individual ribosomes derived from the analysis were plotted back to the original tomograms to visualize the polysome arrangement (Fig 5D, S5). The ribosomes formed a spiral, shape resembling to the reported polysome arrangements (Myasnikov et al., 2014) (Brandt et al., 2010; Mahamid et al., 2016), indicating that they were in a polysome aligned along a strand of RNA. Although most of the observed ER in axons had no bound ribosomes regardless of their morphology, we found a few instances in which ribosomes were attached to the surface of the planar area of the ER mesh network (Fig. 5E–G). The ER-bound ribosomes adopted a polysome-like organization forming a spiral similar to those in the cytoplasm. Those ribosomes synthesize transmembrane proteins, as suggested by a cell biological analysis, but they have not been observed by ultrastructural analyses(Merianda et al., 2009). When the ER formed a thin tubular shape, there were no ribosomes attached to the membrane surface, presumably due to the high curvature. This also explains the absence of ribosomes along the axon shaft.

Discussion

Molecular orchestration at the axon branch

Neuronal polarization is a unique cellular developmental process that is of critical importance. Direct observation of the process is central to gain an overview of the orchestration of the involved players, however it has been long missing. Here, using cryo-electron tomography of mouse primary hippocampal neurons and thalamus explants, we provide snapshots of mature and premature axon branches with maps of the molecular players. Axons are thin and filled with microtubule bundles, therefore, the space for cellular events is limited. That could be attributed to the fact that the mature axon is stable with a tightly packed robust cytoskeleton. At the axon branching point, the microtubule bundle bifurcates at the axon branching point, providing space for additional cellular components and dynamic cellular events. Indeed, at the branching point, we found actual evidence of ongoing cellular activities, including active mitochondria undergoing fission, active ribosomes, spreading of the ER, and fragments of actin filaments.

Our study presents observation for ribosome clusters locally concentrated at the branching point, providing direct proof of local protein synthesis at the axon branching point. In contrast, ribosomes were spread widely within less specialized cells, indicating that protein synthesis is tightly regulated within various regions of the axon. How these ribosomes are regulated and accumulate at the branching site, which is distant from the cell body in the soma, is unknown. Recently it was reported that ribosomal protein components and their coding mRNA are essential for axon branching (Shigeoka et al., 2019), giving a possible scenario that the ribosome itself may as well be remodeled locally. Identifying the steps in ribosome remodeling *in situ* at the branching point would be challenging, However, it would provide visual cues that could explain site-specific regulation of the molecular machinery that controls neuronal dynamics and the processes that lead to the establishment of a new structure like the axon branch.

Cytoskeleton remodeling

The mechanisms that drive the rearrangement of cytoskeleton elements, microtubules and actins, at the axon and the axon branch are poorly understood. Actins are found sparsely along the axon shaft outside of microtubule bundles. Actin rings form perpendicular to the axis of the axon (Vassilopoulos et al., 2019; Xu et al., 2013) and they are predominant actin structure along the axon, although technical limitations constrain our tomographic reconstruction of these rings. At the axon branching point, abundance of short, unaligned fragmented actins accumulated, accompanied by aligned actin filaments forming filopodia-based membrane protrusion. Upon maturation of the branch, actin density decreased at the branched axon, but fragmented actins still remain at the branching point. Where are these actins originated from? Interestingly, actins are indicated to be locally synthesized during the axon branch development (Spillane et al., 2013; Wong et al., 2017). Our data on the colocalization of short actins and active polysome support the notion and bring a hypothesis that ribosomes synthesize actin as part of the machinery to build up filopodia, which is the major central process for forming cell shape.

Stabilization of the microtubules within axons requires neuronal microtubule-associated proteins (MAPs) such as Tau, MAP7, and DCX (Baas et al., 2016; Chen et al., 1992; Moores et al., 2004; Tymanskyj and Ma, 2019), but at the axon branching point, dynamic remodeling of microtubules facilitates new branch formation (Yu et al., 2008). Among the factors involved in the microtubules at the axon branch, we have previously reported a novel microtubule nucleation factor SSNA1, which localizes at the axon branching site, promotes axon branching (Basnet et al., 2018). *In vitro*, we observed a surprising microtubule nucleationthat facilitates the creation of a lattice sharing microtubule branch. Axon branching correlates with the loss of microtubule-branching activity *in vitro*, leaving open questions about the remodeling of the microtubules during axon branching. While these interesting insights are to be addressed, the assessing the microtubule bundles by electron tomography was challenging because the branching axon was too thick to allow visualization of individual microtubules within bundles. Determining how branched cytoskeleton bundles are made will be an important area for future research on axonal development.

Furthermore, we observed the ER and microtubules comigrated to the axon branching point, while the ER was rarely observed in the premature branches. The ER membrane may serve as a lipid source for the growing plasma membrane of the branching axon. The comigrating ER and microtubules may cooperate to grow stably towards branching axons, as they do in the general axon(Farias et al., 2019).

Implications of axon branching in neural network formation

Our study provides a direct close-up view of axon branches that have a remarkable local concentration of cellular machineries, which are critical for axon development and outgrowth. This picture of the branches presents a contrast to the stable structure of the axon shaft, which serves as a rail for the transport of diverse signals and materials. It is intriguing to find a synthesis hub supporting dynamic cellular activities within the confined space of axon branches. Future studies will address the mechanisms by which the cellular machineries are recruited to and regulated at the axon branches. The process of axon branches is critical for neural network formation during the development of the nervous system. Moreover, it plays a critical role in neural homeostasis throughout the life cycle of the brain, including axon pruning during the maturation of the brain and axon regeneration after brain injury. Elucidating the mechanisms governing the formation of axon branches will not only provide insights into fundamental neuronal processes but also be the basis for understanding of neuronal circuit formation and function.

Acknowledgements

We thank Daniel del Toro and Rüdiger Klein (Max Planck Institute of Neurobiology, Germany) for giving us advices for neuronal culture, Elena Conti, Wolfgang Baumeister, particularly, Juergen Plitzko, Ben Engel, and Marion Jasnin (Max Planck Institute of Biochemistry, Germany) for their advice and help in the initial stage of the project. The data was collected at the cryo-EM core facility at Max Planck Institute of Biochemistry, Germany and MICEF at the National Institutes of Health, USA. NM acknowledges the Max Planck Society, Boehringer Ingelheim Foundation Plus 3 Program, and the European Research Council (ERC-CoG, 724209), and the Intramural Research Program of the National Heart Lung and Blood Institute, and the National Institute of Arthritis and Musculoskeletal and Skin Diseases of National Institutes of Health, USA, for funding. NM is a recipient of the EMBO Young Investigator award.

Declaration of interests

The authors declare no competing interests.

Methods

Neuron cultures on EM grids

Quantifoil (R1/4 Au200, MultiA Au300, R1.2/1.3 Au300) gold EM grids were plasma cleaned for 40s and sterilized by UV light for 30 min. Grids were then coated with 1 mg/ml poly-L-lysine in 0.1 M borate buffer (Sigma-Aldrich) overnight, then washed three times in PBS and coated with laminin (Sigma-Aldrich) for 4 hours (5 μg/ml for suspension culture, 20 μg/ml for explants). Grids were washed three times with PBS and covered with neurobasal/B27 medium and incubated at 37 °C.

Primary embryonic mouse neurons were prepared as either dissociated hippocampal cultures or as a tissue explants from thalamus. Neurons were prepared from embryonic day 15.5 (E15.5) mice. Dissected hippocampi were placed into cold HBSS (HBSS supplemented with 1x HEPES, 1x Glutamax, 1x Pen/Strep) media treated with trypsin incubating at 37 °C for 16 min followed by washing with HBSS with FBS and then neurobasal/B27 medium followed by trituration. Thalamus tissue was placed into neurobasal/B27 medium and explants were prepared by cutting thalamus into small pieces which were incubated at 37 °C for 30 min. 11 of the observed cryo-EM images of hippocampus neurons were from the effort of transducing microtubule binding protein SSNA1. The transduction rate was low and furthermore microtubule organization was not assessed in this study. The other components did not show any notable differences to the extent of our experimental evaluation. The dissociated cells were plated on coated EM grids at a concentration 150,000 cell/ml and incubated at 37 °C in 5% CO2. For the explants, they were placed on EM grids covered in neurobasal/B27 medium. The culture medium was NeuroBasal (Invitrogen) supplemented with 1x Glutamax, 1x B27 serum and 1x Pen/Strep (neurobasal/B27 medium). Half of culture media was changed at DIV 1 (day in vitro). Cell cultures were grown for 6-10 days. Then EM grids with neuron cultures were manually vitrified in liquid ethane using home-made plunger or vitrobot (ThermoFisher Scientific).

Cryo-ET data collection and processing

Cryo-electron tomography data were collected on Titan Krios (ThermoFisher Scientific) with a Gatan Quantum 967 LS and K2 Summit direct detector with an option of phase-plate with an acceleration voltage of 300 kV. 63 tilt-series were collected using phase-plate option and 54 tilt-series were collected without phase-plate with defocus range between -3.5 µm to -5 µm. Tilt series were collected -60° to 60° with 2° angular increment using does symmetric scheme using Serial-EM software (Hagen et al., 2017). The total electron dose was around 90 e-/Å and the nominal magnification was 26,000 x, corresponding to the final pixel size of 5.46 Å. Images were taken in super-resolution mode as ten-frame movies and the movie frames were aligned and combined and dose filtered using in-house frame alignment software with implemented MotionCor2. A total of 117 tilt-series were assessed for this study including 52 tilt-series of thalamus explants and 65 tilt-series of hippocampus neurons.

Individual images of the collected tilt-series were assessed manually and low-quality images at the high tilt angle were removed from the dataset. Tilt-series were filtered according to the cumulative radiation dose (Grant and Grigorieff, 2015) and aligned on the basis of the patch tracking algorithm using the IMOD ETOMO package (Kremer et al., 1996). Tomograms were reconstructed from aligned stacks using weighted back-projection in IMOD. Tomograms were further 4x binned, resulting in pixel sizes of 21.8 Å. Tomograms were denoised by edge enhancing diffusion (bnad command in Bsoft(Heymann et al., 2008)).

Tomogram segmentation

Tomograms were manually segmented using Amira software. Additionally when applicable, membranes were segmented automatically using deconvolution filtering(Tegunov and Cramer, 2019) and a tool for membrane segmentation TomoSegMemTV(Martinez-Sanchez et al., 2014). Microtubules were segmented manually in IMOD software. Measurements of mitochondria length (44 mitochondria) and ER tube diameter (19 for thinnest ER measurements and 29 for ER tube diameter) were measured manually in IMOD. The data obtained were represented using box and whiskers graph, where each dot represents measurement for individual mitochondrion or ER and the horizontal line in the graph indicates the median of the distribution. Data was plotted using Prism software.

Subtomogram averaging of ribosomes and distance analysis

1614 ribosome particles from 11 unbinned tomograms were picked using IMOD 3dmod software. The picked coordinates were then transferred into Dynamo a subtomogram averaging software package (Castano-Diez et al., 2012) and the ribosome averages were calculated as follows. The initial template used for the alignment was low pass filtered to >100 Å (EMDB-5224). At this resolution, only general shape and size of the ribosome was visible. The initial alignment was done using standard global settings from Dynamo and the search space and angular increments were then gradually decreased for subsequent refinement. During refinement, the subtomograms were split into odd and even half-sets and Dynamo's adaptive bandpass filtering was performed in order to avoid overfitting and estimate the attained resolution. The attained resolution was estimated by comparing the FSC of separately computed averages from odd and even half-sets. A bandpass filter was then applied in next iteration based on this estimation. Distances between ribosome particles were calculated from refined coordinates from subtomogram averaging runs using Python3 (numpy and scipy libraries). For each particle, the closest neighboring distance was plotted into the distance distribution histogram and fitted with non-linear Gaussian curve in Prism software. The orientation of ribosomes was assessed by placing reconstructed ribosome volume into tomograms in Chimera using coordinates and alignment parameters derived from subtomogram averaging.

References:

Baas, P.W., J.S. Deitch, M.M. Black, and G.A. Banker. 1988. Polarity orientation of microtubules in hippocampal neurons: uniformity in the axon and nonuniformity in the dendrite. *Proc Natl Acad Sci U S A*. 85:8335-8339.

Baas, P.W., and S. Lin. 2011. Hooks and comets: The story of microtubule polarity orientation in the neuron. *Dev Neurobiol*. 71:403-418.

Baas, P.W., A.N. Rao, A.J. Matamoros, and L. Leo. 2016. Stability properties of neuronal microtubules. *Cytoskeleton (Hoboken)*. 73:442-460.

Barnes, A.P., and F. Polleux. 2009. Establishment of axon-dendrite polarity in developing neurons. *Annu Rev Neurosci*. 32:347-381.

Basnet, N., H. Nedozralova, A.H. Crevenna, S. Bodakuntla, T. Schlichthaerle, M. Taschner, G. Cardone, C. Janke, R. Jungmann, M.M. Magiera, C. Biertümpfel, and N. Mizuno. 2018. Direct induction of microtubule branching by microtubule nucleation factor SSNA1. *Nature Cell Biology*. 20:1172-1180.

Bassell, G.J., H. Zhang, A.L. Byrd, A.M. Femino, R.H. Singer, K.L. Taneja, L.M. Lifshitz, I.M. Herman, and K.S. Kosik. 1998. Sorting of beta-actin mRNA and protein to neurites and growth cones in culture. *J Neurosci*. 18:251-265.

Biever, A., C. Glock, G. Tushev, E. Ciirdaeva, T. Dalmay, J.D. Langer, and E.M. Schuman. 2020. Monosomes actively translate synaptic mRNAs in neuronal processes. *Science*. 367.

Brandt, F., L.A. Carlson, F.U. Hartl, W. Baumeister, and K. Grunewald. 2010. The three-dimensional organization of polyribosomes in intact human cells. *Mol Cell*. 39:560-569.

Brandt, F., S.A. Etchells, J.O. Ortiz, A.H. Elcock, F.U. Hartl, and W. Baumeister. 2009. The native 3D organization of bacterial polysomes. *Cell*. 136:261-271.

Chen, J., Y. Kanai, N.J. Cowan, and N. Hirokawa. 1992. Projection domains of MAP2 and tau determine spacings between microtubules in dendrites and axons. *Nature*. 360:674-677.

Cioni, J.M., M. Koppers, and C.E. Holt. 2018. Molecular control of local translation in axon development and maintenance. *Curr Opin Neurobiol*. 51:86-94.

Cui-Wang, T., C. Hanus, T. Cui, T. Helton, J. Bourne, D. Watson, K.M. Harris, and M.D. Ehlers. 2012. Local zones of endoplasmic reticulum complexity confine cargo in neuronal dendrites. *Cell*. 148:309-321.

Dalla Costa, I., C.N. Buchanan, M.D. Zdradzinski, P.K. Sahoo, T.P. Smith, E. Thames, A.N. Kar, and J.L. Twiss. 2021. The functional organization of axonal mRNA transport and translation. *Nat Rev Neurosci*. 22:77-91.

Delgado, T., R.S. Petralia, D.W. Freeman, M. Sedlacek, Y.X. Wang, S.D. Brenowitz, S.H. Sheu, J.W. Gu, D. Kapogiannis, M.P. Mattson, and P.J. Yao. 2019. Comparing 3D ultrastructure of presynaptic and postsynaptic mitochondria. *Biol Open*. 8.

Dent, E.W., and F.B. Gertler. 2003. Cytoskeletal dynamics and transport in growth cone motility and axon guidance. *Neuron*. 40:209-227.

Dent, E.W., and K. Kalil. 2001. Axon branching requires interactions between dynamic microtubules and actin filaments. *J Neurosci*. 21:9757-9769.

Donnelly, C.J., M. Park, M. Spillane, S. Yoo, A. Pacheco, C. Gomes, D. Vuppalanchi, M. McDonald, H.H. Kim, T.T. Merianda, G. Gallo, and J.L. Twiss. 2013. Axonally synthesized beta-actin and GAP-43 proteins support distinct modes of axonal growth. *J Neurosci*. 33:3311-3322.

Farias, G.G., A. Freal, E. Tortosa, R. Stucchi, X. Pan, S. Portegies, L. Will, M. Altelaar, and C.C. Hoogenraad. 2019. Feedback-Driven Mechanisms between Microtubules and the Endoplasmic Reticulum Instruct Neuronal Polarity. *Neuron*. 102:184-201 e188.

Gallo, G. 2011. The cytoskeletal and signaling mechanisms of axon collateral branching. *Dev Neurobiol*. 71:201-220.

Gallo, G. 2013. Mechanisms underlying the initiation and dynamics of neuronal filopodia: from neurite formation to synaptogenesis. *Int Rev Cell Mol Biol*. 301:95-156.

Goldberg, J.L. 2003. How does an axon grow? *Genes Dev*. 17:941-958.

Grant, T., and N. Grigorieff. 2015. Measuring the optimal exposure for single particle cryo-EM using a 2.6 A reconstruction of rotavirus VP6. *Elife*. 4:e06980.

Gumy, L.F., C.L. Tan, and J.W. Fawcett. 2010. The role of local protein synthesis and degradation in axon regeneration. *Exp Neurol*. 223:28-37.

Hagen, W.J.H., W. Wan, and J.A.G. Briggs. 2017. Implementation of a cryo-electron tomography tilt-scheme optimized for high resolution subtomogram averaging. *J Struct Biol*. 197:191-198.

Heyer, E.E., and M.J. Moore. 2016. Redefining the Translational Status of 80S Monosomes. *Cell*. 164:757-769.

Heymann, J.B., G. Cardone, D.C. Winkler, and A.C. Steven. 2008. Computational resources for cryo-electron tomography in Bsoft. *J Struct Biol*. 161:232-242.

Holt, C.E., K.C. Martin, and E.M. Schuman. 2019. Local translation in neurons: visualization and function. *Nat Struct Mol Biol*. 26:557-566.

Hutchins, B.I., and K. Kalil. 2008. Differential outgrowth of axons and their branches is regulated by localized calcium transients. *J Neurosci*. 28:143-153.

Kalil, K., and E.W. Dent. 2014. Branch management: mechanisms of axon branching in the developing vertebrate CNS. *Nat Rev Neurosci*. 15:7-18.

Koenig, E., R. Martin, M. Titmus, and J.R. Sotelo-Silveira. 2000. Cryptic peripheral ribosomal domains distributed intermittently along mammalian myelinated axons. *J Neurosci*. 20:8390-8400.

Kremer, J.R., D.N. Mastronarde, and J.R. McIntosh. 1996. Computer visualization of three-dimensional image data using IMOD. *J Struct Biol*. 116:71-76.

Lewis, S.C., L.F. Uchiyama, and J. Nunnari. 2016. ER-mitochondria contacts couple mtDNA synthesis with mitochondrial division in human cells. *Science*. 353:aaf5549.

Lewis, T.L., Jr., S.K. Kwon, A. Lee, R. Shaw, and F. Polleux. 2018. MFF-dependent mitochondrial fission regulates presynaptic release and axon branching by limiting axonal mitochondria size. *Nat Commun*. 9:5008.

Lowery, L.A., and D. Van Vactor. 2009. The trip of the tip: understanding the growth cone machinery. *Nat Rev Mol Cell Biol*. 10:332-343.

Mahamid, J., S. Pfeffer, M. Schaffer, E. Villa, R. Danev, L.K. Cuellar, F. Forster, A.A. Hyman, J.M. Plitzko, and W. Baumeister. 2016. Visualizing the molecular sociology at the HeLa cell nuclear periphery. *Science*. 351:969-972.

Martinez-Sanchez, A., I. Garcia, S. Asano, V. Lucic, and J.J. Fernandez. 2014. Robust membrane detection based on tensor voting for electron tomography. *J Struct Biol*. 186:49-61.

Merianda, T.T., A.C. Lin, J.S. Lam, D. Vuppalanchi, D.E. Willis, N. Karin, C.E. Holt, and J.L. Twiss. 2009. A functional equivalent of endoplasmic reticulum and Golgi in axons for secretion of locally synthesized proteins. *Mol Cell Neurosci*. 40:128-142.

Moores, C.A., M. Perderiset, F. Francis, J. Chelly, A. Houdusse, and R.A. Milligan. 2004. Mechanism of microtubule stabilization by doublecortin. *Mol Cell*. 14:833-839.

Myasnikov, A.G., Z.A. Afonina, J.F. Menetret, V.A. Shirokov, A.S. Spirin, and B.P. Klaholz. 2014. The molecular structure of the left-handed supra-molecular helix of eukaryotic polyribosomes. *Nat Commun*. 5:5294.

Noma, K., A. Goncharov, M.H. Ellisman, and Y. Jin. 2017. Microtubule-dependent ribosome localization in C. elegans neurons. *Elife*. 6.

Poon, M.M., S.H. Choi, C.A. Jamieson, D.H. Geschwind, and K.C. Martin. 2006. Identification of process-localized mRNAs from cultured rodent hippocampal neurons. *J Neurosci*. 26:13390-13399.

Popov, V., N.I. Medvedev, H.A. Davies, and M.G. Stewart. 2005. Mitochondria form a filamentous reticular network in hippocampal dendrites but are present as discrete bodies in axons: a three-dimensional ultrastructural study. *J Comp Neurol*. 492:50-65.

Sheng, Z.H. 2017. The Interplay of Axonal Energy Homeostasis and Mitochondrial Trafficking and Anchoring. *Trends Cell Biol*. 27:403-416.

Shibata, Y., T. Shemesh, W.A. Prinz, A.F. Palazzo, M.M. Kozlov, and T.A. Rapoport. 2010. Mechanisms determining the morphology of the peripheral ER. *Cell*. 143:774-788.

Shigeoka, T., M. Koppers, H.H. Wong, J.Q. Lin, R. Cagnetta, A. Dwivedy, J. de Freitas Nascimento, F.W. van Tartwijk, F. Strohl, J.M. Cioni, J. Schaeffer, M. Carrington, C.F. Kaminski, H. Jung, W.A. Harris, and C.E. Holt. 2019. On-Site Ribosome Remodeling by Locally Synthesized Ribosomal Proteins in Axons. *Cell Rep*. 29:3605-3619 e3610.

Spillane, M., A. Ketschek, T.T. Merianda, J.L. Twiss, and G. Gallo. 2013. Mitochondria coordinate sites of axon branching through localized intra-axonal protein synthesis. *Cell Rep*. 5:1564-1575.

Stepanova, T., J. Slemmer, C.C. Hoogenraad, G. Lansbergen, B. Dortland, C.I. De Zeeuw, F. Grosveld, G. van Cappellen, A. Akhmanova, and N. Galjart. 2003. Visualization of microtubule growth in cultured neurons via the use of EB3-GFP (end-binding protein 3-green fluorescent protein). *J Neurosci*. 23:2655-2664.

Stiess, M., N. Maghelli, L.C. Kapitein, S. Gomis-Ruth, M. Wilsch-Brauninger, C.C. Hoogenraad, I.M. Tolic-Norrelykke, and F. Bradke. 2010. Axon extension occurs independently of centrosomal microtubule nucleation. *Science*. 327:704-707.

Su, Y., W. Xia, J. Li, T. Walz, M.J. Humphries, D. Vestweber, C. Cabanas, C. Lu, and T.A. Springer. 2016. Relating conformation to function in integrin alpha5beta1. *Proc Natl Acad Sci U S A*. 113:E3872-3881.

Tang, F., and K. Kalil. 2005. Netrin-1 induces axon branching in developing cortical neurons by frequency-dependent calcium signaling pathways. *J Neurosci*. 25:6702-6715.

Taylor, A.M., N.C. Berchtold, V.M. Perreau, C.H. Tu, N. Li Jeon, and C.W. Cotman. 2009. Axonal mRNA in uninjured and regenerating cortical mammalian axons. *J Neurosci*. 29:4697-4707.

Tcherkezian, J., P.A. Brittis, F. Thomas, P.P. Roux, and J.G. Flanagan. 2010. Transmembrane receptor DCC associates with protein synthesis machinery and regulates translation. *Cell*. 141:632-644.

Tegunov, D., and P. Cramer. 2019. Real-time cryo-electron microscopy data preprocessing with Warp. *Nat Methods*. 16:1146-1152.

Tymanskyj, S.R., and L. Ma. 2019. MAP7 Prevents Axonal Branch Retraction by Creating a Stable Microtubule Boundary to Rescue Polymerization. *J Neurosci*. 39:7118-7131.

van Beuningen, S.F., and C.C. Hoogenraad. 2016. Neuronal polarity: remodeling microtubule organization. *Curr Opin Neurobiol*. 39:1-7.

Vassilopoulos, S., S. Gibaud, A. Jimenez, G. Caillol, and C. Leterrier. 2019. Ultrastructure of the axonal periodic scaffold reveals a braid-like organization of actin rings. *Nat Commun*. 10:5803.

Wang, K.H., K. Brose, D. Arnott, T. Kidd, C.S. Goodman, W. Henzel, and M. Tessier-Lavigne. 1999. Biochemical purification of a mammalian slit protein as a positive regulator of sensory axon elongation and branching. *Cell*. 96:771-784.

Wong, H.H., J.Q. Lin, F. Strohl, C.G. Roque, J.M. Cioni, R. Cagnetta, B. Turner-Bridger, R.F. Laine, W.A. Harris, C.F. Kaminski, and C.E. Holt. 2017. RNA Docking and Local Translation Regulate Site-Specific Axon Remodeling In Vivo. *Neuron*. 95:852-868 e858.

Wu, Y., C. Whiteus, C.S. Xu, K.J. Hayworth, R.J. Weinberg, H.F. Hess, and P. De Camilli. 2017. Contacts between the endoplasmic reticulum and other membranes in neurons. *Proc Natl Acad Sci U S A*. 114:E4859-E4867.

Xu, K., G. Zhong, and X. Zhuang. 2013. Actin, spectrin, and associated proteins form a periodic cytoskeletal structure in axons. *Science*. 339:452-456.

Yu, W., L. Qiang, J.M. Solowska, A. Karabay, S. Korulu, and P.W. Baas. 2008. The microtubule-severing proteins spastin and katanin participate differently in the formation of axonal branches. *Mol Biol Cell*. 19:1485-1498.

Zivraj, K.H., Y.C. Tung, M. Piper, L. Gumy, J.W. Fawcett, G.S. Yeo, and C.E. Holt. 2010. Subcellular profiling reveals distinct and developmentally regulated repertoire of growth cone mRNAs. *J Neurosci*. 30:15464-15478.

Figures

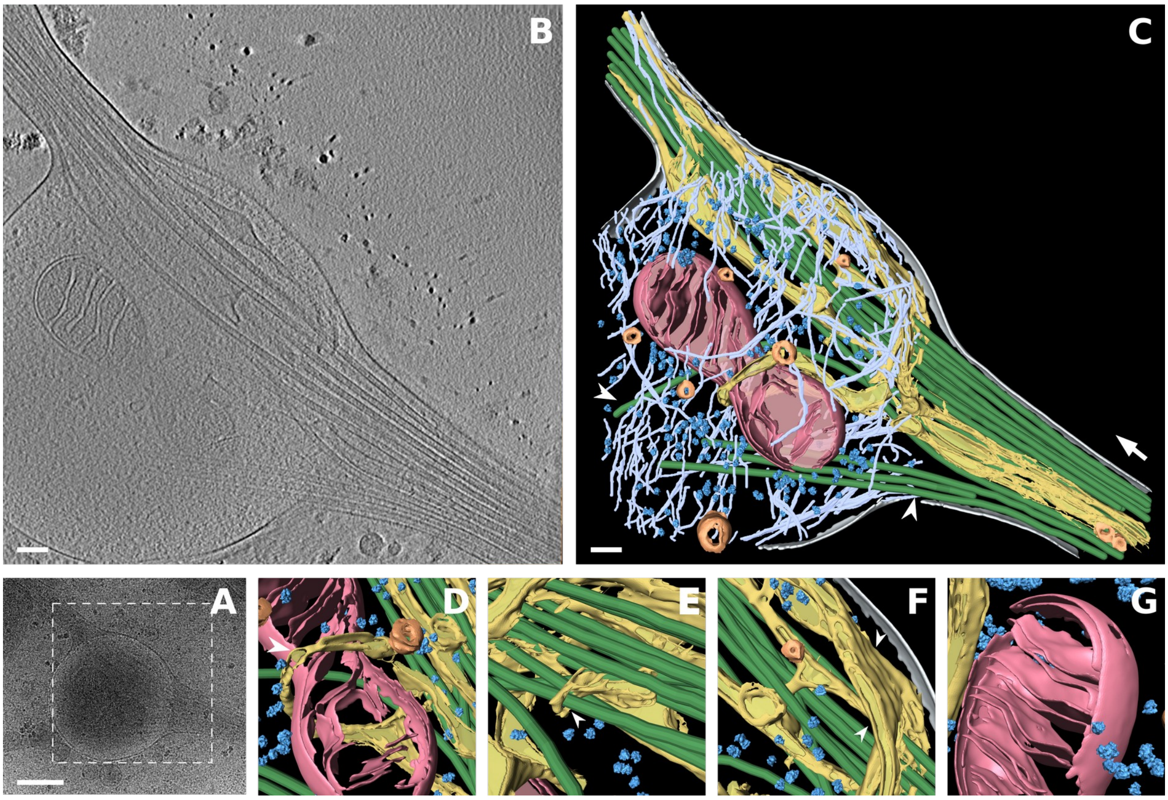

Figure 1. Cryo-electron tomogram of mature axon branch.
A) Low magnification view at a mature axon branching site. White box depicts area of tomographic data collection shown in B. B) A slice of the tomogram reconstruction of the branching site. C) Segmentation of the 430-nm thickness tomographic volume from B. Colour code: grey – cellular membrane, green – microtubules, light blue – actin, pink – mitochondria, yellow – ER, dark blue – ribosomes, orange – vesicles, White arrow shows direction of bundled microtubules following axon growth, white arrowheads depict microtubules entering the branch. D)-G) Zoom in views of segmented volume, D) ER wrapping around mitochondrion (white arrowhead), E) ER wraps around microtubule, F) ER forms a flat sheet (white arrowhead), G) ribosomes in the vicinity of mitochondrion. Scale bars: A, 500 nm; B, C 100 nm.

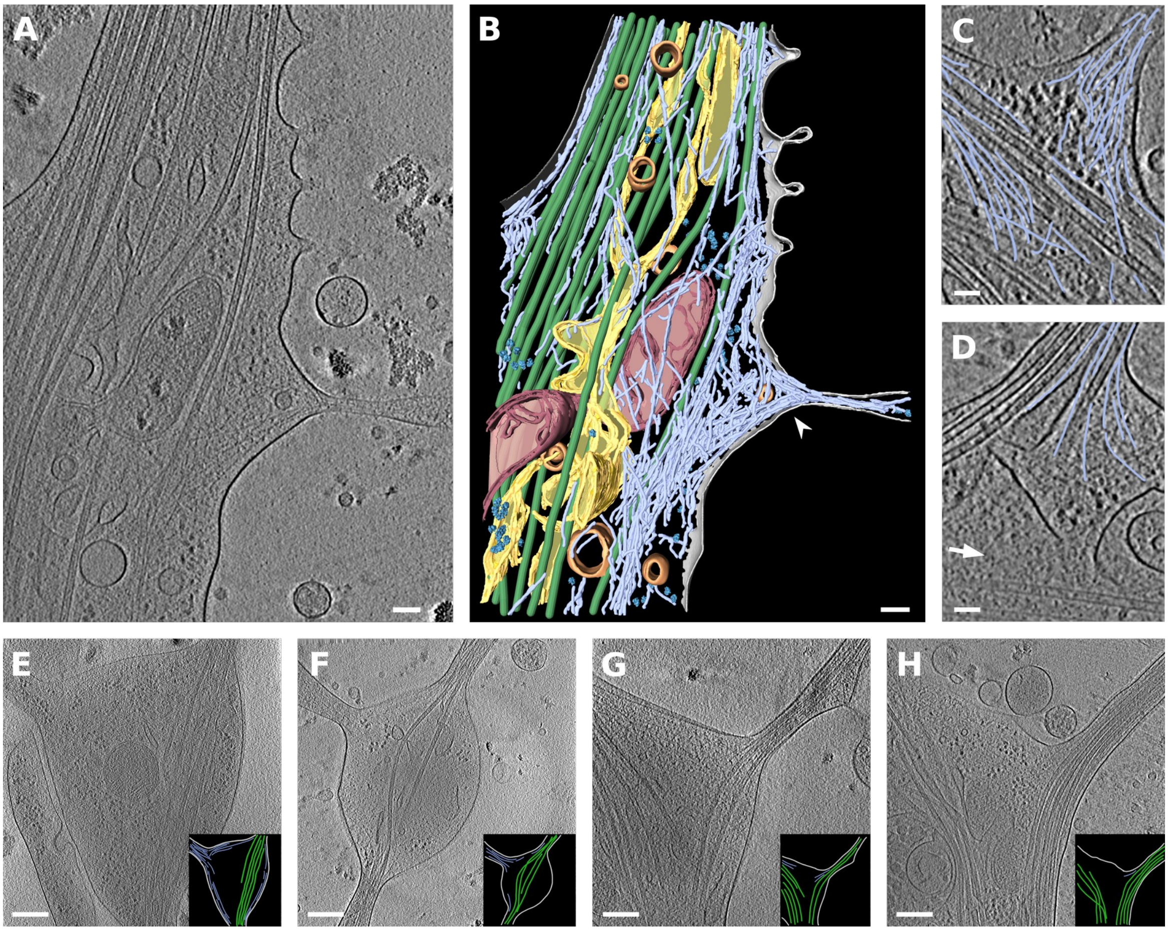

Figure 2. Cryo-electron tomogram of premature axon branch.
A) Slice from tomogram reconstruction of premature branch. B) 353-nm segmented volume of tomogram A. Color code – cellular membrane – grey, microtubules – green, mitochondria - pink, ER – yellow, ribosomes – dark blue, vesicles – orange, actin – light blue. White arrowhead depicts filopodium filled with actin. C) and D) An example of actin arrangement in branch, tomographic slice with traced actin (light blue). C) Actin in the filopodia of premature branch. D) Actin in mature branch, white arrow shows direction of main axon growth. E)-H) A slices from axon branch tomograms. E) and F) premature branches, G) and H) mature branches. Black inserts depict the traced cell membrane – grey, microtubules – green and actin – light blue. Scale bars: A,B 100 nm, C,D 50 nm, E-H – 250 nm.

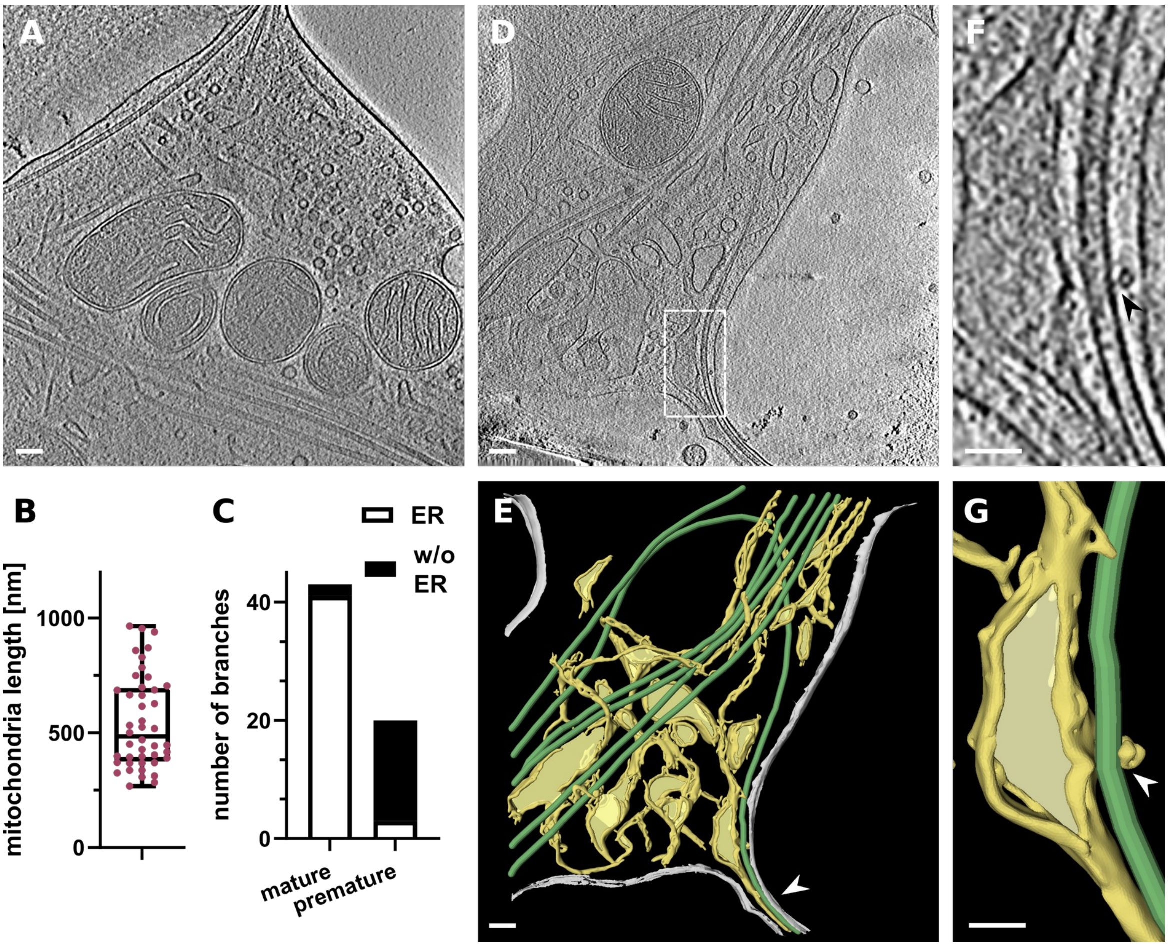
A
D
F
B
C
E
G
mitochondria length [nm]
1000
500
0
number of branches
40
20
0
ER
w/o ER
mature
premature

Figure 3. Mitochondria and ER in axon branch.

A) Tomographic slice of mitochondria enriched in axon branching site. B) Analysis of mitochondria length. Median length: 500.1 nm N=44. C) Bar graph depicting number of branches with and without ER in daughter branch for mature branches with MT and for premature branches with only actin. D) Slice from tomogram showing different kind of ER – thin tubes and flat sheets. White square depicts area in F and G. E) Segmented tomogram D, color code: grey – cell membrane, green – microtubules, yellow –ER, white arrowhead shows ER in branch together with microtubules. F) ER – MT contact (black arrowhead). G) Segmentation of ER tube wrapping around microtubule (white arrowhead). Scale bar: A,D,E 100 nm, F,G = 50 nm.

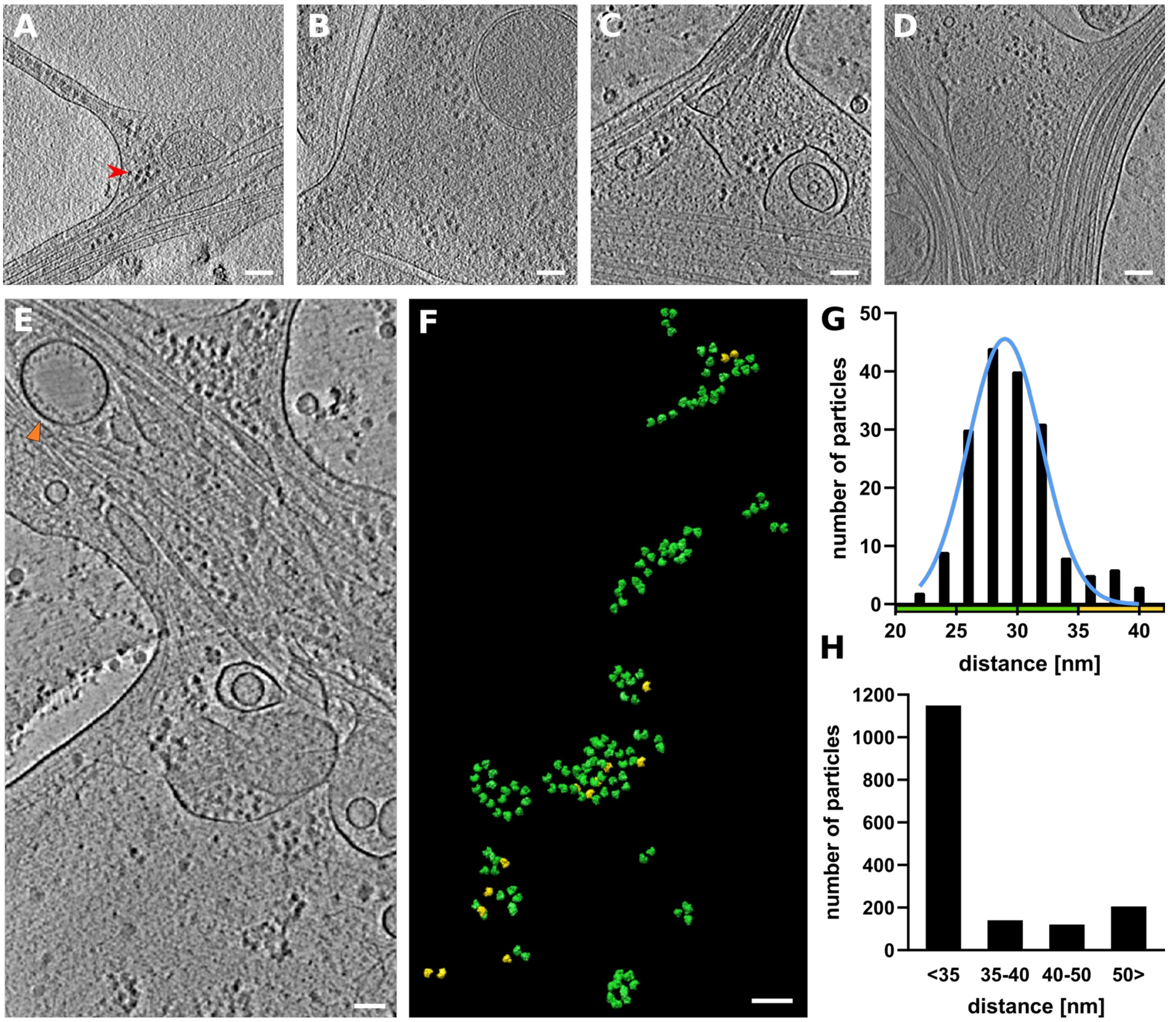
A
B
C
D
E
F
G
50
40
30
20
10
0
number of particles
20
25
30
35
40
distance [nm]
H
1200
1000
800
600
400
200
0
number of particles
<35
35-40
40-50
50>
distance [nm]

Figure 4. Ribosome clusters at axon branch.

A)-D) Examples of clustered ribosomes in axon branches. A) and B) Ribosomes filling premature branch. Red arrowhead depicts an example of ribosome density. C) and D) Ribosomes present at mature branch site. E)-G) Analysis of distance between ribosomes. E) Slice of analyzed tomogram. (Of interest: Orange triangle shows vesicle with inner membrane densities) F) Distribution of ribosomes in the 3D volume of tomogram in E, color code by distance between ribosome particle coordinates: green < 35 nm, yellow > 35 nm. G) Distance distribution of ribosome particles in tomogram E, graph shows particles with closest neighbor distance value bellow 40 nm, N=178. H) Cumulative distance distribution for all analyzed ribosomes. N=1614. Scale bar: A-F = 100 nm.

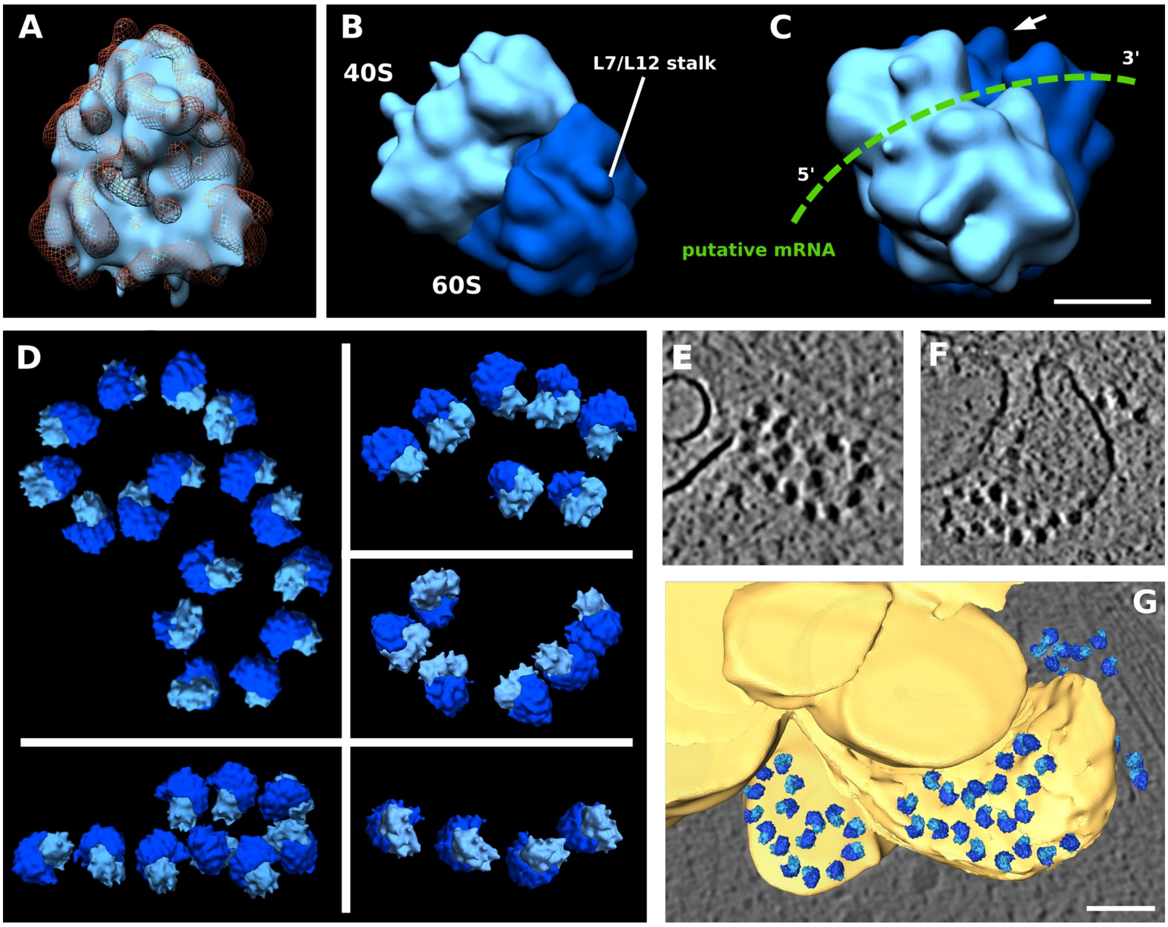

Figure 5. Ribosome reconstruction and polysome orientation.

A) Reconstructed ribosome (light blue) fitted into the 80S ribosome volume from database (orange mesh, EMD-3420). B) Reconstructed ribosome volume with depicted 40S (light blue) and 60S (dark blue) subunits and L7/L12 stalk. C) Rotated view of ribosome from B, Putative path of mRNA depicted inn green, White arrow shows L7/L12 stalk. D) Polysomes found in various tomograms. E)-G) Ribosomes on the surface of ER. E), F) slice from tomogram, G) Segmented view for E and F. Scale bar: C = 10 nm, G = 100 nm.

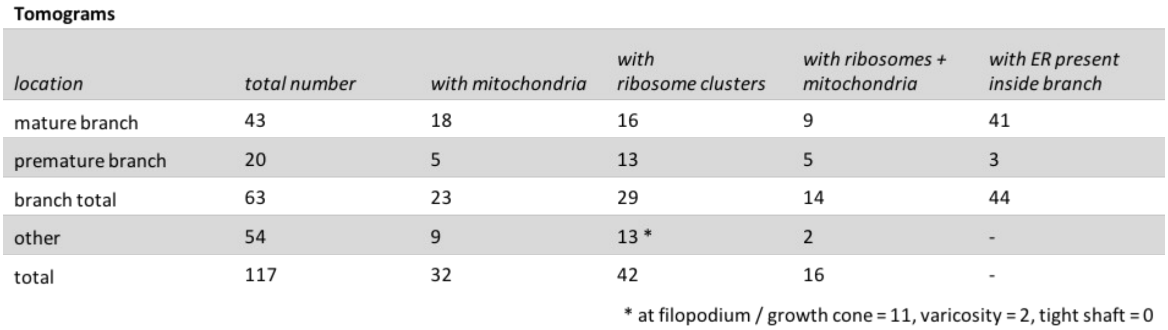

Tomograms

location	*total number*	*with mitochondria*	*with ribosome clusters*	*with ribosomes + mitochondria*	*with ER present inside branch*
mature branch	43	18	16	9	41
premature branch	20	5	13	5	3
branch total	63	23	29	14	44
other	54	9	13 *	2	-
total	117	32	42	16	-

* at filopodium / growth cone = 11, varicosity = 2, tight shaft = 0

Table 1. Numeric summary of analysed tomograms.

Showing localization of tomographic data collection site within axon and individual cellular features observed at the given locality.

Movie 1. Reconstructed tomogram of axon branch.

Slice view through 430-nm thick tomographic volume in Figure 1 and segmentation. Colour code: grey – cellular membrane, green – microtubules, light blue – actin, pink – mitochondria, yellow – ER, dark blue – ribosomes, orange – vesicles. In final slice, upper layer of segmented actin was removed for better clarity.

Supplementary material

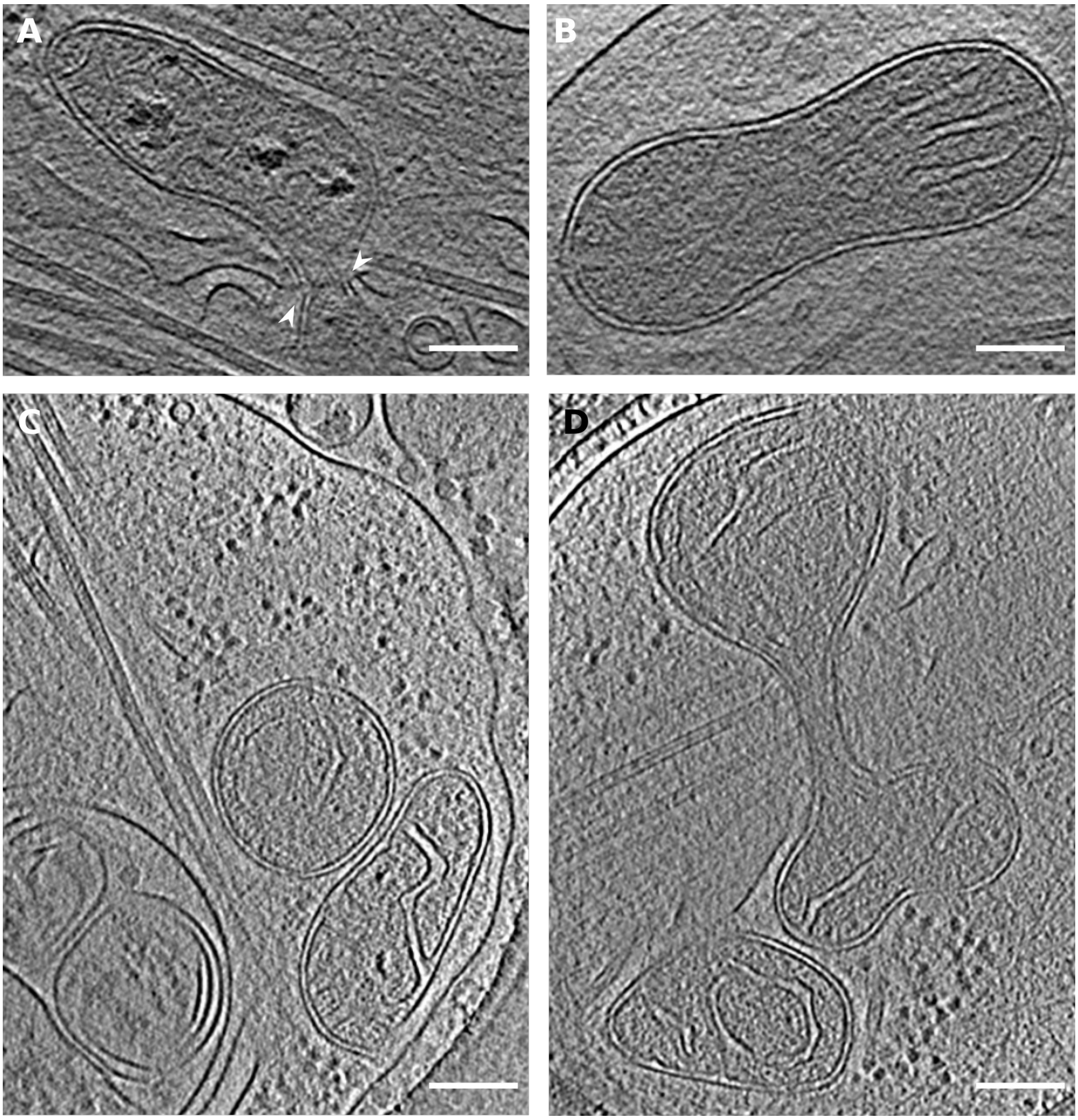

Figure S1. Examples of mitochondria found at axon branch.
A) Mitochondrion undergoing fission facilitated by ER. White arrowheads depict ER pinching at mitochondria membrane. B) Possibly dividing mitochondrion. C) Examples of different sizes of mitochondria. D) Mitochondrion presumably undergoing fission. Scale bar: A-D = 100 nm.

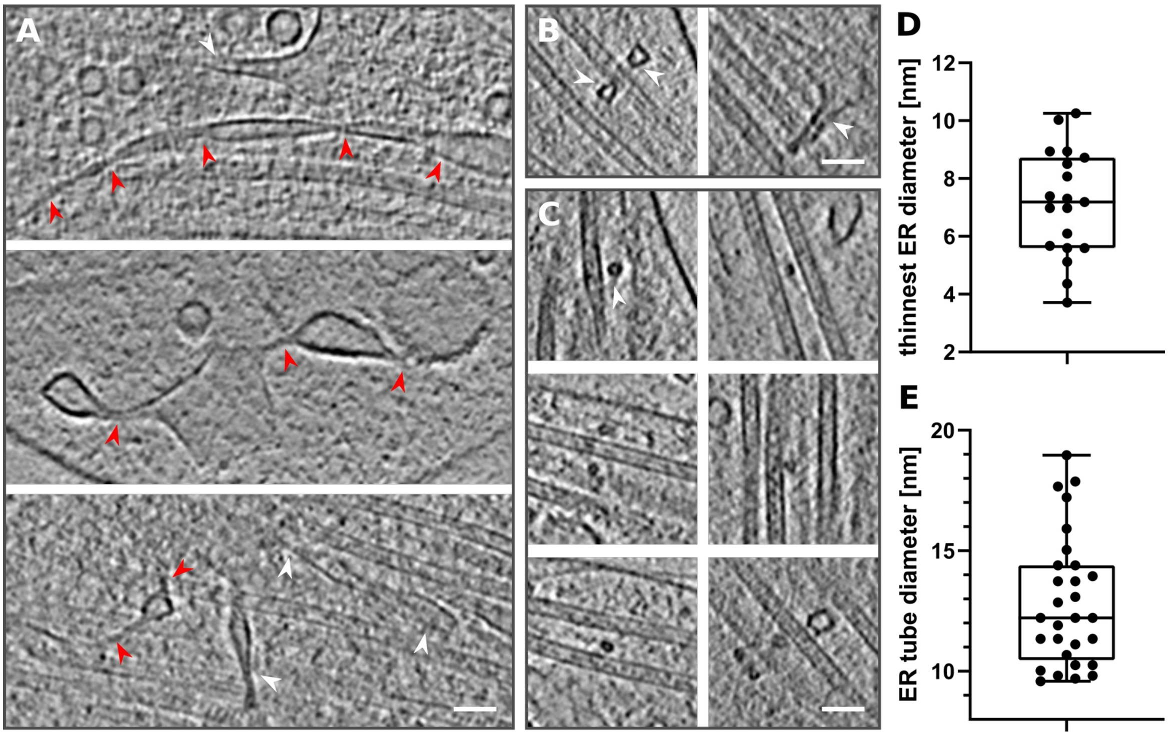
A
B
C
D
thinnest ER diameter [nm]
12
10
8
6
4
2
E
ER tube diameter [nm]
20
15
10

Figure S2. Thin ER tubes in axon branches.

A) Examples of ER tube reaching extremely thin diameters. Red arrowheads follow continuous ER tubes, White arrowheads depict different ER. B) ER (white arrowheads) wrapping around microtubules. C) Cross-section of ER tube (white arrowhead) wrapping around microtubules. D) Diameter of thinnest ER tubes found in tomograms, median diameter: 7.19 nm, N=19. E) Diameter of ER tube wrapping around microtubule, median diameter: 12.21 nm, N= 29. Scale bar: A-C = 50 nm.

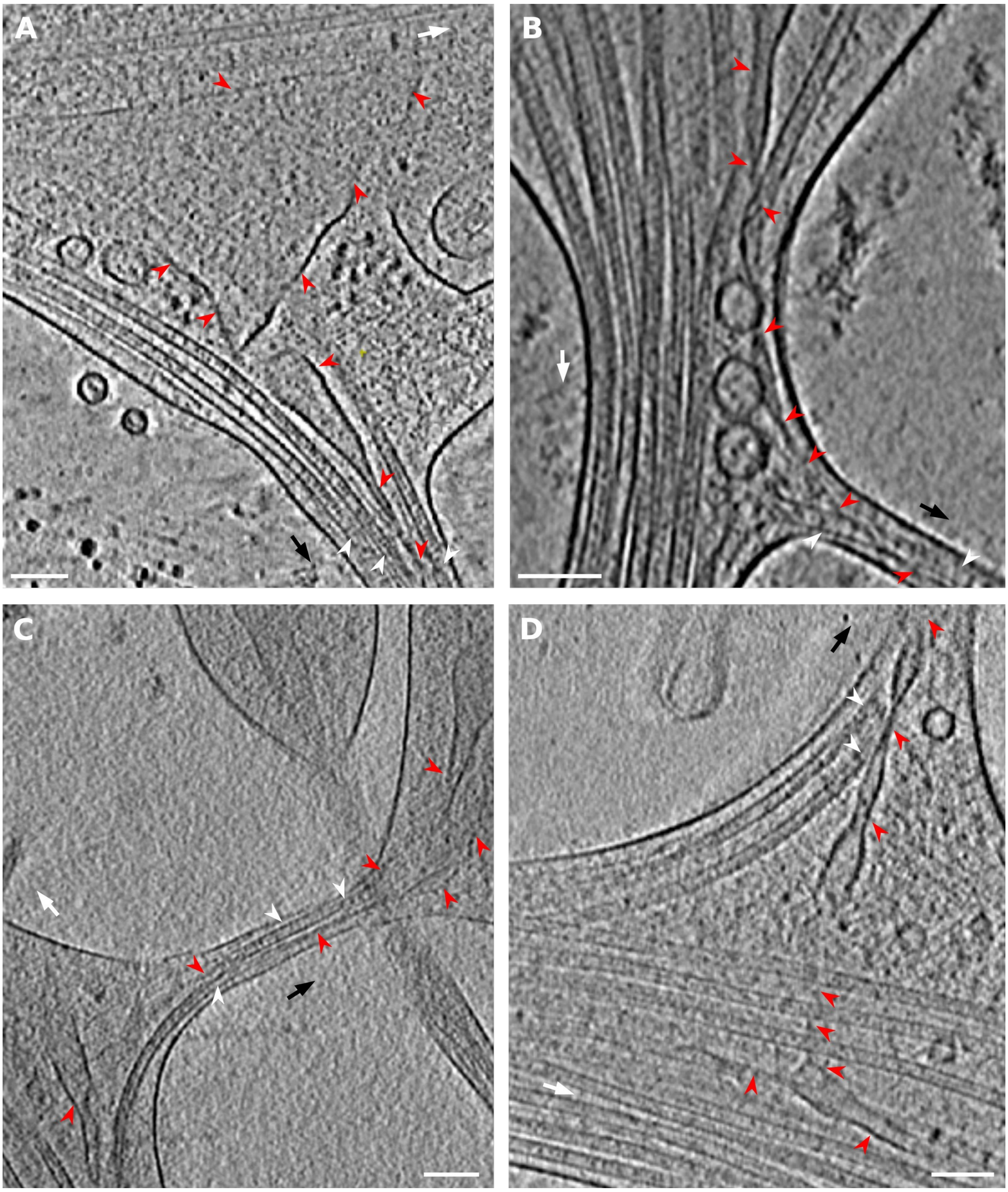

Figure S3. ER enters axon branches together with microtubules.

A)-D) Examples of ER tube present in axon branch together with microtubules, red arrowheads – ER, white arrowheads – microtubules, black arrow shows direction of new branch, white arrow points in the direction of main axon growth. Scale bar: A-D = 100 nm.

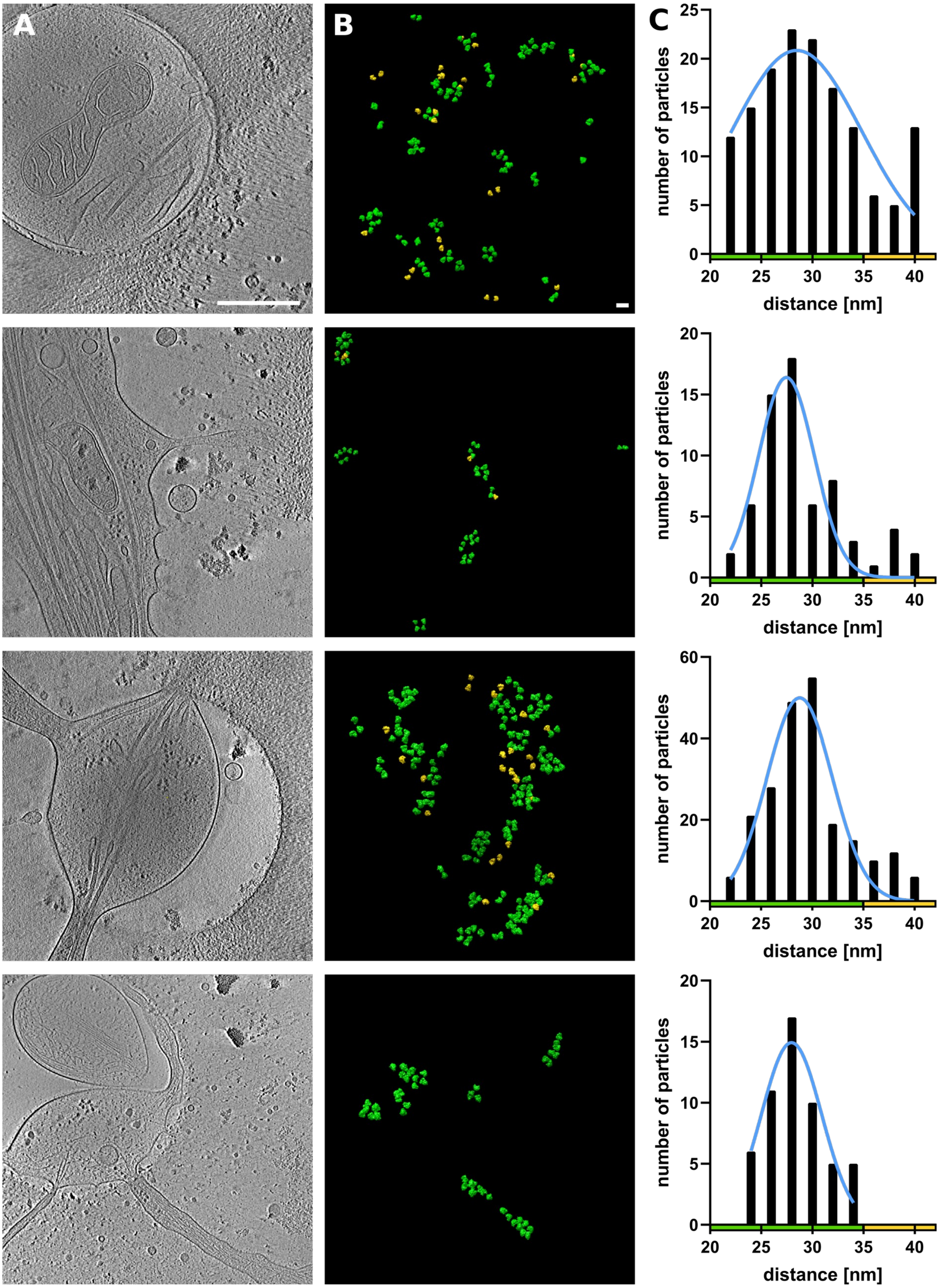

Figure S4. Visual representation of the ribosome distance distribution.

A) Slice from tomogram. B) Ribosome particles placed into the tomogram volume in color representation according their closest neighbor distance, green < 35 nm, yellow > 35 nm. C) Graph representing the distance distribution between clustered ribosomes. Scale bar: A = 500 nm, B = 50 nm.

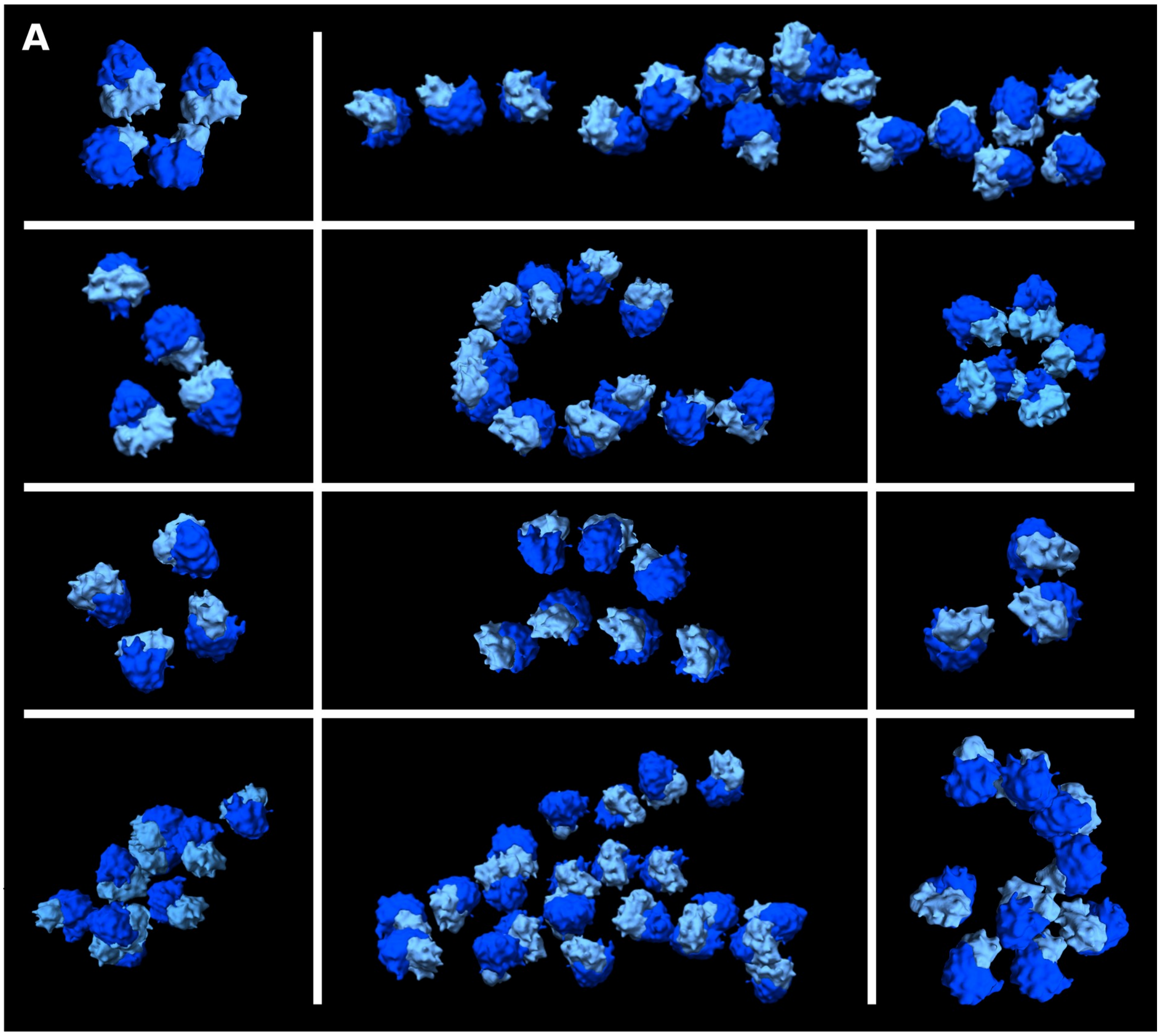

Figure S5. Clustered ribosomes form polysomes.

Examples of strings of ribosomes found in axon branches forming polysomes.

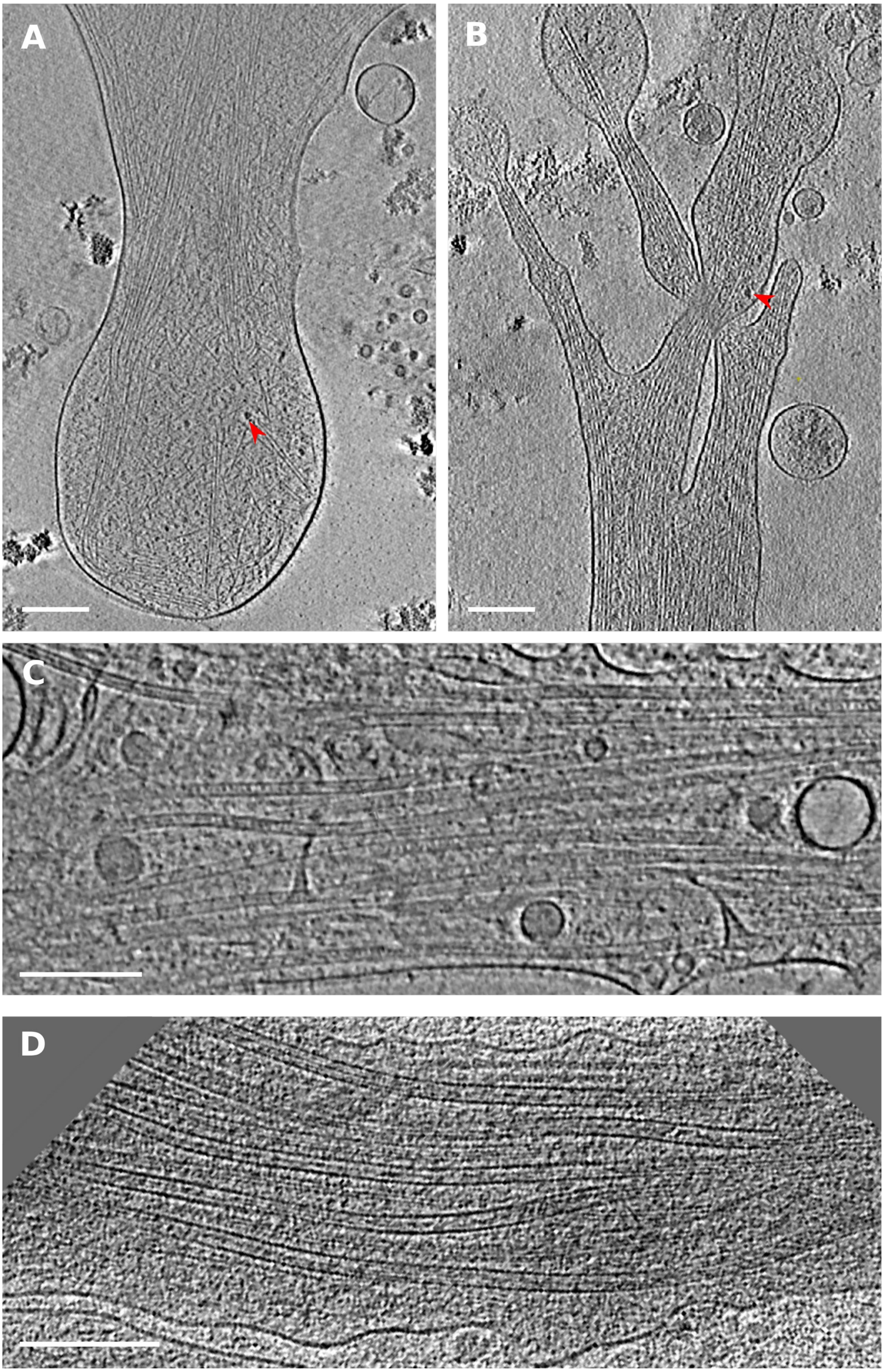

Figure S6. Growth cone and axon shaft.

A), B) Slices of tomograms showing growth cone filled with actin, red arrowhead depicts ribosome. C) Axon shaft packed with bundled microtubules, thin ER tubes and vesicles. Scale bar: A-C = 200 nm.

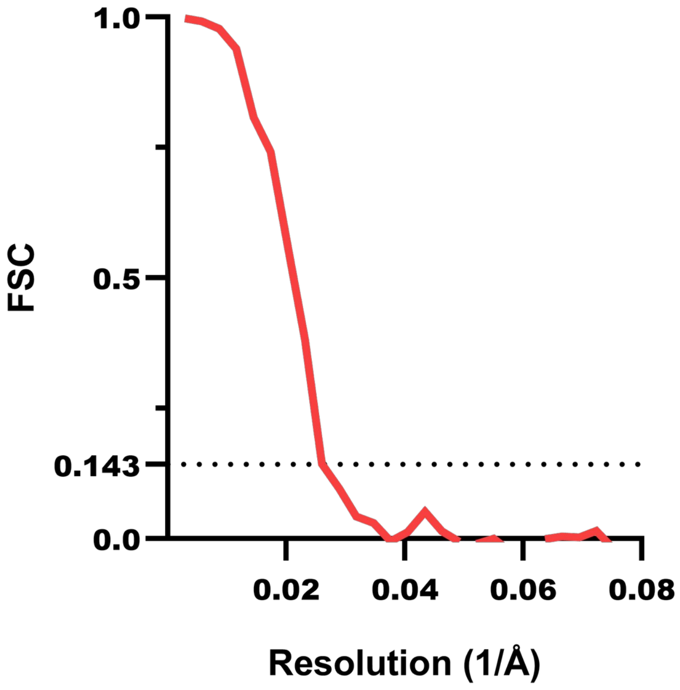

Figure S7. Ribosome reconstruction resolution estimation, FCS curve.

2.2 Direct induction of microtubule branching by microtubule nucleation factor SSNA1

Basnet N., Nedozralova H., Crevenna A.H., Bodakuntla S., Schlichthaerle T., Taschner M., Cardone G., Janke C., Jungmann R., Magiera M.M., Biertuempfel Ch., Mizuno N., (2018). *Nature Cell Biology* 20, 1172–1180.

During my PhD, I was able to contribute to the project about microtubule nucleation factor SSNA1. This study shows that SSNA1 can nucleate and induce the remodeling of the microtubule into a branched structure where a new microtubule directly branches out from the existing old microtubule. The remodeling or branching property of SSNA1 is related to its ability of self-assembly and the mutants which abrogate the self-assembly of SSNA1 also abolish microtubule branching. These SSNA1 mutants that abolish microtubule branching in-vitro also fail to promote axon branching when overexpressed in neurons.

For this study, I performed tomogram segmentation of microtubule branches, prepared neuron samples for cellular DNA-PAINT experiments, and analyzed light microscopy data. Detailed author contributions are included in the attached article.

ARTICLES
https://doi.org/10.1038/s41556-018-0199-8

nature cell biology

Direct induction of microtubule branching by microtubule nucleation factor SSNA1

Nirakar Basnet[1], Hana Nedozralova[1], Alvaro H. Crevenna[2], Satish Bodakuntla[3,4], Thomas Schlichthaerle[1,5,6], Michael Taschner[1,7], Giovanni Cardone[1], Carsten Janke[3,4], Ralf Jungmann[1,5], Maria M. Magiera[3,4], Christian Biertümpfel[1] and Naoko Mizuno[1]*

Microtubules are central elements of the eukaryotic cytoskeleton that often function as part of branched networks. Current models for branching include nucleation of new microtubules from severed microtubule seeds or from γ-tubulin recruited to the side of a pre-existing microtubule. Here, we found that microtubules can be directly remodelled into branched structures by the microtubule-remodelling factor SSNA1 (also known as NA14 or DIP13). The branching activity of SSNA1 relies on its ability to self-assemble into fibrils in a head-to-tail fashion. SSNA1 fibrils guide protofilaments of a microtubule to split apart to form daughter microtubules. We further found that SSNA1 localizes at axon branching sites and has a key role in neuronal development. SSNA1 mutants that abolish microtubule branching in vitro also fail to promote axon development and branching when overexpressed in neurons. We have, therefore, discovered a mechanism for microtubule branching and implicated its role in neuronal development.

Cell-shape control is critical in a number of physiological processes. Microtubules, the major cytoskeletal component determining cell shape, are mostly nucleated at the centrosome in proliferating cells. During specialized cell-shaping events, such as mitosis or cell polarization, cytoskeletal remodelling is thought to be driven by local nucleation of microtubules using a centrosome-independent mechanism[1–3].

Neuronal cells are a distinctive example of cells with highly complex morphologies. Neurons are shaped in an extremely polarized fashion with a unique-shaped axon protruding from the cell body and stretching over long distances. Individual cells develop branch points from their axons to connect to neighbouring cells, creating an intricate communication network in the nervous system. As the shape of axons is determined by microtubules, these branch points require remodelling of microtubules to split the cytoskeletal path into separate branches[1–5]. As the centrosome is not necessary for the morphological development of the axon[6], it is possible that axonal transformation occurs in a locally regulated manner within the axon. At axon branching points, the local destabilization and fragmentation of microtubules is mediated by the microtubule-severing enzyme spastin, which leads to the emergence of short microtubules[7]. However, the process of splitting the microtubule networks and, specifically, how the local rearrangement of spastin-processed tubulin oligomers or short microtubule fragments occurs has been enigmatic.

Due to its importance in various cell activities, the microtubule cytoskeleton has been well characterized in vitro. In the classical view, microtubules are considered as cylindrical polymers made of ~13 protofilaments. However, in living cells, it has been suggested that microtubules form higher-order branched networks to regulate their distribution within complex cytoskeletal networks[1,8,9]. The branched networks could be envisioned either through the attachment of new microtubule modules onto the side of an existing microtubule, or through direct branching of microtubules. So far, only one example of branching microtubule network has been shown, involving the microtubule nucleators augmin and γ-tubulin, which allow microtubules to grow out from nucleation points that attach to the side of existing microtubules[8,10–13]. There was, however, no evidence that protofilaments in a single microtubule can split apart to form a branched structure. Particularly at axon branch sites, augmin is less likely to be involved in generating branched microtubule networks, but has rather been implicated in determining microtubule orientation by crosslinking adjacent microtubules within an axon[14].

Here we focused on the protein SSNA1, a microtubule-binding protein implicated in the dynamic assembly of microtubules. SSNA1 is found at centrosomes or basal bodies in sperm cells[15,16], and at the midbody in dividing cells[17]. A recent study reported that SSNA1 accelerates neuronal development by promoting axon elongation and branch formation[17]. These observations collectively suggest a versatile role for SSNA1 in microtubule remodelling. However, the nature of its activity in controlling microtubule dynamics is unclear.

We now demonstrate that SSNA1 is a powerful microtubule-nucleating and -branching factor. In vitro reconstitution of SSNA1-mediated microtubule nucleation showed an induction of branched microtubules, where new daughter microtubules directly branch out from existing microtubules. SSNA1 attaches along single protofilaments, guiding them to grow away from a microtubule and template a branched microtubule. Mutation of residues essential for the oligomerization and the microtubule-branching activity of SSNA1, which we designed by structure-guided in vitro experiments, leads to defective axonal branching in primary neurons, showing that the

---

[1]Max Planck Institute of Biochemistry, Martinsried, Germany. [2]Biomolecular Self-Organization, Instituto de Tecnologia Química e Biológica António Xavier, Universidade Nova de Lisboa, Oeiras, Portugal. [3]Institut Curie, PSL Research University, CNRS, Orsay, France. [4]Universite Paris Sud, Universite Paris-Saclay, Orsay, France. [5]Department of Physics and Center for Nanoscience, Ludwig Maximilian University, Munich, Germany. [6]Graduate School of Quantitative Biosciences Munich (QBM), Ludwig Maximilian University, Munich, Germany. [7]Present address: Department of Fundamental Microbiology, University of Lausanne, Lausanne, Switzerland. *e-mail: mizuno@biochem.mpg.de

simple scaffolding mechanism of SSNA1 can lead to vast morphological changes in neurons.

Results

SSNA1 localizes at axon branching sites in primary neurons. A previous study implicated SSNA1 in the promotion of axon branching[17], but the underlying mechanism remained elusive. To investigate how SSNA1 plays a role in neuron development, we transduced wild-type murine primary hippocampal neurons with lentiviral particles encoding GFP-2A-mouse_SSNA1. Overexpression of SSNA1 led to the promotion of axon outgrowth (Fig. 1a,c), in agreement with a previous report[17]. In addition, we found a striking accumulation of SSNA1 at axon branches (Fig. 1b and Supplementary Fig. 1), which was also observed at secondary branch sites that emanate from an already existing axon branch (Fig. 1b, panel 4, and Supplementary Fig. 1). In agreement with its localization, SSNA1 overexpression led to increased and more complex branching as characterized by the Strahler number (Fig. 1d). Since SSNA1 localizes at the cytosolic compartments where microtubule are dynamic[15–17], we hypothesized that clusters of SSNA1 at branching sites in neurons might facilitate local microtubule nucleation.

SSNA1 induces direct microtubule branching. To assess the influence of SSNA1 on microtubules, we prepared recombinant SSNA1 (from *Chlamydomonas reinhardtii*, CrSSNA1, Supplementary Fig. 2A–C) and tested its interaction using cryo-electron microscopy (cryo-EM; Fig. 2a and Supplementary Fig. 2D). CrSSNA1 induced a formation of direct microtubule branches that split from a single microtubule (Fig. 2a, arrowheads), in contrast to an attachment of a second microtubule on the microtubule surface. Branching occurs by splitting the lattice of the microtubule, and protofilaments of mother microtubules directly continue into the outer surface of the branched microtubule. The bending angle was variable (Fig. 2b,c, 47° ± 15°, and Supplementary Fig. 2D,E), which suggests a rather flexible junction, in contrast to the more rigid, 70° Arp2/3-mediated actin branching[18,19]. Moreover, microtubules occasionally formed fork-like structures with several branches or junctions (Fig. 2b and Supplementary Fig. 2D). This has so far not been observed in any other system, and further underpins the uniqueness of SSNA1-mediated microtubule branching.

Cryo-ET shows diverging microtubules with a break in the microtubule lattice. To further understand the organization of microtubule branches, we performed cryo-electron tomography (cryo-ET) on branched microtubules (Fig. 3 and Supplementary Fig. 2F). Even though SSNA1 itself was not detectable due to the resolution limit of tomographic reconstructions, the microtubule lattice was clearly visible (Fig. 3a,b) and facilitated a tracing of individual protofilaments at the branch (Fig. 3c–e). The tracing showed that two branching microtubules shared a subset of protofilaments with their mother microtubule. In addition, we traced newly assembled protofilaments that were not connected to the mother microtubule (Fig. 3d), as the number of protofilaments doubles compared to the mother microtubule. This shows a discontinuity in the microtubule lattice at the splitting point of the branch.

SSNA1 self-clusters and nucleates microtubules. To explore the dynamic behaviour of SSNA1 causing this unique action in microtubules, we tested the interaction of SSNA1 with unpolymerized tubulin using fluorescence microscopy (Fig. 4a). Considering the average cellular concentration of SSNA1 of 187 nM[20], we mixed 200 nM CrSSNA1 and 8 µM tubulin in the presence of polyethylene glycol (PEG)[21]. Above a concentration of 5% PEG (Fig. 4b), we observed condensates of CrSSNA1 clustering with tubulin (Fig. 4a–c). Interestingly, several microtubules emerged from these CrSSNA1–tubulin clusters (Fig. 4a,b), reminiscent of aster

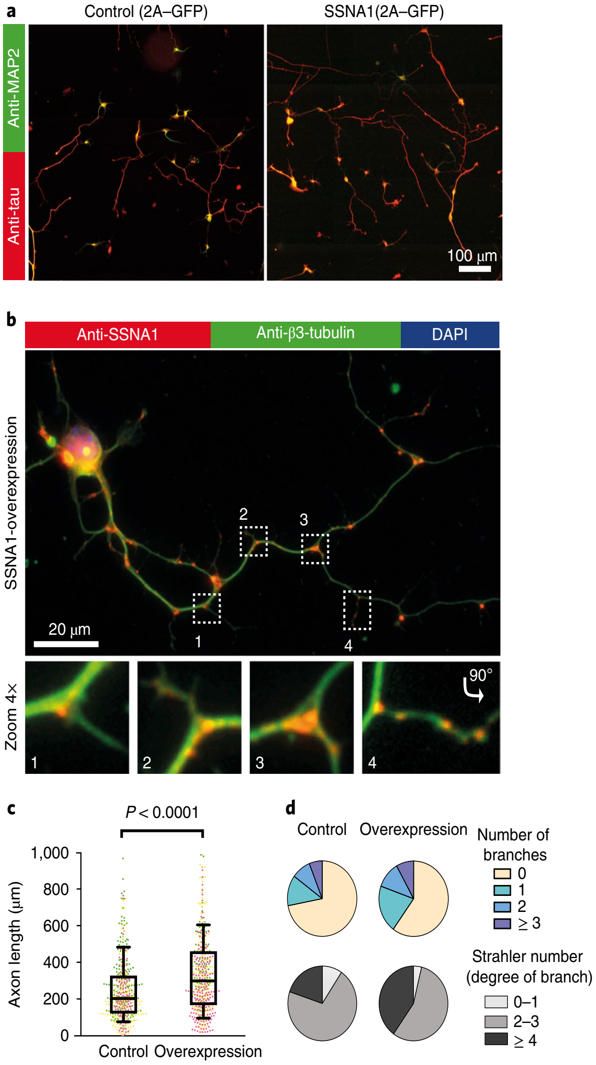

Fig. 1 | The effect of SSNA1 overexpression on primary hippocampal neurons. a, Immunostaining of MAP2 (green) and Tau (red) in control (GFP overexpression) and SSNA1-wild-type overexpression. **b**, Immunostaining of SSNA1 (red) and βIII-tubulin (green) in neurons overexpressing SSNA1 wild type shows the localization of SSNA1 at axon branch sites. **c**, Scatter dot plots of axon length under overexpression of SSNA1. The longest protrusion from the soma was defined as the axon, and cells with very short protrusions were also included in the counting, so that underdeveloped neurons could be assessed as well. The promotion of axon development occurs only in overexpression of wild-type SSNA1. Experiments were performed in triplicates, shown in magenta, green and yellow. Every cell is represented by a single point: control ($n = 505$ cells), wild type ($n = 499$ cells), pooled from 3 independent experiments, and the overlaid box-and-whisker plots cover 50% (boxes) and 90% (whiskers) of the entire population, with median values indicated as lines within the boxes. The results show statistical significance ($P < 0.0001$) as tested using the Kruskal–Wallis test, followed by Dunn's multiple comparison post hoc test. **d**, Pie graphs showing the distribution of the number of branches under overexpression conditions (control ($n = 496$ cells), wild type ($n = 490$ cells) pooled from 3 independent experiments) and Strahler number (degree of sub-branch formations on the existing branches; control ($n = 266$ cells), wild type ($n = 289$ cells) pooled from 3 independent experiments). Distributions of the branches and the Strahler number in SSNA1-expressing neurons differ significantly from the control (GFP overexpression) according to χ^2 two-sample test ($\chi^2 = 20.7$, $P < 0.01$ and 18.6, $P < 0.005$, respectively). See Supplementary Table 3 for source data.

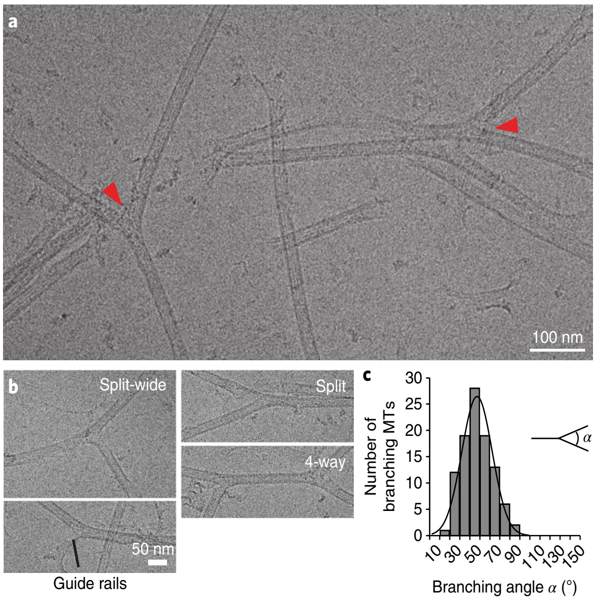

Fig. 2 | Characterization of in vitro-reconstituted microtubule branching. **a**, A cryo-EM image of branched microtubules. The arrowheads show examples of branching points. Microtubules were stabilized with 1 mM GMPCPP. **b**, Snapshots of branching microtubules. The 'guide rail' depicts thin lines of density often seen at the split of the branch point. **c**, Distribution of branching angles (47 ± 15°, *n* = 99 branch points). These experiments were performed three independent times.

formation seen during microtubule nucleation[1,22], and thus indicating that CrSSNA1 nucleates microtubules. This process was effective at a CrSSNA1 concentration of as little as 50 nM (Fig. 4d,e). Nucleation events were confined to the local condensates of CrSSNA1 and tubulin did not polymerize without CrSSNA1, highlighting the effect of the SSNA1 condensates and the requirement of a high local concentration. The number of growing asters and microtubules (Fig. 4d,e) correlated well with the concentration of CrSSNA1. We also observed new microtubules emerging from already formed microtubules (Supplementary Videos 1 and 2).

SSNA1 induces microtubule nucleation from mother microtubules. To understand and assess SSNA1-mediated nucleation from template microtubules, we mixed (3 or 30 μM) CrSSNA1 with tubulin in the presence of GTP with GMPCPP-stabilized microtubule seeds[23]. Several microtubules were able to grow out from the ends or the wall of pre-existing microtubules (Fig. 4f,g, Supplementary Fig. 3A,B and Supplementary Videos 3 and 4), agreeing with the cryo-EM observation (Fig. 2a). By differentially labelling pre-existing microtubules (red) and newly polymerized dynamic microtubules (green), we could categorize the branching events into: 'splitting', in which newly formed microtubules split from the end of a pre-formed microtubule; 'end-joining', showing three pre-existing microtubules connected through newly formed tubulin oligomers; 'side branching', seen as new microtubules coming out from the side of pre-existing microtubules; and 'dynamic branching', in which newly generated dynamic microtubules form a branch. The 'side branching' is reminiscent of local microtubule nucleation mediated by augmin and γ-tubulin in cell extracts[8,13]. However, in contrast to the augmin-mediated mechanism, the formation of CrSSNA1-mediated branching did not require γ-tubulin, indicating that SSNA1 works by a novel mode of action.

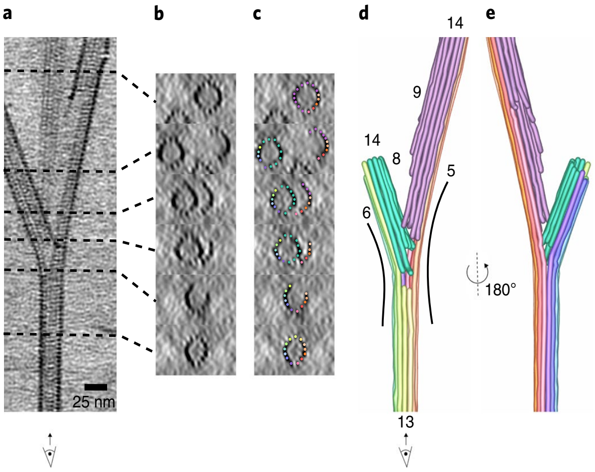

Fig. 3 | The cryo-ET reconstruction of SSNA1-mediated microtubule branching. **a**, A 25-nm slice of a tomographic reconstruction highlighting a branching point of a microtubule. With this view, individual protofilaments and tubulin units are visible, but the SSNA1 density is too thin to be visualized. **b**, Cross-sections of the branched microtubules in **a**. **c**, Individual protofilaments are overlaid with colour represented in the segmentation in **d**. **d**, Tracing of protofilaments in the 3D density map in **a**. Individual protofilaments are coloured in rainbow-colour coding. The newly formed protofilaments from the branched microtubules are coloured in green (left) and in pink (right). The number of protofilaments in this particular branched microtubule is counted to be 13 (mother microtubule), 14 (left branched microtubule) and 14 (right, branched microtubule). Thirteen mother protofilaments are split to 6 to the left and 5 to the right side of branched microtubules. **e**, 180°-rotated segmentation of the branched microtubule.

SSNA1 forms a fibril-like assembly on the surface of the microtubule with 11-nm periodicity. Although cryo-ET did not visualize the decoration of SSNA1 on microtubules, we observed that the free ends of microtubules are often extended with thin fibrils (Supplementary Fig. 2D, red arrowheads). These fibrils extend from splitting microtubules, seemingly to work as a 'guide rail' for the growth of branched microtubules (Fig. 2b; and Supplementary Fig. 2D, 'guide rail'). Computational averages of the cryo-EM images of microtubules allowed the visualization of CrSSNA1 directly attached to the surface of microtubules, revealing a ladder-like pattern (Fig. 5a, compare to 'microtubule-only control') with a periodicity of ~11 nm (Fig. 5b). We observed that CrSSNA1 facilitated preferential assembly of 13-protofilament microtubules similar to doublecortin[24] and EBs[25]. In contrast, 14-protofilament microtubules are predominantly polymerized in the absence of SSNA1 (Fig. 5c).

SSNA1 forms a head-to-tail fibril with 11-nm periodicity and covers the C-terminal tail of microtubules. SSNA1 is a protein with a relative molecular mass of 14,000 Da predicted to adopt a tropomyosin-like single parallel coiled-coil configuration[26,27] (Supplementary Fig. 3E). Fibril formation has previously been observed as a result of head-to-tail self-assembly[27,28]. Accordingly, we observed that CrSSNA1 readily forms short fibrillar appearances with occasional long fibril formations (Fig. 5g, 'FL'). Furthermore, the shorter fibrils of CrSSNA1 were converted into longer, organized bundles of fibrils after ~24 h incubation (Supplementary Fig. 3F). A closer look at these bundles revealed a striped, knob-like pattern, which leads to the formation of a sheet (Supplementary Fig. 3F, 24 h) with a 11-nm periodicity (Supplementary Fig. 3F, inset), and the inter-fibril distance of 3.5 nm. This pattern is comparable to that observed on the microtubule surface (Fig. 5a), indicating that the fibrils are covering microtubules along their long axis, giving a 11-nm spaced ladder-like pattern.

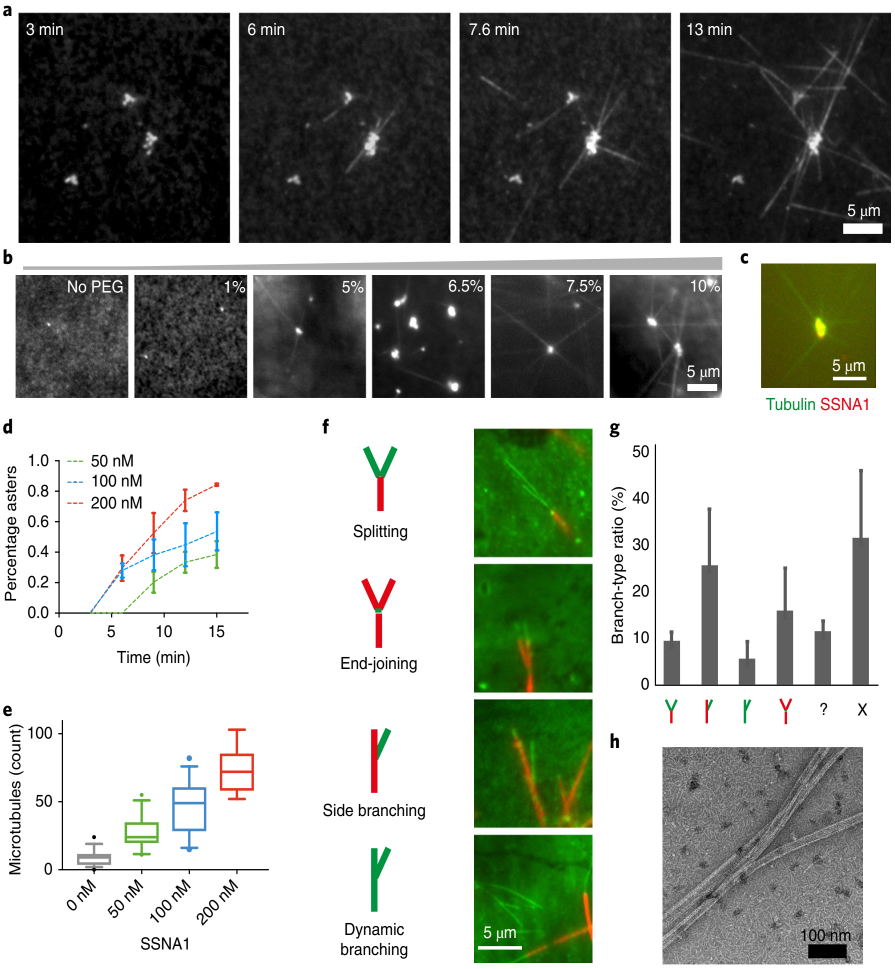

Fig. 4 | Nucleation and branching of microtubules mediated by CrSSNA1 under various conditions. **a**, Aster-like formation of microtubules (20% HiLyte488 tubulin) occurs within 3 min after mixing tubulin with a lower concentration (200 nM) of CrSSNA1 (upper) under conditions mimicking molecular crowding (7.5% PEG, typically used as a crowding agent), where tubulin alone does not form any polymers. Microtubules propagate out from tubulin concentrate, serving as a nucleation centre. These experiments were performed three independent times with similar results. **b**, 200 nM CrSSNA1 and 8 µM tubulin self-associate, forming clusters in the presence of PEG with concentration >~5%. **c**, SSNA1 antibody recognizes the microtubule nucleation centre. **d**, A plot of the percentage of the concentrates growing into asters with microtubules as a function of time (min) in the presence of 50, 100 and 200 nM CrSSNA1. The error bars are mean ± s.d. from $n = 3$ independent experiments. As little as 50 nM of CrSSNA1 is sufficient to observe aster formation in the presence of 7.5% PEG. **e**, Counts of microtubules observed per field of view, in the presence of different concentrations of CrSSNA1. The box plots cover 50% (boxes) and 90% (whiskers) of the entire population, with median values indicated as lines within the boxes. Sample size: 0 nM: $n = 42$ fields of view; 50 nM: $n = 29$; 100 nM: $n = 30$; 200 nM: $n = 25$. Data were pooled from three independent experiments except for the first point (0 nM) for which data were pooled from four independent experiments. **f**, Green coloured dynamic microtubules on red-microtubule GMPCPP seeds in the presence of a higher concentration of CrSSNA1 (30 µM) without molecular crowding agents to achieve globally concentrated conditions. 'branch-like' nucleation is observed. Branches were categorized as 'splitting', 'end-joining', 'side branching' or 'dynamic branching'. **g**, Ratios of different branch types ($n = 895$ branches, mean ± s.d. pooled from 3 independent experiments). '?' shows the bundled microtubules, which are difficult to categorize. 'X' shows microtubules without branching. Branch-like nucleation can be seen from the locally concentrated SSNA1 condition described in **a**–**e**; however observations of individual microtubules are challenging due to the high local protein concentrations. **h**, A negative-stain EM image of SSNA1-mediated branched microtubules in the presence of 200 nM CrSSNA1 and 7.5% PEG, representative of 3 independent experiments. See Supplementary Table 3 for source data.

To further characterize the interaction between SSNA1 and microtubules, we obtained a cryo-EM three-dimensional (3D) structure of CrSSNA1 in complex with microtubules (Fig. 5d–f and Supplementary Fig. 4A) with an overall resolution of 6.1 Å (Supplementary Fig. 4B). Due to the symmetry mismatch between microtubules (4- or 8-nm periodicity) and SSNA1 (11-nm periodicity), SSNA1 was averaged out, and the fibril appeared as a 'cloud' of protein density running parallel to the microtubule surface, with an apparent local resolution of ~11 Å (Supplementary Fig. 4C). However, it was possible to visualize thin lines of additional densities running parallel to the microtubule surface (Fig. 5e,f), which we interpreted as SSNA1 filaments. The SSNA1 filaments run between two protofilaments, proximal to the unstructured, highly acidic carboxy-terminal tails (E-hooks) of tubulin (Fig. 5f labelled 'C'). Removal of E-hooks resulted in weakening of SSNA1 crosslinking with microtubules as determined by EDC (~49% less crosslinked; Supplementary Fig. 4E). E-hooks create a negative electrostatic cloud by their periodical arrangement on the microtubule surface[29], which could attract the SSNA1 fibrils. This could explain why SSNA1 interacts with microtubules despite the symmetry mismatch. It also suggests that the head-to-tail assembly of SSNA1 fibrils could guide protofilament assembly and microtubule polymerization by covering and neutralizing the E-hooks as shown previously[30].

The head-to-tail fibril formation of SSNA1 is essential for microtubule branching. On the basis of the observation that SSNA1 fibrils appear to guide the protofilaments of microtubules, we hypothesized that the microtubule branching activity is mediated by the formation of long SSNA1 fibrils that curve away and guide the protofilament out of the lattice (guide rail, Fig. 2b and Supplementary Fig. 2D). To test this, we created a series of truncated SSNA1 fragments that abolish fibril formation. On the basis of a PHYRE2 analysis[31] and previous reports[27], we found that SSNA1 contains a well-conserved α-helical region (residues 6–104) followed by an unstructured C-terminal tail (Supplementary Fig. 3E). A series of amino-terminal truncations showed that the first 19 residues were not necessary for fibril formation, as CrSSNA1(20–111) (20-C) formed cable-like bundled fibrils, which were less ordered compared to full-length protein (CrSSNA1 FL), but displayed an ~11-nm pattern (Fig. 5g,h, Supplementary Fig. 5A and Supplementary Table 1). In contrast, CrSSNA1(21-C), a truncation missing one more residue, Glu 20, was unable to form fibrils (Fig. 5g,h, Supplementary Fig. 5A and Supplementary Table 1). This observation correlates with the ability of CrSSNA1(20-C), but not CrSSNA1(21-C), to mediate microtubule branching (Supplementary Fig. 5A and Supplementary Table 1). The key role of the residue Glu 20 for fibril-formation and microtubule-branching activity of SSNA1 was further underpinned by point mutations E20A and E20A/D21A, which drastically reduced microtubule branch formation (Supplementary Fig. 5A and Supplementary Table 1). These mutants may form fibrils, but with much lower frequency and without a distinct higher-order organization.

In the C-terminal region of CrSSNA1, three distinctive lysine residues (Lys 105, Lys 106 and Lys 107) mark the beginning of the unstructured C terminus. CrSSNA1 truncations 1–104 and 1–105 (Fig. 5g,h, Supplementary Fig. 5A and Supplementary Table 1) showed that CrSSNA1(1–104) can no longer form fibrillar oligomers, or induce microtubule branching (Fig. 5g,h), while CrSSNA1(1–105) was purified as fibrils and showed microtubule branching activity (Supplementary Fig. 5A) at a similar efficiency to CrSSNA1-FL. These results indicate that the positive charge of the lysine residues is essential for the ability of CrSSNA1 to form fibrils. We confirmed this by generating a triple point mutant, K105A/K106A/K107A, which indeed abolished fibril formation and microtubule branching (Supplementary Fig. 5A and Supplementary Table 1) for both the full length and the 1–107 fragment. Altogether, our mutational analyses indicate that the key interaction for longitudinal fibril formation is mediated by Glu 20 of one unit and the C-terminal tail (Lys 105–107) of the adjacent interacting unit (Fig. 5i). To confirm this, we created mutants in which the charges of residues Glu 20/Asp 21 and Lys 105/Lys 106/Lys 107 were swapped. When two of the opposite charges were swapped (E20K/D21K/K105E/K106E or E20K/D21K/K106E/K107E), both cable-like formation and microtubule branching activity of SSNA1 were retained. In contrast, swapping of the two negative residues at the N terminus and the three positive residues at the C terminus (E20K/D21K/K105E/K106E/K107E), resulting in a change of net charge from +1 to −1, abolished microtubule branching (Supplementary Fig. 5B). However, this construct was still able to form SSNA1 fibrils and cable-like structures, indicating that the microtubule branching activity depended not only on fibril formation of SSNA1, but also on the presence of an extra negative charge at the unstructured SSNA1 C terminus. This was confirmed by the mutant E20A/D21A/K105A/K106A/K107A, termed 5A, showing a complete loss of microtubule branching activity (Fig. 5g).

Microtubule-branching-deficient SSNA1 mutants abolished the promotion of axon branches. Having gained insights into the molecular organization of SSNA1 and its effect on microtubule nucleation and branching, we hypothesized that the promotion of axon growth and branching observed in neurons overexpressing wild-type SSNA1 might be altered when microtubule-branching-deficient SSNA1 versions are expressed. Our results indeed showed that, in contrast to the SSNA1 wild type (Figs. 1 and 6a–c), SSNA1 with mutations abolishing microtubule branching in vitro also failed to promote the growth of axons or axon branches (Fig. 6a–c and Supplementary Fig. 6A–E) in primary neurons. Notably, a dominant-negative effect was also observed when the 5A mutant was overexpressed for the number of total neurite processes (Fig. 6c), showing a decreased number of major and minor branches. This dominant-negative effect was also found when the two negative residues at the N terminus and the three positive residues at the C terminus were swapped (swap-KK/EEE). Notably, swapping only two opposite charges and leaving the third C-terminal lysine intact (swap-KK/EE) could still promote axon growth (Supplementary Fig. 6D,E). Together these findings show that the ability of SSNA1 to induce fibril formation and microtubule branching at the molecular level correlates with its function of mediating axon branching and development, suggesting the intriguing possibility that it locally generates branched microtubules at axon branch sites.

Morphological change of microtubule networks in non-neuronal cells. To test whether the function of SSNA1 is conserved in different cell types, we used fibroblasts, which are structurally less specialized than neurons, and tested whether overexpression of SSNA1 has the capacity to change the microtubule organization (Fig. 6e–j). Super-resolution light microscopy with DNA-PAINT showed that individual microtubules are well resolved in the control cells with a wide-ranging network (Fig. 6e–g). In contrast, microtubules were rather short in SSNA1-overexpressing cells (Fig. 6h–j), suggesting that SSNA1 can promote nucleation, generating more but shorter microtubules. We also occasionally found microtubules forming three-way intersections, as if one microtubule emerged out of another in both control and SSNA1-overexpressing cells (Fig. 6g,j, arrowheads). These events occurred more often in SSNA1-overexpressing cells (2.8 ± 1.2 occurrences per 100 μm of microtubule) than control cells (1.0 ± 0.35 occurrences per 100 μm of microtubule). Although the limited resolution in light microscopy prevented us from discerning whether microtubules branched with a shared lattice or if two microtubules only attached to each other, the observations were consistent with our in vitro studies by electron microscopy.

Discussion

During cell polarization, the dynamics and distribution of the microtubule cytoskeleton is tightly regulated. Although the centrosome has a major role as a microtubule-organizing centre in less differentiated cells, the inactivation of centrosomes in neurons does not affect axon growth, a process strongly dependent on microtubule assembly[6]. Thus far, the molecular mechanisms regulating axonal microtubule nucleation, especially in the form of branching, have remained a mystery. Here, we show that SSNA1 accumulates at axon branches and promotes axon branching in primary neurons, and can nucleate microtubules in vitro. Mutations interfering with SSNA1 in vitro nucleation activity also affect the occurrence of axon branches in neurons. Together, these results suggest that SSNA1 could act as a microtubule nucleator at axon branch sites.

Strikingly, our work revealed that SSNA1 independently mediates microtubule branching by causing protofilaments to splay apart from the lattice. To our knowledge, no other microtubule-binding protein shows this activity. When tested, EB3 and ch-TOG, known regulators of microtubule dynamics, under the same conditions,

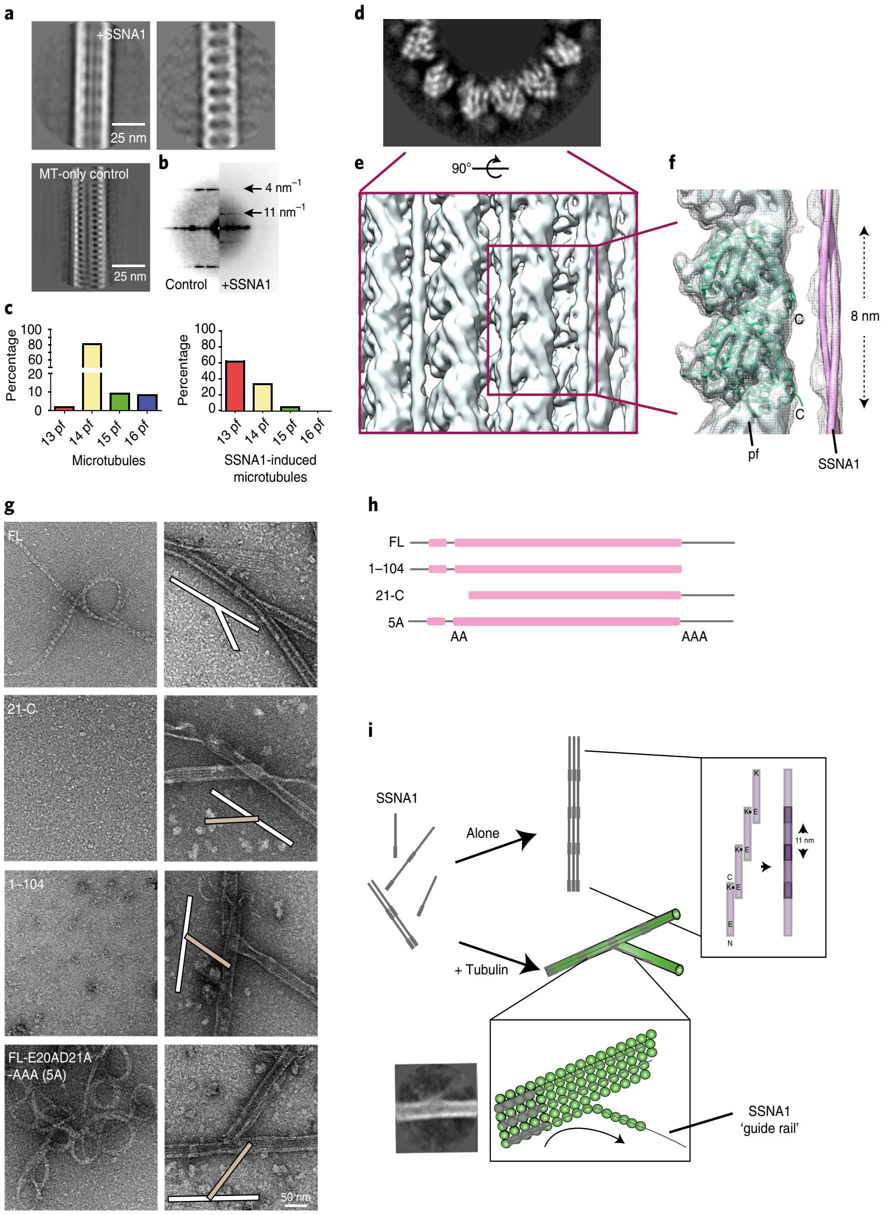
a
+SSNA1
25 nm
MT-only control
25 nm
b
4 nm−1
11 nm−1
Control
+SSNA1
c
Percentage
100
80
60
20
10
0
13 pf
14 pf
15 pf
16 pf
Microtubules
Percentage
100
80
60
40
20
0
13 pf
14 pf
15 pf
16 pf
SSNA1-induced microtubules
d
e
90°
f
C
C
8 nm
pf
SSNA1
g
FL
21-C
1–104
FL-E20AD21A -AAA (5A)
50 nm
h
FL
1–104
21-C
5A
AA
AAA
i
SSNA1
Alone
+ Tubulin
K
K•E
K•E
C
K•E
E
N
11 nm
SSNA1 'guide rail'

Fig. 5 | Molecular characterization of the branching action of SSNA1. **a**, Left: representative class average of the SSNA1-induced microtubules. Right: SSNA1 decoration emphasized by computationally subtracting microtubule densities[35]. Bottom left: average of microtubules without decoration for comparison. **b**, The power spectrum of microtubule class averages shows an additional 11 nm periodicity in the presence of SSNA1. **c**, Distribution of protofilament (pf) numbers of microtubules reconstituted from brain tubulin in the absence (left) and in the presence of SSNA1 (right) shifting the majority from 14- to 13-protofilament microtubules. **d**, Greyscale slice from the density map of the plus-end-on view of the SSNA1–microtubule 3D reconstruction. SSNA1 decoration and the secondary structures of tubulin density are well resolved. **e**, Rendering of the microtubule surface decorated with SSNA1. The resolution of the microtubule surface (~10 Å) is not as high as the core (<8 Å) due to the SSNA1 decoration. **f**, Tubulin atomic model (PDB ID: 3jal) fitted to the map. The SSNA1 coiled-coil fibril is indicated as a tube representation. Note that the periodical feature of SSNA1 is averaged out because of the symmetrical mismatch between tubulin dimers (8 nm) and SSNA1 fibrils (11 nm). **g**, Morphological observation of SSNA1 and its branching activity. Left: observation of the purified protein at 0 h incubation (that is, immediately after purification). Right: a magnified view of the co-polymerized microtubules. Microtubule branching was observed with SSNA1-FL, while other protein fragments do not facilitate branching. For the proteins that do not cause the branching, examples of typical crossing of microtubules (white and beige bars at the scheme within the image), instead of branching, are shown. Detailed observations are available in Supplementary Fig. 5A. **h**, A graphical scheme of the SSNA1 constructs used in **g**. **i**, A scheme of the SSNA1 self-assembly and microtubule nucleation mediated by SSNA1. While SSNA1 oligomers alone can also undergo a slow self-assembly process, the SSNA1 oligomers interact with tubulin dimers to promote their co-polymerization. The polymerized SSNA1 may further act as a guide rail (bottom inset) for protofilament splitting, resulting in microtubule branch formation. A class average indicating the guide rail mechanism is shown. Other class averages are available in Supplementary Fig. 2E.

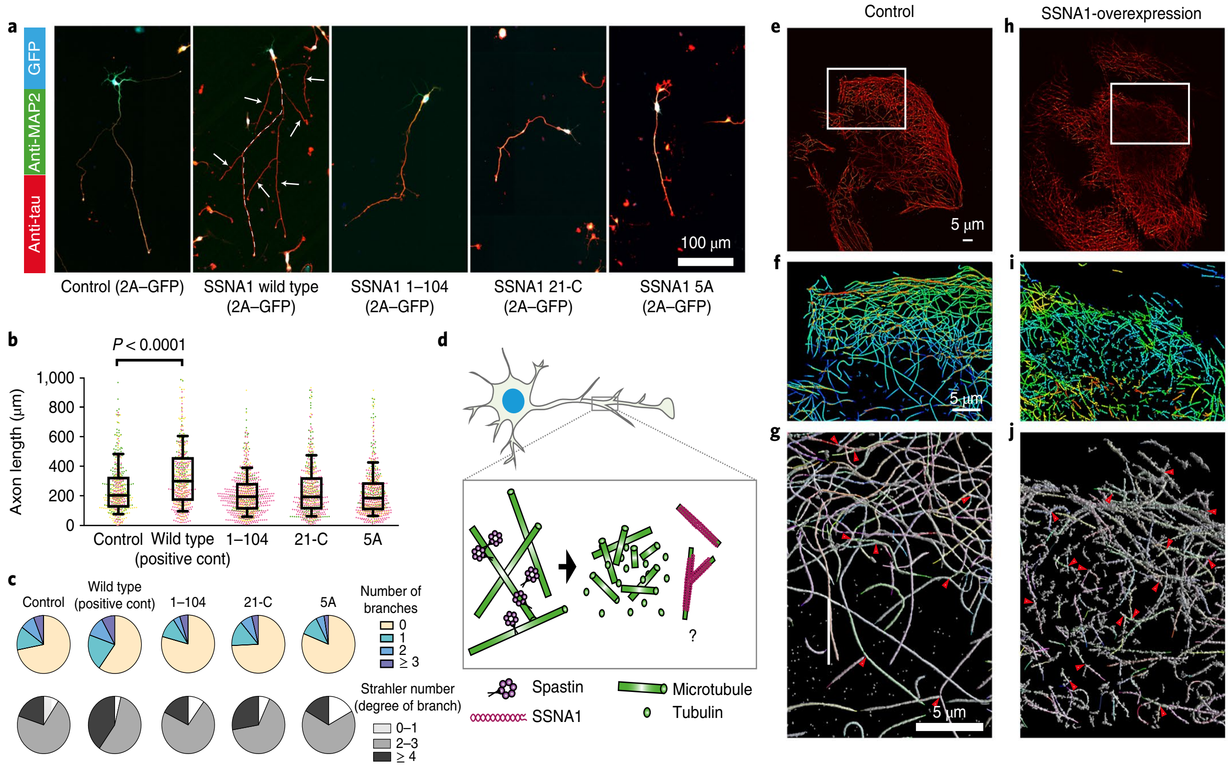

Fig. 6 | The effect of various SSNA1 constructs on primary hippocampal neurons and fibroblast cells a, Immunostaining of MAP2 (green), Tau (red) and GFP (blue, expression control) in SSNA1-overexpressing cells. For the SSNA1 wild type, the axon is indicated with a dashed line. **b**, Scatter dot plots of axon length under overexpression of various SSNA1 constructs. The control and wild-type profiles shown in Fig. 1 are placed as a negative and positive control, respectively. The promotion of axon development occurs only in overexpression of wild-type SSNA1, while no apparent effect was observed for the constructs that fail to mediate microtubule branching. Every cell is represented by a single point; control ($n = 496$ cells), wild type ($n = 490$), 1-104 ($n = 788$), 21-C ($n = 610$), 5A ($n = 642$) from 3 independent experiments, shown in magenta, green and yellow, and the overlaid box-and-whisker plots cover 50% (boxes) and 90% (whiskers) of the entire population, with median values indicated as lines within the boxes. **c**, Pie graphs showing the distribution of the number of branches and Strahler number under different overexpression conditions. The GFP-expression-control and SSNA1-wild-type-overexpression profiles in Fig. 1 are placed as controls. **d**, A schematic model describing how SSNA1-mediated microtubule nucleation could contribute to axon branch formation. Spastin has been shown to localize at axon branches[7] and to interact with SSNA1[36]. Taken together with our finding of SSNA1 localization at axon branches, it is possible that the two proteins work sequentially by spastin severing microtubules to provide tubulin oligomers, and SSNA1 nucleating microtubules at the branching site. **e**, A DNA-PAINT image of a 500-nm slice of the microtubule network in untreated cells (control). **f**, Zoomed-in view from **e**; the object is coloured in a rainbow code according to the depth. **g**, Individually recognized microtubules are highlighted in various colours. Three-way intersections are indicated with red arrowheads. **h–j**, Corresponding view of a 500-nm slice of the microtubule network in SSNA1 overexpressing cells. For analysis, 3 independent SSNA1-overexpressing and control cells were assessed each, containing the total microtubule lengths of 5,700 µm, 7,900 µm and 1,900 µm and 7,700 µm, 8,500 µm and 7,700 µm, respectively. See Supplementary Table 3 for source data.

did not induce branching (Supplementary Fig. 6F,G). In addition, we showed that microtubule branching requires co-polymerization of SSNA1 with microtubules, as well as specific amino-acid interactions. Taken together, these results indicate that the observed branching activity is highly specific to SSNA1.

Our work has uncovered a surprising example of how co-polymerization of a simple coiled-coil protein with tubulin can induce global remodelling of the microtubule network. Association of SSNA1 may reinforce longitudinal connections of tubulin oligomers, facilitate protofilament formation and act as a polymerization seed for microtubule formation. Concomitantly, the preference of SSNA1 for lateral connections may facilitate the lateral associations between microtubule protofilaments. Polymerized SSNA1 may precede microtubule protofilaments, guiding protofilaments out of the microtubule axis, thus providing a template for a new microtubule branch ('guide rail' mechanism). In a cellular context, however, the situation is more complex as SSNA1 activity is probably modulated by other factors. Further experiments are necessary to test this mode of action of SSNA1 for microtubule branching in cells.

Our in vitro reconstitutions showed that SSNA1 self-assembles into clusters together with tubulin at a high local concentration. As axons are densely packed with cytoskeletal components, this organization is a plausible prerequisite for the physiological function of SSNA1, allowing SSNA1 to concentrate locally, self-assemble and become a microtubule nucleation centre at designated locations. Alternatively, the requirement of a high local concentration of SSNA1 may be a means to limit the microtubule-remodelling activity of SSNA1 to specific subcellular areas such as axon branches, the midbody in dividing cells and the base of cilia.

As microtubules are much less dynamic in axons compared to less polarized cells[32–34], SSNA1-mediated branching may be restricted to locally destabilized sites of the microtubule cytoskeleton. Interestingly, SSNA1 interacts with spastin, a protein important for the initiation of axon branching and thought to increase the pool of soluble tubulin through microtubule fragmentation[7].

It is tempting to speculate that short, spastin-severed microtubules (that is, tubulin oligomers) provide the building blocks for SSNA1-mediated microtubule nucleation and branching. Thus, the synergistic action of spastin and SSNA1 could facilitate the formation of axonal branch points (Fig. 6d). Further investigation of SSNA1 activity in situ will provide valuable insights into the initiation and organization of axon branches. In particular, it will be interesting to explore whether SSNA1-mediated microtubule branching is a direct driving force for axon branching, or an intermediate state during early stages of neuronal morphogenesis. Considering the diverse sites at which SSNA1 is localized in various cell types[17,27], the microtubule-branching mechanism discovered here could have broad implications for understanding the regulation of various microtubule functions, providing new clues to previously unanswered questions about cytoskeleton and intracellular transport.

Online content

Any methods, additional references, Nature Research reporting summaries, source data, statements of data availability and associated accession codes are available at https://doi.org/10.1038/s41556-018-0199-8.

Received: 19 November 2017; Accepted: 20 August 2018;
Published online: 24 September 2018

References

1. Ishihara, K., Nguyen, P. A., Groen, A. C., Field, C. M. & Mitchison, T. J. Microtubule nucleation remote from centrosomes may explain how asters span large cells. *Proc. Natl Acad. Sci. USA* **111**, 17715–17722 (2014).
2. Meunier, S. & Vernos, I. Acentrosomal microtubule assembly in mitosis: the where, when, and how. *Trends. Cell Biol.* **26**, 80–87 (2016).
3. Petry, S. & Vale, R. D. Microtubule nucleation at the centrosome and beyond. *Nat. Cell Biol.* **17**, 1089–1093 (2015).
4. Kalil, K. & Dent, E. W. Branch management: mechanisms of axon branching in the developing vertebrate CNS. *Nat. Rev. Neurosci.* **15**, 7–18 (2014).
5. Lewis, T. L., Courchet, J. & Polleux, F. Cell biology in neuroscience: cellular and molecular mechanisms underlying axon formation, growth, and branching. *J. Cell Biol.* **202**, 837–848 (2013).
6. Stiess, M. et al. Axon extension occurs independently of centrosomal microtubule nucleation. *Science* **327**, 704–707 (2010).
7. Yu, W. et al. The microtubule-severing proteins spastin and katanin participate differently in the formation of axonal branches. *Mol. Biol. Cell* **19**, 1485–1498 (2008).
8. Petry, S., Groen, A. C., Ishihara, K., Mitchison, T. J. & Vale, R. D. Branching microtubule nucleation in *Xenopus* egg extracts mediated by augmin and TPX2. *Cell* **152**, 768–777 (2013).
9. Decker, F., Oriola, D., Dalton, B. & Brugués, J. Autocatalytic microtubule nucleation determines the size and mass of *Xenopus laevis* egg extract spindles. *eLife* **7**, e31149 (2018).
10. Murata, T. et al. Microtubule-dependent microtubule nucleation based on recruitment of gamma-tubulin in higher plants. *Nat. Cell Biol.* **7**, 961–968 (2005).
11. Janson, M. E., Setty, T. G., Paoletti, A. & Tran, P. T. Efficient formation of bipolar microtubule bundles requires microtubule-bound gamma-tubulin complexes. *J. Cell Biol.* **169**, 297–308 (2005).
12. Goshima, G., Mayer, M., Zhang, N., Stuurman, N. & Vale, R. D. Augmin: a protein complex required for centrosome-independent microtubule generation within the spindle. *J. Cell Biol.* **181**, 421–429 (2008).
13. Kamasaki, T. et al. Augmin-dependent microtubule nucleation at microtubule walls in the spindle. *J. Cell Biol.* **202**, 25–33 (2013).
14. Sánchez-Huertas, C. et al. Non-centrosomal nucleation mediated by augmin organizes microtubules in post-mitotic neurons and controls axonal microtubule polarity. *Nat. Commun.* **7**, 12187 (2016).
15. Pfannenschmid, F. et al. Chlamydomonas DIP13 and human NA14: a new class of proteins associated with microtubule structures is involved in cell division. *J. Cell Sci.* **116**, 1449–1462 (2003).
16. Lai, C. K. et al. Functional characterization of putative cilia genes by high-content analysis. *Mol. Biol. Cell* **22**, 1104–1119 (2011).
17. Goyal, U., Renvoisé, B., Chang, J. & Blackstone, C. Spastin-interacting protein NA14/SSNA1 functions in cytokinesis and axon development. *PLoS ONE* **9**, e112428 (2014).
18. Blanchoin, L. et al. Direct observation of dendritic actin filament networks nucleated by Arp2/3 complex and WASP/Scar proteins. *Nature* **404**, 1007–1011 (2000).
19. Volkmann, N. et al. Structure of Arp2/3 complex in its activated state and in actin filament branch junctions. *Science* **293**, 2456–2459 (2001).
20. Itzhak, D. N., Tyanova, S., Cox, J. & Borner, G. H. Global, quantitative and dynamic mapping of protein subcellular localization. *eLife* **5**, e16950 (2016).
21. Woodruff, J. B. et al. The centrosome is a selective condensate that nucleates microtubules by concentrating tubulin. *Cell* **169**, 1066–1077.e10 (2017).
22. Wilde, A. & Zheng, Y. Stimulation of microtubule aster formation and spindle assembly by the small GTPase Ran. *Science* **284**, 1359–1362 (1999).
23. Hyman, A. A., Salser, S., Drechsel, D. N., Unwin, N. & Mitchison, T. J. Role of GTP hydrolysis in microtubule dynamics: information from a slowly hydrolyzable analogue, GMPCPP. *Mol. Biol. Cell* **3**, 1155–1167 (1992).
24. Bechstedt, S. & Brouhard, G. J. Doublecortin recognizes the 13-protofilament microtubule cooperatively and tracks microtubule ends. *Dev. Cell* **23**, 181–192 (2012).
25. Des Georges, A. et al. Mal3, the *Schizosaccharomyces pombe* homolog of EB1, changes the microtubule lattice. *Nat. Struct. Mol. Biol.* **15**, 1102–1108 (2008).
26. Ramos-Morales, F., Infante, C., Fedriani, C., Bornens, M. & Rios, R. M. NA14 is a novel nuclear autoantigen with a coiled-coil domain. *J. Biol. Chem.* **273**, 1634–1639 (1998).
27. Price, H. P. et al. The orthologue of Sjögren's syndrome nuclear autoantigen 1 (SSNA1) in *Trypanosoma brucei* is an immunogenic self-assembling molecule. *PLoS ONE* **7**, e31842 (2012).
28. Rodríguez-Rodríguez, M. et al. Characterization of the structure and self-recognition of the human centrosomal protein NA14: implications for stability and function. *Protein Eng. Des. Sel.* **24**, 883–892 (2011).
29. Janke, C. The tubulin code: molecular components, readout mechanisms, and functions. *J. Cell Biol.* **206**, 461–472 (2014).
30. Wang, Q., Crevenna, A. H., Kunze, I. & Mizuno, N. Structural basis for the extended CAP-Gly domains of p150(glued) binding to microtubules and the implication for tubulin dynamics. *Proc. Natl Acad. Sci. USA* **111**, 11347–11352 (2014).
31. Kelley, L. A., Mezulis, S., Yates, C. M., Wass, M. N. & Sternberg, M. J. E. The Phyre2 web portal for protein modeling, prediction and analysis. *Nat. Protoc.* **10**, 845–858 (2015).
32. Witte, H. & Bradke, F. The role of the cytoskeleton during neuronal polarization. *Curr. Opin. Neurobiol.* **18**, 479–487 (2008).
33. Conde, C. & Cáceres, A. Microtubule assembly, organization and dynamics in axons and dendrites. *Nat. Rev. Neurosci.* **10**, 319–332 (2009).
34. Kapitein, L. C. & Hoogenraad, C. C. Building the neuronal microtubule cytoskeleton. *Neuron* **87**, 492–506 (2015).
35. Mizuno, N., Narita, A., Kon, T., Sutoh, K. & Kikkawa, M. Three-dimensional structure of cytoplasmic dynein bound to microtubules. *Proc. Natl Acad. Sci. USA* **104**, 20832–20837 (2007).
36. Errico, A., Claudiani, P., D'Addio, M. & Rugarli, E. I. Spastin interacts with the centrosomal protein NA14, and is enriched in the spindle pole, the midbody and the distal axon. *Hum. Mol. Genet.* **13**, 2121–2132 (2004).

Acknowledgements

We thank C. Grashoff, E. Lorentzen and J. von Blume for assistance at various stages of the project, E. Conti, W. Baumeister and the imaging, biochemistry and cryo-EM core facilities for resources and infrastructure (Max Planck Institute of Biochemistry). We thank A. Carter (University of Cambridge) and C. Kelley (Max Planck Institute of Biochemistry) for careful proofreading of the manuscript and helpful discussions. We thank PICT-IBiSA@Orsay and S. Leboucher (Institut Curie, Orsay) for technical assistance. We are grateful to G. Woehlke (Technical University Munich, Germany) for combined efforts of purification of tubulin, and to C. Gonzalez-Billault and C. Villablanca (University of Chile, Santiago) for help with the analysis of neurons. We also acknowledge C. Sindelar and R. Zhang for providing the software package for microtubule analysis and giving guidance on its use. The EM map of the SSNA1–microtubule complex is deposited with EMDB ID: EMD-4188. N.M., R.J. and C.B. acknowledge the Max Planck Society for the financial support. This study was supported by the DFG through grants within GRK1721, MI 1745/1, and the European Research Council (ERC-CoG-724209 to N.M., ERC-StG-680241 to R.J.). N.M. is a recipient of an EMBO Young Investigator award and a Boehringer Ingelheim Foundation Plus 3 Program grant. R.J. is supported by the DFG Emmy Noether Program (DFG JU 2957/1-1). C.J. is supported by the Institut Curie, the CNRS, the ANR-10-LBX-0038, ANR-10-IDEX-0001-02 PSL, ANR-12-BSV2-0007, INCA 2013-1-PLBIO-02-ICR-1 and 2014-PLBIO-11-ICR-1. A.H.C. acknowledges LISBOA-01-0145-FEDER-007660 and FCT.

Author contributions

N.B. and N.M. performed electron and light microscopy, designed mutant constructs and performed biochemistry experiments, analysed the data and prepared the figures. S.B. and M.M.M. performed experiments with neuron primary culture. N.B. and A.H.C. performed light microscopy experiments. N.B., C.B. and M.T. cloned and purified proteins. N.M., N.B., H.N., S.B., M.M.M. and C.J. analysed neuron data and G.C.

facilitated the automation of neuron analysis. N.M., N.B. and H.N. performed electron microscopic data collection and analysed the data. H.N. and T.S. performed super-resolution light microscopy experiments and N.M., H.N., G.C., C.B and R.J. analysed the data. Experiments were designed by N.M. and the manuscript was written by N.M. with contributions from the other authors.

Competing interests

The authors declare no competing interests.

Additional information

Supplementary information is available for this paper at https://doi.org/10.1038/s41556-018-0199-8.

Reprints and permissions information is available at www.nature.com/reprints.

Correspondence and requests for materials should be addressed to N.M.

Publisher's note: Springer Nature remains neutral with regard to jurisdictional claims in published maps and institutional affiliations.

Methods

Protein preparation and purification. The DNAs of CrSSNA1 and mouse SSNA1 were obtained by gene synthesis (GeneArt, ThermoFisher) and cloned into self-generated LIC (ligation-independent cloning) vectors. The SSNA1 fragments were prepared as hexahistidine (His) fusion proteins with a TEV-protease recognition site. The proteins were expressed in *Escherichia coli* BL21(DE3) (Merck) by induction with 0.4 mM IPTG (Carl Roth) overnight at 18 °C. Cells were sonicated in lysis buffer (50 mM Na-phosphate buffer pH 7.5, 150 mM NaCl, 10% (v/v) glycerol, 5 mM β-mercaptoethanol) supplemented with protease inhibitors (1 mM pepstatin A, 1 mM AEBSF and 1 mM leupeptin) and clarified. The soluble fraction was purified by Ni-NTA affinity chromatography. The His tag was either removed by TEV cleavage or left on the protein. Biochemical analysis did not show any differences with or without the tag. For CrSSNA1(1–104), an additional step of size-exclusion chromatography (Superdex 200, GE Healthcare) was applied. Circular dichroism spectra were obtained on a JASCO 715 CD spectrometer equipped with a Peltier thermostat, at 4 °C, 25 °C and 37 °C. Tubulin was purified from porcine brains (The Bayerische Landesanstalt für Landwirtschaft) according to a previously published protocol[37] or purchased from Cytoskeleton. The oligomerizations of SSNA1 variants were monitored for 0 h (immediately after purification), 24 h and 48 h.

The DNAs for mouse ch-TOG (amino acids 1–505) and human EB3 (amino acids 1–281) were obtained from the Mammalian Gene Collection (MGC, Source BioScience LifeSciences). mTOG protein was expressed in *E. coli* BL21(DE3)pLysS by induction with 0.5 mM IPTG and cells were grown overnight at 16 °C. Cells were sonicated in lysis buffer (50 mM Tris, pH 8.0, 300 mM NaCl, 10 mM imidazole,1 mM dithiothreitol) supplemented with protease inhibitors (1 mM pepstatin A, 1 mM leupeptin and 1 mM phenylmethylsulfonyl fluoride (PMSF)) and clarified. The protein was purified using Ni-affinity chromatography followed by ion exchange chromatography (Hi Trap S, GE Healthcare) and size-exclusion chromatography (Superdex 200, GE Healthcare). His tag was removed by 3C protease. EB3 was expressed in *E. coli* BL21(DE3). Cells were sonicated in lysis buffer (20 mM Pipes, 1 mM $MgCl_2$, 1 mM EGTA 500 mM NaCl, pH 6.8, 1 mM dithiothreitol) supplemented with protease inhibitors (1 mM pepstatin A, 1 mM leupeptin and 1 mM PMSF) and clarified. The protein was purified using Ni-affinity chromatography followed by size-exclusion chromatography (Superdex 200; GE Healthcare). His tag was removed by 3C protease.

Electron microscopy of SSNA1. SSNA1 constructs (0.05 mg ml^{-1}) of different time points of incubation (0, 24 and 48 h) were applied on manually prepared carbon-coated grids and stained with 1% (w/v) uranyl acetate. The specimens were observed using a CM200 (Thermo Fisher Scientific) at 160 kV at a nominal magnification of 50,000×, corresponding to 2.16 Å per pixel.

Electron microscopy of SSNA1–microtubule complex and image processing. For screening conditions that were also used for light microscopic observations, 8 or 15 µM of tubulin was mixed with 0.1 to 30 µM of SSNA1 in BRB80 buffer (80 mM Pipes-KOH pH 6.8, 1 mM $MgCl_2$, 1 mM EDTA) supplemented with 1 mM GTP or GMPCPP for 5 min, and directly applied on an EM grid for negative staining. The cluster of the microtubules observed in light microscopic environments was only partially preserved under the negative stain condition, due to the fixation process of the sample for negative-stain EM. The centre of the cluster is not visible due to high electron densities.

For cryo-EM, we used 15 µM of tubulin and two to five times excess of SSNA1 to maximize the decoration with the protein. Microtubules were stabilized using a non-hydrolysable GTP analogue mimicking GTP-bound conditions, GMPCPP. After 5 min, 5 µl of sample without dilution was applied to glow-discharged grids with holey carbon (Quantifoil, Cu, R1.2/1.3) and vitrification was carried out in liquid ethane using a home-made manual plunger. The cryo-EM specimens were observed on a Tecnai F20 (Thermo Fisher Scientific) at 200 kV with a magnification of 29,000×. Images were taken using a Falcon2 direct detector (Thermo Fisher Scientific), corresponding to 3.46 Å per pixel with a defocus of about −2.5 µm. The total 98 images with the dose of 50 electrons per square ångström were used for image analysis.

For counting the numbers of the protofilaments of the microtubules, we referred to a well-known specific interference pattern (moiré pattern) of the microtubules[38] observed under cryo-EM.

For the measurement of the branching angles, we used 99 branched microtubules. Using FIJI software, two-connector segments were drawn with each segment approximately 50 nm long, placing the junction of the segments at the centre of the branching points. Then the two segments were aligned along the direction of the two branched microtubules. Examples of branches with various angles are shown in Supplementary Fig. 2D.

For the initial analysis visualizing the 11-nm periodicity of SSNA1 on the microtubule surface, a data set acquired on the F20 (described above) was used. The EMAN2[39] e2helixboxer scheme was used to extract the segments of microtubules. The box size was set to 256 pixels corresponding to 886 Å with 90% overlap and 6,160 segments were extracted in total. For classification and averaging of the images, RELION2[40] software was used.

Data sets were collected using a Titan Arctica microscope (Thermo Fisher Scientific) working at 200 kV and equipped with a Falcon3 direct detector (Thermo Fisher Scientific), at a magnification of 92,000×, corresponding to 1.6 Å per pixel, and a Titan Krios microscope (Thermo Fisher Scientific) working at 300 kV and equipped with a K2 Summit direct electron detector, and controlled with SerialEM software, at a magnification of 105,000×, corresponding to 1.34 Å per pixel. The final reconstruction included in this report was carried out using the data set taken with the Titan Krios. For the data set that was included in the final reconstruction, 762 images were collected with defocus varying from −1.5 µm to −3.5 µm. The detector was operated in counting mode with a dose rate of 10.1 electrons per pixels per second. A total exposure time of 6 s, corresponding to an accumulative dose of 34.08 electrons per square ångström was fractionated into 24 video frames with 0.25 s exposure time and a dose of 1.42 electrons per square ångström for each frame. The video frames were aligned, and averaged using the UCSF Motioncorr2 program[41].

For the 2D classification of branched microtubules, RELION2 was used. Two hundred and twenty-six branched microtubules not overlapping with other microtubules were selected from the data set recorded with the Titan Krios and boxed out with a box size of 1,000 pixels, corresponding to 1,340 Å. The branch angles were variable, causing structural heterogeneity, limiting the resolution of averages.

For image analysis leading to the 3D reconstruction of the microtubule–SSNA1 complex, quality, defocus and astigmatism of each micrograph were assessed using CTFFIND4[42]. Out of 762 images, 478 images containing microtubules were selected for further processing. A total of 1,774 selected microtubules were segmented with a box size of 480 Å with 90% of overlap. As microtubules with 13 protofilaments were the majority, we chose to process 13-protofilament microtubules further. The 13-protofilament microtubules contain a seam that breaks the helical continuity of tubulin dimers, which is a building block. To circumvent this problem, a specially designed package described earlier[43] was used in combination with the method described previously[44–46]. Briefly, multi-reference alignment was performed using 20 Å low-pass-filtered, 2D projections of a microtubule with 13 protofilaments as a reference. The package uses a reference that was computationally synthesized using the atomic structure of tubulin decorated by kinesin. The alignment revealed the polarity and the position of the seam by following the segmented boxes that position along a single microtubule. After the determination of the seam, re-segmentation of the microtubules from the micrograph was performed using the alignment information and with the box size of 600 Å and every 80 Å as an interval. The FREALIGN[47] package was implemented in the package for refinement with options of helical analysis. For this, the known helical parameter of a microtubule with 13 protofilaments was used (helical_rise: −9.37308 Å, helical_twist: 27.692 degree, helical_subunit: 13). Afterwards, the method in refs [44–46] was implemented for refinement as this method follows the consistency of patterns within individual microtubules, independent of the kinesin-decorated pattern, as a reference of alignment. We however observed that the SSNA1 decoration on the microtubules affected the accuracy of the particle alignment as well as the seam detection as indicated in the local resolution estimation shown in Supplementary Fig. 4. While the reconstruction of the microtubules could be further improved by a more laborious strategy, SSNA1 on the contrary cannot be better resolved because of the existing symmetry mismatch with the microtubules. The resulting reconstruction is nevertheless informative, as it allows us to visualize a long SSNA1 fibril attached along a protofilament of microtubules. The global resolution was determined to be 6.1 Å by calculating the Fourier shell correlation of two independent reconstructions. However, we note that the alpha and beta tubulins are not sufficiently separated and the higher resolutions are only effective in the core of tubulin. The reconstruction was filtered based on local resolution estimation by the 'blocres' scheme[48] with a scan box size of 50 pixels.

Cryo-ET of SSNA1–microtubule complex and image processing. Ten-nanometre BSA-coated gold (Aurion) was used as a fiducial marker. A 4 µl volume of sample was mixed with 1 µl fiducial marker and then applied to glow-discharged grids (Quantifoil, Cu, R2/2). Plunge freezing immediately followed using Vitrobot (Thermo-Scientific). Tomographic tilt series were collected on a Titan Krios (Thermo-Scientific) operated at an acceleration voltage of 300 kV, equipped with a Gatan K2 Summit direct electron detector, with magnification of 64,000× corresponding to 2.23 Å per pixel. Images were collected in a sequential manner, starting at 0° and increasing to +59° with 1° increments. After acquiring +59°, the stage was returned to 0° and the tilt series was collected until −59° with 1° increments as well. Each tilt series was collected with the defocus value set between 3 and 7 µm. Images were acquired as videos in counting mode using a dose rate of 4.7 electrons per pixels per second. The total accumulative dose of the tilt series was 112.46 electrons per square ångström. The video frames were aligned using the UCSF Motioncorr2 program.

Tomogram reconstruction was performed using the IMOD package[49]. Tilt series were aligned using fiducial gold markers and further binned by a factor of 4 (final pixel size of 8.92 Å per pixel). Tomograms were reconstructed by back projection and a simultaneous iterative reconstruction technique with seven iterations in IMOD.

Subtilisin treatment of microtubules and crosslinking. Taxol-stabilized microtubules (20 μM) were mixed with 7.4 μM subtilisin (Sigma Aldrich) and incubated for 0–60 min at 37 °C. The reaction was stopped by adding 2.5 mM PMSF. In 10 min, subtilisin completes the cleavage of β-tubulin E-hooks and the cleavage of α-tubulin E-hooks follows. For the crosslinking assay, 5 μM microtubules were mixed with 25 μM of SSNA1, and 1-ethyl-3-[3-dimethylaminopropyl]carbodiimide hydrochloride (EDC) (Fisher) was added to a final concentration of 5 mM. Samples were incubated at room temperature for 1 h. The densities of SDS–PAGE were measured using Fiji.

Light microscopy of in vitro SSNA1-mediated microtubule nucleation. Flow cells were assembled with cover glass and passivated coverslips as described before[50]. The use of the GODCAT oxygen scavenging system, common for microtubule growth observation, blocked the effects of CrSSNA1 on microtubule polymerization in our assays. Therefore, instead we used the PCA/PCD/Trolox oxygen scavenging system[51], which contains 10 nM protocatechuate 3,4-dioxygenase from the *Pseudomonas* species, 2.5 mM 3,4-dihydroxybenzoic acid 'PCA' and 1 mM Trolox (Sigma). Total internal reflection fluorescence microscopy was performed on a DeltaVision Elite imaging system (GE Healthcare). For the formation of 'asters', the conditions used were: 8 μM tubulin (20% HiLyte488 Tubulin, Cytoskeleton), 50–200 nM CrSSNA1, 0–10 % PEG and 2 mM GTP. Further experiments containing PEG were performed in the presence of 7.5% PEG. For the detection of the localization of CrSSNA1, after 5 min of the incubation of the mixture of the samples, an anti-SSNA1 antibody was added, and then an anti-rabbit antibody labelled with Alexa Fluor 568 (Life Technology) was added for the visualization of the antibody. We observed that PEG causes formations of concentrate of SSNA1, which is detectable with >4% of PEG, and can mediate microtubule formation with >5% PEG, in good agreement with other proteins previously reported to nucleate microtubules[21]. With any of the above-mentioned conditions, it is confirmed that spontaneous formations of microtubules do not occur without SSNA1. As little as 50 nM CrSSNA1 was effective to mediate a microtubule formation in the presence of 7.5% PEG.

To mimic the nucleation event, seeds were used as a template. The seeds were formed by incubating 30 μM of tubulin with 15% of atto565-labelled tubulin in the presence of 0.5 mM GMPCPP at 37 °C for 30 min and then centrifuged at 15,800*g* for 8 min to remove excess GMPCPP. Pellets were dissolved in BRB80 buffer. Seeds (1 μM) were mixed with 15 μM tubulin containing 20% HiLyte488 tubulin, 2 mM GTP and 3–30 μM CrSSNA1, and then the microtubule growth was immediately observed. Snapshots were taken after 30 min of incubation. Videos were made by acquiring one frame every 15–20 s for 15–20 min. All experiments were performed at least three times independently. We observed branch formations both from templated GMPCPP-stabilized microtubules as well as dynamic microtubules. At 3 μM, branch-like microtubules started appearing (20%, 115 out of 559 microtubules) and at 30 μM, 50% (448 out of 895 microtubules) had branch-like protrusions of microtubules. To categorize the types of branch, the snapshots of microtubules in the presence of 30 μM SSNA1 were used, and all of the microtubules ($n = 895$) were selected out of 89 snapshots from 3 independent experiments ($n = 47$, 21, 21) and categorized into: 'splitting'—dynamic microtubules with GTP are growing out from the end of the preformed microtubules; 'end joining'—two pre-existing microtubules are annealed through dynamic tubulin oligomers; 'side branching'—dynamic microtubules are growing out of the wall of the pre-existing microtubules; 'dynamic branching'—newly formed dynamic microtubules branch out; 'indistinguishable'; and 'no branch'—microtubules without branching.

Mouse hippocampal primary neuron cultures. Animal care and use for this study were performed in accordance with the recommendations of the European Community (2010/63/UE). Experimental procedures were specifically approved by the ethics committee of the Institut Curie CEEA-IC no. 118 (authorization no. 04395.03 given by the National Authority) in compliance with the international guidelines. The study is compliant with all relevant ethical regulations regarding animal research.

Mouse hippocampal neurons were cultured as described previously[52]. Briefly, wild-type dams at 17.5 days of pregnancy were euthanized using cervical dislocation, the embryos were decapitated and their hippocampi were dissected. Hippocampi were digested with 0.25% trypsin–EDTA (ThermoFisher, 15090046) for 20 min at 37 °C, followed by mechanical dissociation with glass pipettes. Dissociated neurons were then plated in plating medium (MEM supplemented with 10% FBS and 0.6% w/v glucose (Sigma G-8769)) on coverslips coated with poly-D-lysine (no. 354210, Corning). Four hours after plating, media were replaced with neurobasal media containing 1% glutamate, 2% B27 and with/without lentivirus.

Overexpression of SSNA1 in cultured mouse hippocampal neurons. Mouse SSNA1(FL), SSNA1(1–104), SSNA1(21–119) (corresponding to 21-C), SSNA1(E20A/E21A/K105A/K112A/K117A) (corresponding to 5A), SSNA1 swap-KK/EE (E20K/E21K/K105E/K112E) and swap-KK/EEE (E20K/E21K/K105E/K112E/K117E) were cloned into modified lentiviral vector pTRIP using a one-step sequence and ligation-independent cloning method. The pTRIP vector contains a 2A peptide sequence between the EGFP and SSNA1 sequence so that the expression of protein constructs can be ensured with the expression of GFP signals without tagging. Lentiviral particles for the mouse SSNA1 constructs were produced as described previously[53]. Briefly, lentiviral vectors along with viral packaging vectors (psPAX2 and pCMV-VSV-G) were co-transfected in Lenti-X-293T cells using TransIT-293 transfection reagent (Mirus Bio LLC). The virus-containing medium was filtered and stored at −80 °C. The amount of virus to be used for experiments was determined by adding different volumes of virus to the neurons. Mouse hippocampal neurons were cultured as described in ref. [52]. On DIV0 (days in vitro 0), 4 h after plating, neurons were transduced with lentiviruses encoding different SSNA1 constructs. On DIV3, neurons were fixed as described in ref. [54].

Immunofluorescence analyses of primary neuron. Primary neurons fixed on DIV3 were stained with anti-MAP2 and Tau1 antibodies. Cells were then incubated with anti-mouse Alexa Fluor 647 and anti-rabbit Alexa Fluor 568. Nuclei were stained with DAPI (0.02 μg ml^{-1}, ThermoFisher Scientific). For immunostaining of SSNA1, anti-SSNA1 and anti-βIII tubulin were used. Antibody information is provided in Supplementary Table 2. Cells were mounted using ProLong Gold anti-fade (ThermoFisher Scientific). Cells were imaged on a Zeiss Axio Imager.M2 with 20× or 40× objectives. Acquired images were analysed using FIJI[55]. Cells with very short axons were included in the analysis so that underdeveloped neurons could be assessed as well. Note for the data set overexpressing swap-KK/EE and swap-KK/EEE, primary neurons were prepared at a different time, causing the change in general growth profiles of axons. Control (GFP transfected) was used as a standard for comparison of promotion or reduction of axon development of different mutants. Axons, defined as the longest protrusion from the soma, were selected using the Simple Neurite Tracer plugin[56]. The collateral branches longer than 15 μm were defined as major branches. The total number of collateral branches and the total length of all the branches for each axon was determined by tracing of the neuron morphology. In each image, the position of the cell bodies was determined by segmentation of the nuclei: after applying a Gaussian filter and subtracting the background, the image was thresholded using Otsu's method. In the overexpression experiments, the neurons were screened for transduction efficiency, as measured by EGFP expression. The branch network was obtained by segmenting and combining the intensity in the Tau1 and MAP2 fluorescence images: for each channel, the neurites were highlighted by mapping the curvature of the image (Compute Curvature plugin) and thresholding this quantity using Otsu's method. The resulting binary mask was then skeletonized to outline all of the neurites detected. By overlapping the traced axons with this image, only the neurites branching from the axons were kept and measured. The branching complexity of each neuron was summarized with the Strahler number[57,58] (Strahler Analysis plugin), using the location of its corresponding cell body to mark the root branch, which is the start point of the axon.

Immunostaining for DNA-PAINT. DNA-labelled antibodies were prepared as previously reported[59]. In brief, 300 μl of 1 mg ml^{-1} secondary donkey anti-rat antibody (Jackson ImmunoResearch, 711-005-152) was reacted with 10× mole excess maleimide–PEG2–succinimidyl ester crosslinker (Sigma-Aldrich, 746223), and then 10× mole excess of DNA was added to the antibody-crosslinker. Final usage concentration was 10 μg ml^{-1}.

Mouse embryonic fibroblast cells were transfected with pTRIP_2A_EGFP vector using Lipofectamine 2000 (Thermo Fisher Scientific). Cells were fixed and stained as described previously[59], and then were incubated at 4 °C overnight with primary rat α-tubulin (YL1/2) antibody. Antibody information is provided in Supplementary Table 2. DNA-labelled secondary antibody (10 μg ml^{-1}) was added and incubated for 1 h. Samples were then incubated for 5 min with 90-nm gold particles (Cytodiagnostics, G-90-100) at a 1:10 ratio in PBS, and then residual gold was washed away. Cells were kept at 4 °C until they were used for imaging within 48 h.

DNA-PAINT. Fluorescence imaging was carried out on an inverted Nikon Eclipse Ti microscope (Nikon Instruments) with the Perfect Focus System, applying an objective-type total internal reflection fluorescence (TIRF) configuration with an oil-immersion objective (Apo SR TIRF 100×, NA 1.49, oil). Two lasers were used for excitation: 561 nm (200 mW, Coherent Sapphire) or 488 nm (200 mW, Toptica iBeam smart). The laser beam was passed through a cleanup filter (ZET488/10× or ZET561/10×, Chroma Technology) and coupled into the microscope objective using a beamsplitter (ZT488rdc or ZT561rdc, Chroma Technology). Fluorescent light was spectrally filtered with two emission filters (ET525/50 m and ET500lp for 488 nm excitation and ET600/50 and ET575lp for 561 nm excitation, Chroma Technology) and imaged on a sCMOS camera (Andor Zyla 4.2) without further magnification, resulting in an effective pixel size of 130 nm after 2 × 2 binning. The camera readout sensitivity was set to 16-bit, and the readout bandwidth was set to 200 MHz.

Transfected cells were screened using 488 nm laser excitation at 0.01 kW cm^{-2}. The excitation was switched to 561 nm, the focal plane and TIRF angle were readjusted and imaging was subsequently performed using ~1.5 kW cm^{-2} 561 nm laser excitation. The imager strand concentration varied dependent on the measurement from 2 nM to 5 nM Cy3b-P1 and was adjusted to minimize double-binding events. Imaging was performed in 1 × PCA (Sigma-Aldrich, 37580-25G-F)/1 × PCD (Sigma-Aldrich, P8279-25UN)/1 × Trolox (Sigma-Aldrich, 238813-1G) in Buffer C (PBS + 500 mM NaCl) and imaged for 20,000–40,000 frames at 200 ms exposure time. 3D imaging was performed using a cylindrical lens in the detection path as previously reported[60].

Super-resolution data analysis. Raw data videos were reconstructed with the Picasso software[59]. Drift correction was performed with a redundant cross-correlation and/or gold particles as fiducials. Using Picasso, the localization information was converted to an image volume with isotropic pixel sampling of 10 nm. The volumes were denoised by applying a Gaussian filter with a standard deviation of 30 nm. The topology of the microtubules was derived using stretching open active contour modelling, as implemented in the SOAX software[61]. Three independent SSNA1-overexpressing fibroblasts and control cells were assessed each, containing the total tube lengths (that is, microtubule lengths) of 7,700 µm, 8,500 µm and 7,700 µm for control cells and 5,700 µm, 7,900 µm and 1,900 µm for SSNA1-overexpressing cells. In each cell, the occurrences of the three-way intersections were counted to be 0.96, 0.78 and 1.2 per 100 µm for control cells and 1.6, 3.2 and 4.2 per 100 µm for SSNA1-overexpressing cells. As the expression level of SSNA1 varies between individual cells, the transfected cells were selected on the basis of the signal of GFP, which was co-expressed with SSNA1. Three independent cells containing the strongest signals out of >500 cells have been selected.

Statistics and reproducibility. All microtubule nucleation assays and TIRF-based assays were performed independently at least three times unless otherwise stated. Similar results were observed in all of the replicates performed. Primary neuron preparation was performed from three independent mice.

The χ^2 two-sample test was performed to determine the significance of differences between two data sets. The Kruskal–Wallis test, followed by Dunn's multiple comparison post-hoc test, was performed to test the significance across multiple independent samples. Reproducibility was confirmed.

Reporting Summary. Further information on experimental design is available in the Nature Research Reporting Summary linked to this article.

Code availability. Morphology analysis of the neurons (total number of collateral branches and total length of all the branches for each axon) was performed using Fiji, with the help of scripts written ad hoc for the task. All scripts are available from the corresponding author upon request.

Data availability

The cryo-EM structure of the SSNA1–microtubule is available through EMDB with the accession code EMD-4188. The additional tomography images are available in Figshare (https://figshare.com/articles/Microtubule_branch_png/6809795). Source data for Figs. 1, 4, 6 and Supplementary Fig. 6 have been provided as Supplementary Table 3. Other data supporting the findings of this study such as the cryo-tomography data are available from the corresponding author on reasonable request.

References

37. Shelanski, M. L., Gaskin, F. & Cantor, C. R. Microtubule assembly in the absence of added nucleotides. *Proc. Natl Acad. Sci. USA* **70**, 765–768 (1973).
38. Chrétien, D., Kenney, J. M., Fuller, S. D. & Wade, R. H. Determination of microtubule polarity by cryo-electron microscopy. *Structure* **4**, 1031–1040 (1996).
39. Tang, G. et al. EMAN2: an extensible image processing suite for electron microscopy. *J. Struct. Biol.* **157**, 38–46 (2007).
40. Scheres, S. H. W. RELION: implementation of a Bayesian approach to cryo-EM structure determination. *J. Struct. Biol.* **180**, 519–530 (2012).
41. Li, X. et al. Electron counting and beam-induced motion correction enable near-atomic-resolution single-particle cryo-EM. *Nat. Methods* **10**, 584–590 (2013).
42. Rohou, A. & Grigorieff, N. CTFFIND4: Fast and accurate defocus estimation from electron micrographs. *J. Struct. Biol.* **192**, 216–221 (2015).
43. Shang, Z. et al. High-resolution structures of kinesin on microtubules provide a basis for nucleotide-gated force-generation. *eLife* **3**, e04686 (2014).
44. Zhang, R. & Nogales, E. A new protocol to accurately determine microtubule lattice seam location. *J. Struct. Biol.* **192**, 245–254 (2015).
45. Zhang, R., Alushin, G. M., Brown, A. & Nogales, E. Mechanistic origin of microtubule dynamic instability and its modulation by EB proteins. *Cell* **162**, 849–859 (2015).
46. Alushin, G. M. et al. High-resolution microtubule structures reveal the structural transitions in αβ-tubulin upon GTP hydrolysis. *Cell* **157**, 1117–1129 (2014).
47. Grigorieff, N. Frealign: an exploratory tool for single-particle cryo-EM. *Methods Enzymol.* **579**, 191–226 (2016).
48. Cardone, G., Heymann, J. B. & Steven, A. C. One number does not fit all: mapping local variations in resolution in cryo-EM reconstructions. *J. Struct. Biol.* **184**, 226–236 (2013).
49. Kremer, J. R., Mastronarde, D. N. & McIntosh, J. R. Computer visualization of three-dimensional image data using IMOD. *J. Struct. Biol.* **116**, 71–76 (1996).
50. Crevenna, A. H. et al. Side-binding proteins modulate actin filament dynamics. *eLife* **4**, e04599 (2015).
51. Wieczorek, M., Bechstedt, S., Chaaban, S. & Brouhard, G. J. Microtubule-associated proteins control the kinetics of microtubule nucleation. *Nat. Cell Biol.* **17**, 907–916 (2015).
52. Kaech, S. & Banker, G. Culturing hippocampal neurons. *Nat. Protoc.* **1**, 2406–2415 (2006).
53. Lahaye, X. et al. The capsids of HIV-1 and HIV-2 determine immune detection of the viral cDNA by the innate sensor cGAS in dendritic cells. *Immunity* **39**, 1132–1142 (2013).
54. Magiera, M. M. & Janke, C. Investigating tubulin posttranslational modifications with specific antibodies. *Methods Cell Biol.* **115**, 247–267 (2013).
55. Schindelin, J. et al. Fiji: an open-source platform for biological-image analysis. *Nat. Methods* **9**, 676–682 (2012).
56. Longair, M. H., Baker, D. A. & Armstrong, J. D. Simple Neurite Tracer: open source software for reconstruction, visualization and analysis of neuronal processes. *Bioinformatics* **27**, 2453–2454 (2011).
57. Hollingworth, T. & Berry, M. Network analysis of dendritic fields of pyramidal cells in neocortex and Purkinje cells in the cerebellum of the rat. *Phil. Trans. R. Soc. Lond. B* **270**, 227–264 (1975).
58. Vormberg, A., Effenberger, F., Muellerleile, J. & Cuntz, H. Universal features of dendrites through centripetal branch ordering. *PLoS Comput. Biol.* **13**, e1005615 (2017).
59. Schnitzbauer, J., Strauss, M. T., Schlichthaerle, T., Schueder, F. & Jungmann, R. Super-resolution microscopy with DNA-PAINT. *Nat. Protoc.* **12**, 1198–1228 (2017).
60. Huang, B., Wang, W., Bates, M. & Zhuang, X. Three-dimensional super-resolution imaging by stochastic optical reconstruction microscopy. *Science* **319**, 810–813 (2008).
61. Xu, T. et al. SOAX: a software for quantification of 3D biopolymer networks. *Sci. Rep.* **5**, 9081 (2015).

nature cell biology
SUPPLEMENTARY INFORMATION
https://doi.org/10.1038/s41556-018-0199-8

In the format provided by the authors and unedited.

Direct induction of microtubule branching by microtubule nucleation factor SSNA1

Nirakar Basnet[1], Hana Nedozralova[1], Alvaro H. Crevenna[2], Satish Bodakuntla[3,4], Thomas Schlichthaerle[1,5,6], Michael Taschner[1,7], Giovanni Cardone[1], Carsten Janke[3,4], Ralf Jungmann[1,5], Maria M. Magiera[3,4], Christian Biertümpfel[1] and Naoko Mizuno[1]*

---

[1]Max Planck Institute of Biochemistry, Martinsried, Germany. [2]Biomolecular Self-Organization, Instituto de Tecnologia Química e Biológica António Xavier, Universidade Nova de Lisboa, Oeiras, Portugal. [3]Institut Curie, PSL Research University, CNRS, Orsay, France. [4]Universite Paris Sud, Universite Paris-Saclay, Orsay, France. [5]Department of Physics and Center for Nanoscience, Ludwig Maximilian University, Munich, Germany. [6]Graduate School of Quantitative Biosciences Munich (QBM), Ludwig Maximilian University, Munich, Germany. [7]Present address: Department of Fundamental Microbiology, University of Lausanne, Lausanne, Switzerland. *e-mail: mizuno@biochem.mpg.de

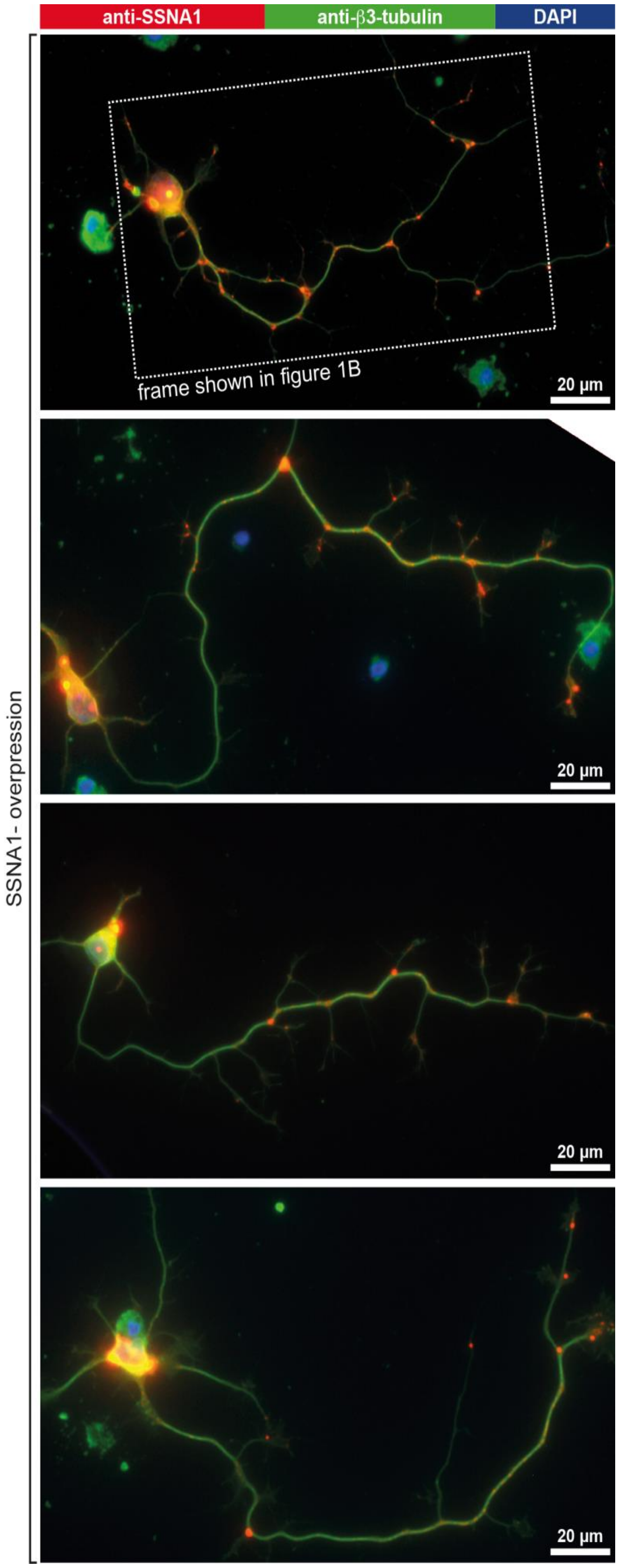
anti-SSNA1
anti-β3-tubulin
DAPI
SSNA1- overexpression
frame shown in figure 1B
20 µm
20 µm
20 µm
20 µm

Supplementary Figure 1

Gallery of primary neurons (DIV3) showing the localization of SSNA1 (red) at the axon branching sites. β3-tubulin is shown in green. These images are representing three independent experiments.

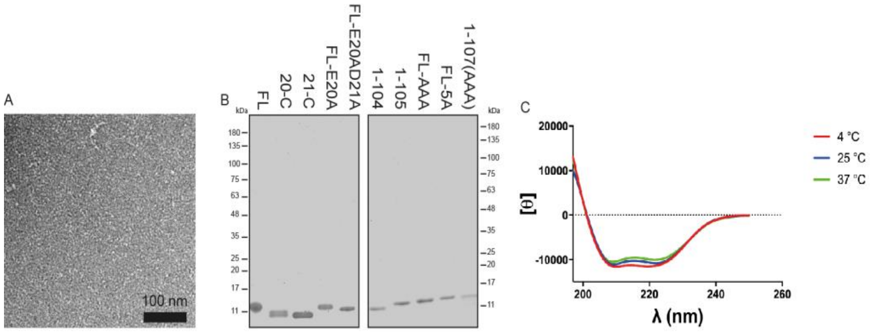

D Cryo-EM snapshots of branched microtubules

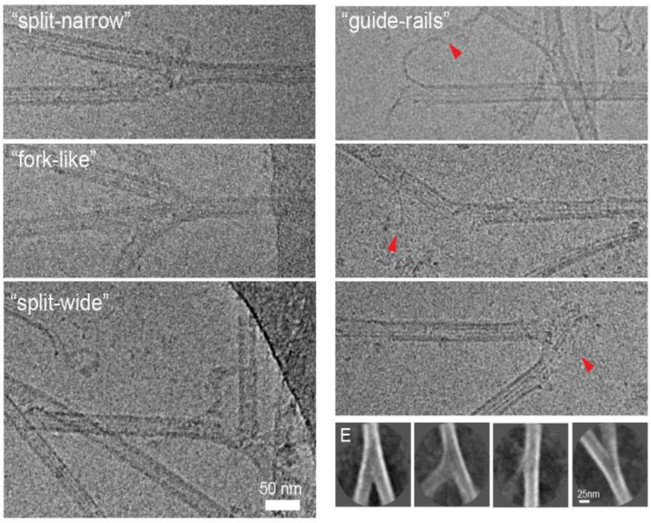
"split-narrow"
"guide-rails"
"fork-like"
"split-wide"
50 nm
E
25nm

F Cryo electron tomography of branched microtubules

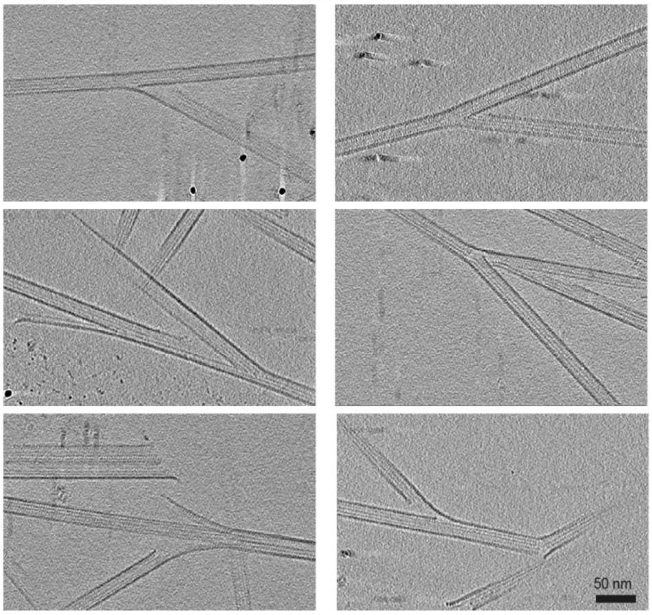

Supplementary Figure 2

(A) Purified CrSSNA1 FL observed under negative stain EM, showing no aggregation. Fibril formation can also occur concomitantly, which is shown in Fig. S5A. **(B)** SDS-PAGE of purified protein fragments reported in the study. **(C)** Circular dichroism spectra (Mean residue ellipticity (MRE: □) of the purified CrSSNA1 FL at different temperatures, showing well folded alpha-helical configurations. **(D)** Snapshots of microtubule branching during nucleation observed by cryo-EM in addition to the images shown in Fig. 2B. In addition to typically observed split of microtubules (“split”, see Fig. 2B), widely or narrowly opened split (“split-wide” and “split-narrow”), microtubules branched into 3 splits (“fork-like”) or a microtubule splitting both ways was observed. Red arrowheads indicate the split protofilaments or the cloud of molecules that are joining to the polymerizing microtubules. **(E)** Representative 2D class averages of microtubule branches (n = 226 branches) showing wide-range of branching formation. Due to the flexible junction points, 2D averages do not resolve details. **(F)** Gallery of cryo-electron tomographic slices of microtubule branches. At the branching points, the breakage of the protofilament lattice can be observed. These images represent 15 cryo-tomograms.

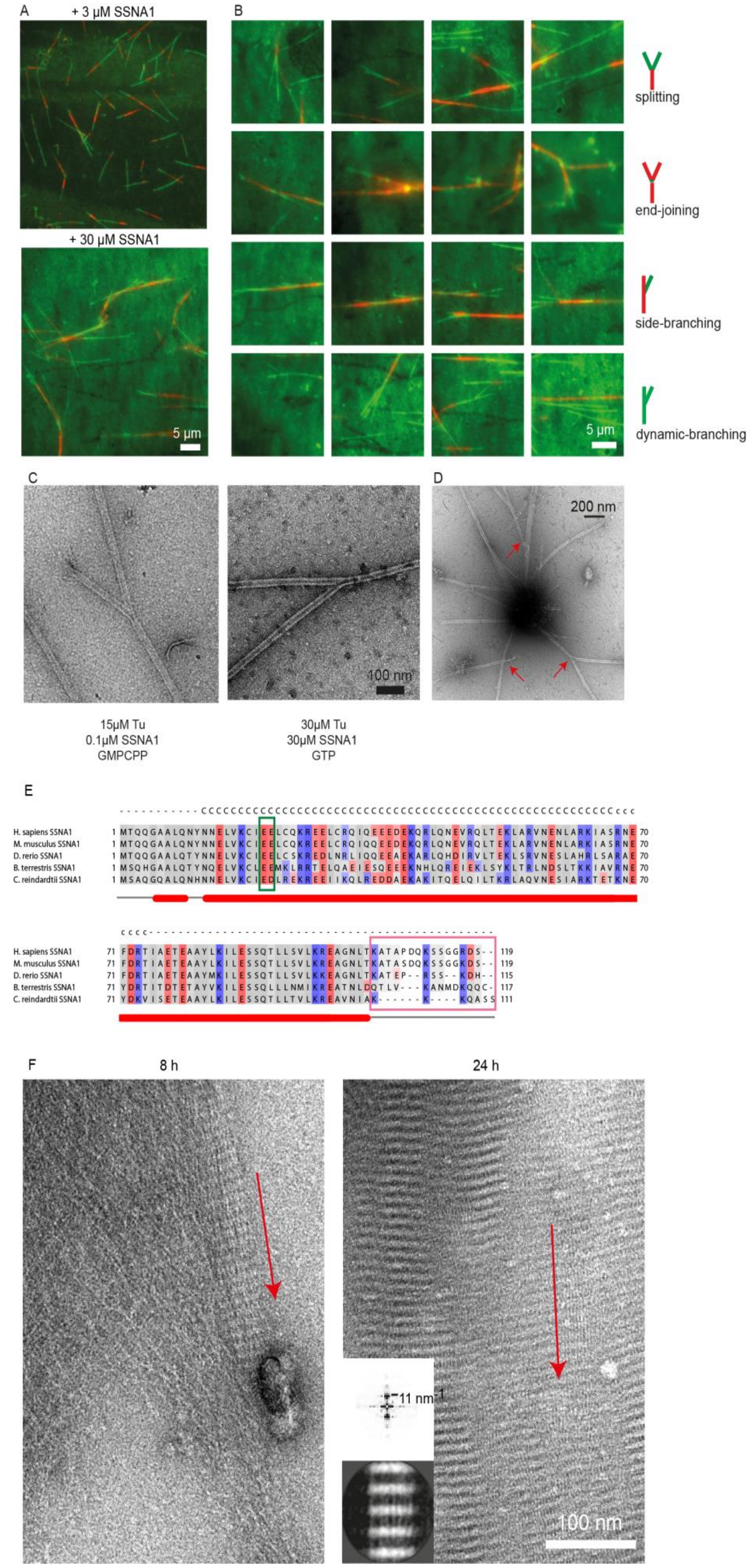
A
+ 3 µM SSNA1
+ 30 µM SSNA1
5 µm
B
splitting
end-joining
side-branching
dynamic-branching
5 µm
C
100 nm
15µM Tu
0.1µM SSNA1
GMPCPP
30µM Tu
30µM SSNA1
GTP
D
200 nm
E
-----------ccccccccccccccccccccccccccccccccccccccccccccccccccccccccccc
H. sapiens SSNA1 1 MTQQGAALQNYNNELVKCIEELCQKREELCRQIQEEEDEKQRLQNEVRQLTEKLARVNENLARKIASRNE 70
M. musculus SSNA1 1 MTQQGAALQNYNNELVKCIEELCQKREELCRQIQQEEDEKQRLQNEVRQLTEKLARVNENLARKIASRNE 70
D. rerio SSNA1 1 MTQQGAALQTYNNELVKCIEELCSKREDLNRLIQQEEAEKARLQHDIRVLTEKLSRVNESLAHRLSARAE 70
B. terrestris SSNA1 1 MSQHGAALQTYNQELVKCLEEMKLRRTELQAEIESQEEEKNHLQREIEKLSYKLTRLNDSLTKKIAVRNE 70
C. reindardtii SSNA1 1 MSAQGQALQNHNNELVKCIEDLREKREEIIKQLREDDAEKAKITQELQILTKRLAQVNESIARKTETKNE 70
cccc---
H. sapiens SSNA1 71 FDRTIAETEAAYLKILESSQTLLSVLKREAGNLTKATAPDQKSSGGRDS-- 119
M. musculus SSNA1 71 FDRTIAETEAAYLKILESSQTLLSVLKREAGNLTKATASDQKSSGGKDS-- 119
D. rerio SSNA1 71 FDRTIAETEAAYMKILESSQTLLSVLKKEAGNLTKATEP--RSS--KDH-- 115
B. terrestris SSNA1 71 YDRTITDTETAYVKILESSQLLLNMIKREATNLDQTLV---KANMDKQQC- 117
C. reindardtii SSNA1 71 YDKVISETEAAYLKILESSQTLLTVLKREAVNIAK------K----KQASS 111
F
8 h
24 h
11 nm⁻¹
100 nm

Supplementary Figure 3

(A) Dynamic microtubules (green) on microtubule seeds (red) in the presence of high concentration of SSNA1 (3 or 30 µM) without molecular crowding agent, to achieve globally concentrated conditions. At 3 µM, branch-like microtubules started appearing (20%, 115 out of 559 microtubules observed) and at 30 µM, 50% (448 out of 895 microtubules) had branch-like protrusion of microtubules. **(B)** Snapshots of microtubules showing 'branch-like' formations. Branches were categorized as 'splitting', 'end-joining', 'side-branching' or 'dynamic-branching'. **(C)** Negative-stain EM snapshots of branched microtubules with conditions tested in a fluorescence microscopy-based dynamic assay, showing branching happens under various conditions. **(D)** Snapshot of branched microtubules protruding out of a nucleation center in the presence of GMPCPP, used for cryo-EM ultrastructure observation. **(E)** The sequence based alignment of the SSNA1 proteins. Secondary structure elements, based on the prediction from PHYRE2 are depicted below the sequences with red bars for α-helices. Coiled-coil prediction from the Marcoil server is shown above the sequences. The charged amino acids are colored in blue for the positive, and red for the negative charge. The colors or grey-scale (for uncharged amino acids) are intensified based on the degree of conservation of the amino acids. The green box highlights residues E20/E(D)21, and the red box shows the unstructured tail region, which are both essential for microtubule branching. **(F)** A snapshot of SSNA1-FL fibrils forming sheet-like structure after 8 hours and 24 hours of incubation. The red arrows show the direction of a fibril. Fibrils laterally assemble together making an ordered sheet. This allows us to assess the basic arrangement of individual fibrils, showing 11-nm of repeat within a fibril as indicated in power spectrum of an average of fibril sheets. These images are representing three independent experiments.

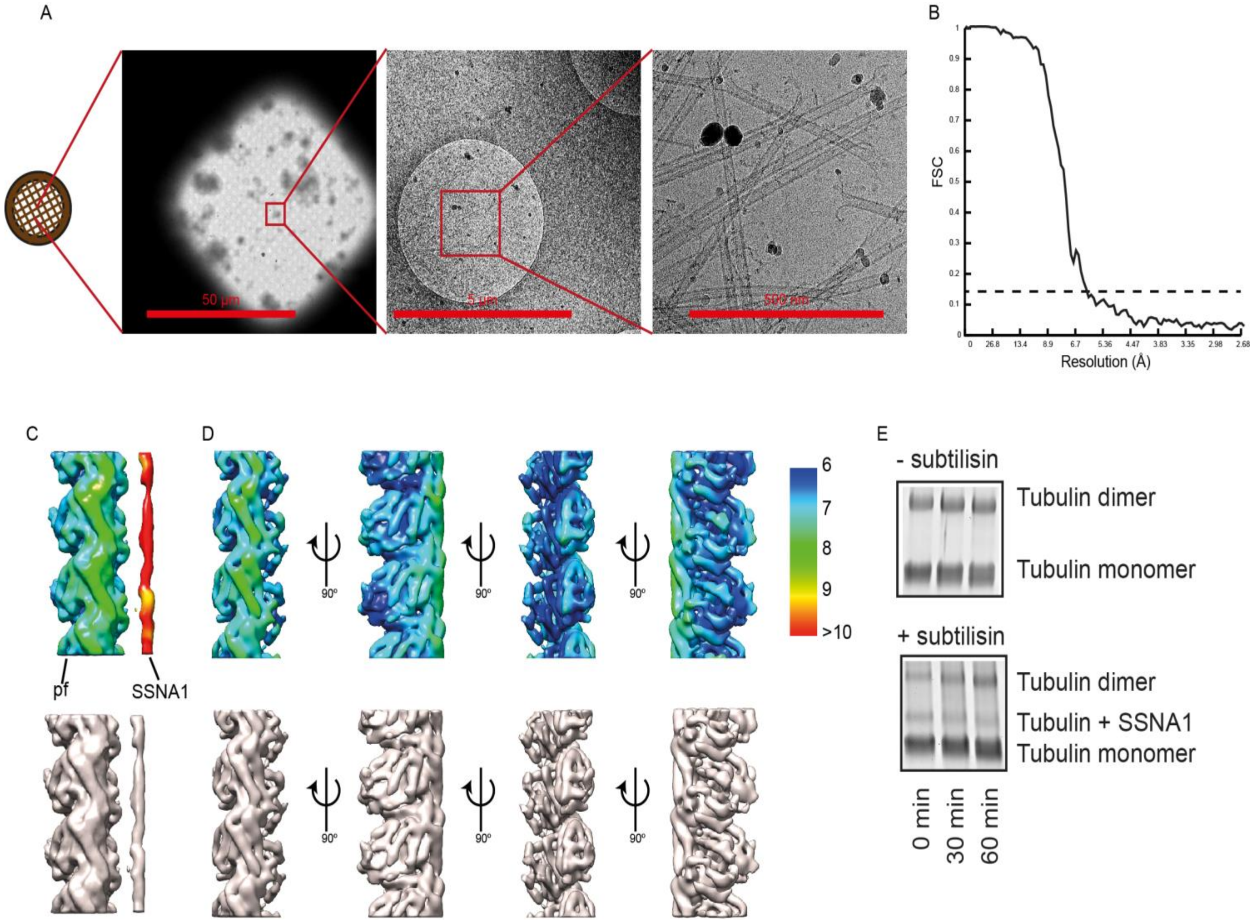
A
50 µm
5 µm
500 nm
B
FSC
Resolution (Å)
0
0.1
0.2
0.3
0.4
0.5
0.6
0.7
0.8
0.9
1
0
26.8
13.4
8.9
6.7
5.36
4.47
3.83
3.35
2.98
2.68
C
pf
SSNA1
D
90°
90°
90°
90°
90°
90°
6
7
8
9
>10
E
- subtilisin
Tubulin dimer
Tubulin monomer
+ subtilisin
Tubulin dimer
Tubulin + SSNA1
Tubulin monomer
0 min
30 min
60 min

Supplementary Figure 4

(A) Snapshots showing ‘cluster’ formation embedded in vitreous ice for cryo-EM observation. The centers of microtubule nucleation clusters have high densities of microtubules. **(B)** Fourier Shell Correlation (FSC) of the 3D reconstruction of the SSNA1-microtubule complex. The global resolution of the 3D reconstruction is 6.1 Å according to the FSC=0.143 criteria, though it is only effective for the core of tubulin according to the local resolution mapping shown in D. **(C and D)** Local resolution representation of the 3D reconstruction according to the resolution-color code on the right color bar. **(C)** with a threshold that includes the SSNA1 decoration and **(D)** with the threshold that allows the visualization of the secondary structure elements in the tubulin core. While the tubulin core part shows a resolution ~6 Å, the decorated SSNA1 fibril is not resolved due to the symmetry mismatch between microtubules and SSNA1. The surface of the microtubules is not resolved either, presumably due to the coverage of SSNA1 knob-like pattern with 11 nm periodicity, blurring surrounding densities. Note the 11-nm knob-like pattern is averaged out due to the symmetry mismatch to the microtubule symmetry. **(E)** Chemical crosslinking of microtubules in the absence (top) and presence (bottom) of SSNA1. Subtilisin proteolyzes tubulin E-hooks, and subsequent crosslinking shows the loss of SSNA1-tubulin binding.

A Truncations and point mutants

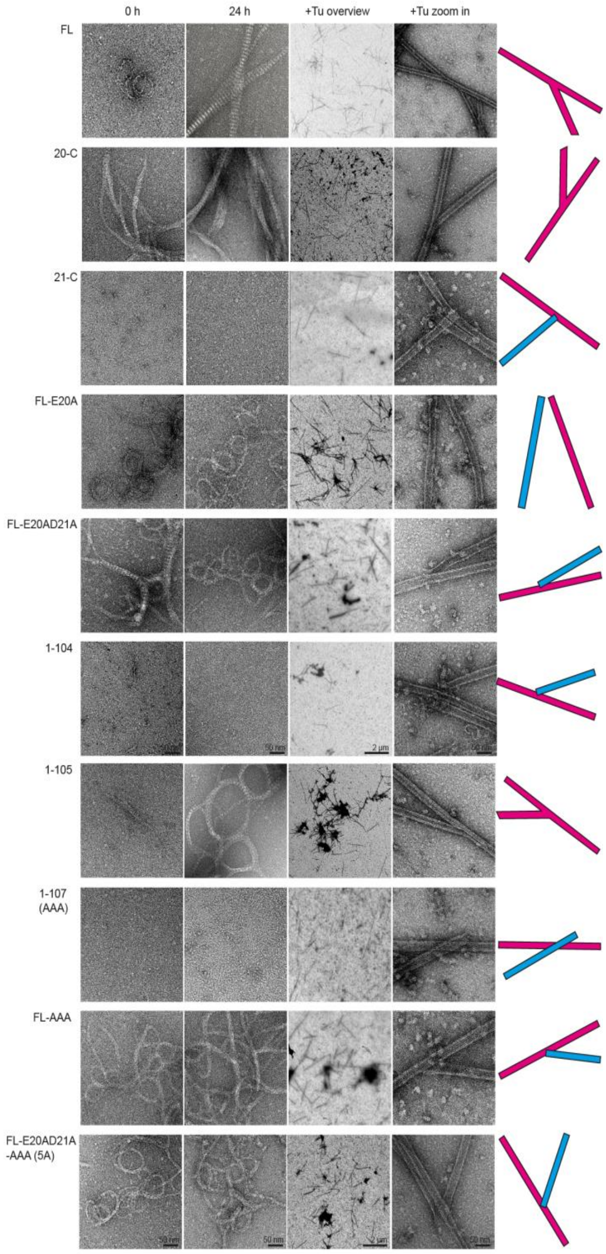
0 h
24 h
+Tu overview
+Tu zoom in
FL
20-C
21-C
FL-E20A
FL-E20AD21A
1-104
1-105
1-107
(AAA)
FL-AAA
FL-E20AD21A
-AAA (5A)
50 nm
2 µm
50 nm

B Swap mutants

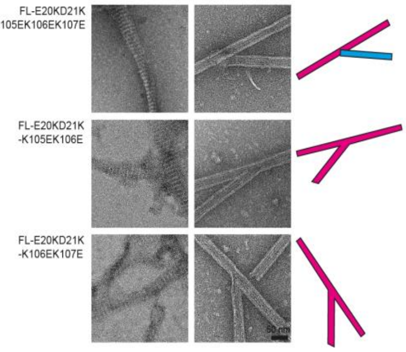
FL-E20KD21K
-K105EK106EK107E
FL-E20KD21K
-K105EK106E
FL-E20KD21K
-K106EK107E
50 nm

Supplementary Figure 5

(A) Gallery of electron micrographs of various CrSSNA1 truncation series tested for microtubule nucleation and branching. From left, observation of the purified protein at 0 h incubation (i.e. immediately after purification), 24h incubation at RT, an overview after the addition of tubulin resulting in co-polymerized microtubules, and a magnified view of the copolymerized microtubules. Microtubule branching is shown with FL, 20-C and 1-105, while other protein fragments do not facilitate branching. For the proteins that do not cause the branching, examples of typical crossing of microtubules (red and blue bars at the scheme at the right column), instead of branching are shown. **(B)** Gallery of electron micrographs of various CrSSNA1 swap mutants. Left – all the mutants form cable-like fibrils. Right - branch formation is not induced with the E20K/D21K/K105E/K106E/K107E mutant. These images are representing three independent experiments.

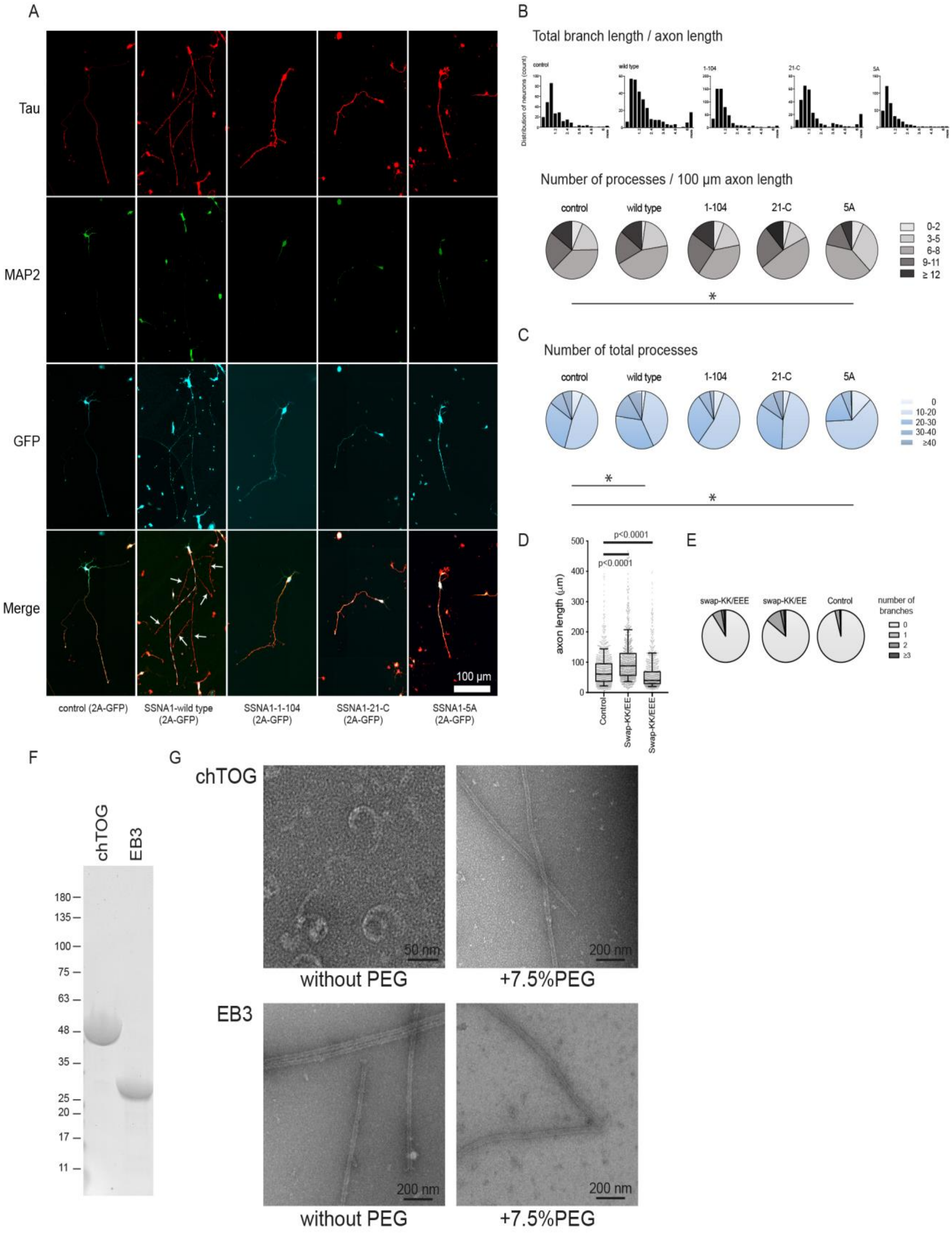
A
Tau
MAP2
GFP
Merge
100 µm
control (2A-GFP)
SSNA1-wild type (2A-GFP)
SSNA1-1-104 (2A-GFP)
SSNA1-21-C (2A-GFP)
SSNA1-5A (2A-GFP)
B
Total branch length / axon length
Distribution of neurons (count)
control
wild type
1-104
21-C
5A
Number of processes / 100 µm axon length
control
wild type
1-104
21-C
5A
0-2
3-5
6-8
9-11
≥ 12
*
C
Number of total processes
control
wild type
1-104
21-C
5A
0
10-20
20-30
30-40
≥40
*
*
D
p<0.0001
p<0.0001
axon length (µm)
500
400
300
200
100
0
Control
Swap-KK/EE
Swap-KK/EEE
E
swap-KK/EEE
swap-KK/EE
Control
number of branches
0
1
2
≥3
F
chTOG
EB3
180
135
100
75
63
48
35
25
20
17
11
G
chTOG
50 nm
200 nm
without PEG
+7.5%PEG
EB3
200 nm
200 nm
without PEG
+7.5%PEG

Supplementary Figure 6

(A) Unmerged images of primary neurons (DIV3) overexpressing various SSNA1 variants shown in Fig. 6. The axons are labeled in red by Tau1 antibody (first row, red), while the dendrites are marked with the MAP2 antibody (second row, green). The expression of the SSNA1 proteins was confirmed by concomitant GFP expression (third row, cyan). In the merged view of the SSNA1 WT, axon is guided with a dotted line. **(B-E)** Neuron morphology analysis of various overexpression conditions **B**) Distribution of neurons based on total branch length/axon length and pie graphs showing the distribution of the number of processes (major branches plus minor protrusions along axon). Sample size: Control (n=266 cells), wild type (n=289 cells), 1-104 (n=537 cells), 21-C (n=274 cells), 5A (n=358 cells) pooled from 3 independent experiments and **(C)** Pie graphs showing the distribution of the total number of processes. Sample size: Control (n=266 cells), wild type (n=289 cells), 1-104 (n=537 cells), 21-C (n=274 cells), 5A (n=358 cells) pooled from 3 independent experiments. In **(B)** and **(C)**, statistics of 5A show significant difference ($\chi2 = 23.0$, $p < 0.001$ and 36.3, $p < 0.001$ respectively) compared to control, indicating a negative effect of the 5A mutant overexpression to neurons. In **(C)**, wild type overexpressed neurons show the significant difference ($\chi2 = 12.83$, $p < 0.01$). **(D)** Scatter dot plots of axon length under over-expression of various SSNA1 swap mutants. The promotion of axon development occurs in over-expression of swap-KK/EE, while slight dominant negative effect (shortening of axon) was observed in over-expression of swap-KK/EEE. Every cell is represented by a single point: Control (n=1348 cells), swap-KK/EE (n=789 cells), swap-KK/EEE (n=1129 cells) and the overlaid box-and-whisker plots cover 50% (boxes) and 90% (whiskers) of the entire population, with median values indicated as lines within the boxes. **(E)** Pie graphs showing the distribution of the number of branches. Distributions of the branches in swap-mutants expressed neurons differ significantly from control (GFP over-expression) according to χ^2 two-sample test ($\chi^2 = 14.4$, $p < 0.005$ and 29.1, $p < 0.000005$, respectively). Sample size: Control (n=1348 cells), swap-KK/EE (n=789 cells), swap-KK/EEE (n=1127 cells). **(F)** Purification of chTOG and EB3. **(G)** Mixtures of tubulin with chTOG (upper) and EB3 (lower) were treated in the same way as SSNA1-tubulin mixture to test the induction of microtubule branches. No microtubule branching was observed in the tested conditions.

Supplementary Tables

Table 1: Series of truncations and mutations created and their microtubule branching activities

Table 2: Information of antibodies used in Immunoflourescence and DNA Paint experiments

Table 3: Statistics Source Data

Supplementary Videos

Supplementary video 1: Aster-like microtubule formation in the presence of SSNA1

TIRF microscopy showing aster-like microtubule formation in the presence of 200 nM SSNA1, 8 µM tubulin, 2 mM GTP and 7.5 % (w/v) PEG. The movie was recorded at 22 ºC for 15 min, 20 s each frame. The movie is played at 20 fps. Microtubules propagate out from the tubulin concentrate, which serves as nucleation center.

Supplementary video 2: Nucleation of microtubules from the side of a microtubule with 100 nM SSNA1

TIRF microscopy showing nucleation of microtubules from the side of a microtubule (pointed by the arrow) in the presence of 100 nM CrSSNA1, 8 µM tubulin, 2 mM GTP and 7.5% (w/v) PEG. The movie was recorded at 22 ºC for 15 min, 20 s each frame. The movie is played at 20 fps.

Supplementary video 3: Nucleation of microtubules from the side of a microtubule with 30 µM SSNA1

TIRF microscopy showing nucleation of microtubules from the side of a microtubule (pointed by the arrow) in the presence of 30 µM CrSSNA1 15 µM tubulin, 2 mM GTP and 7.5% (w/v) PEG. The movie was recorded at 22 ºC for 15 min, 15 s each frame. The movie is played at 20 fps.

Supplementary video 4: Nucleation of microtubules from the end of the microtubule seed

TIRF microscopy showing nucleation of microtubules (green) from the end of the red microtubule seed (pointed by the arrow) in the presence of 30 µM CrSSNA1, 15 µM tubulin, 2 mM GTP. The seed (red) was incubated with tubulin (green) and CrSSNA1 and the movie was recorded at 22 ºC for 15 min, 15 s each frame. The movie is played at 20 fps.

.

3. Discussion

3.1 Visualization of axon branch

Axon branching is an important neuronal development process facilitating the creation of the complex neural network, allowing one axon to generate multiple synaptic connections simultaneously. Direct observation of the branching process is key to gain a comprehensive overview of the orchestration of the involved cellular components, however, the view had been long missing. In our study, We used in-situ cryo-ET to elucidate the axon branching of mouse primary hippocampal neurons and thalamus explants. We obtained a direct snapshot view into the structure of mature and premature axon branches and provided the segmented maps of the molecular players.

Based on our observations we report that along the shaft axons are thin, tightly filled with bundled microtubules intertwined with thin ER tubes, and that the space along the shaft is limited for cellular events to take place. That could be attributed to the fact that the areas of axon which are not currently undergoing remodeling need to maintain robust stability. At the branching points, the microtubule bundle loosens up and splits into two and there is space that can be filled with other cellular components. More space could mean that the area is more prone to have the occurrence of dynamic cellular events. Indeed, we found series of evidence of ongoing activities, i.e., colocalization of active mitochondria undergoing fission, active ribosomes, spreading ER, and short pieces of actin filaments.

In particular, our study highlights the presence of the ribosome clusters, the direct proof of local protein synthesis at the axon branching point. Remarkably these clusters are locally concentrated to the branching point whereas there are almost no ribosomes along the axon outside the branch regions. This is an indication that the activity of the protein synthesis is tightly regulated to the location of the designated spot within the axon. How these ribosomes accumulate and how are regulated at the site so distal from the soma is still to be elucidated. Recently it has been reported that ribosomal protein components and their coding mRNA are essential for axon branching [190], suggesting a possible scenario that the ribosome itself may as well be locally synthesized or parts of them repaired. Analyzing the steps of ribosome biogenesis at the local site in-situ would be technically challenging, but could offer a visual clue on how the local translation is regulated at the specific sites.

3.2 Cytoskeleton remodeling

The details of cytoskeleton elements remodeling at the axon branch are still not fully understood. Actin is sparsely found in the axon along with the microtubule bundles, instead, a lattice of actin rings perpendicular to the axis of the axon is present [191, 6], even though our tomographic reconstruction does not enable the visualization of the actin rings due to the technical limitations of the method.

However, at the axon branching point, we observed an accumulation of short actin filaments without apparent alignment at the base of the membrane protrusion and aligned actin filaments in the filopodia protrusion. Upon the branch maturation, after the insertion of microtubules into the protrusion, the density of actin decreased and the remaining actin filaments are either aligned along the cell membrane at the branching point or are occupying the enlarged area from where the branch emerges out of the axon shaft. The accumulation of short actin filaments and their colocalization with active polysomes are suggesting that the actin needed to form the filopodia protrusion is locally synthesized. This observation is in accordance with the reports of locally translated actin mRNA transcripts during axon branching induced described previously [25, 31]. Altogether these observations indicate that the local protein synthesis might be a central process that controls the dynamics of branch filopodium formation.

Microtubules within the axon shaft are stabilized by interactions with neuronal MAPs such as Tau, MAP7, and DCX [192, 193, 194, 195], which are regulating microtubule dynamics and thus maintaining the integrity of microtubule filaments over long distances and time. However, at the axon branching point, microtubules undergo dynamical remodeling in order to facilitate the new branch formation [117] and so the MAPs interactions change. Among the factors involved in the dynamics of microtubules at the axon branch, we have previously reported a novel microtubule nucleation factor SSNA1, which localizes at the axon branching site in-vivo as an axon branching promoting factor [110]. The in-vitro structural study revealed the surprising microtubule nucleation effect of SSNA1 and the unique ability of SSNA1 to facilitate the direct microtubule branching when the microtubule filament splits into two to create a lattice sharing microtubule branch. We also reported a correlation between the loss of microtubule-branching activity in-vitro and axon branching, leaving an open question if the described mechanism also contributes to the remodeling of the microtubules during axon branching. While we hoped that these interesting insights might be addressed by our cryo-ET observation of axon branches, the assessment of the microtubules in axons was challenging with our current data, due to the sample thickness and dense microtubule bundling. We were unable to clearly visualize the individual microtubules within bundles, due to the technical challenges of electron tomography and the limitations of our sample preparation options. Understanding the mechanism by which microtubules enter the newly forming branch is an important future topic to elucidate axonal development. Our study provided a two-stage snapshot view of the axon branching event. The actin-filled filopodium of premature branch and mature branch with already inserted microtubules. Nevertheless, the steps in between, when microtubules start to enter the filipodium, are still to be understood and the interactions between actin and microtubule cytoskeleton to be visualized.

3.3 Role of ER

Furthermore, our study showed enrichment of ER at the axon branching points. We observed a loosened ER tubular network intertwined with microtubules at the axon branches, in contrast to the tight and thin ER tubes within microtubule bundles along the axon shaft. We found ER tubes wrapping around microtubule filaments, possibly representing ER-microtubule interaction sites. We could not interpret whether the interactions serve to stabilize or loosen the microtubule bundles, but we hypothesize that possibly both, depending on the context, to stabilize bundles along the axon shaft and to loosen them up at the branching point. Moreover, we observed ER comigrating with microtubules into the axon branch, while in premature branches, ER was rarely observed inside the filopodia. We speculate that, ER and microtubules may stabilize each other to facilitate the stabilization and maturation of the axon branch by comigrating together, similarly like the case of general axon growth [36].

ER membrane is also an important lipid source for the production of growing plasma membrane, presumably providing lipids by contacts with the plasma membrane and by producing vesicles for exocytosis [167]. Since the growth of the new axon branch is dependent on cell membrane extension it can be expected that the presence of ER in the axon branch is also important as the source of new lipids. In our data, we observed ER in the proximity of the plasma membrane, but the direct contact between them has not been resolved. In some tomographs we observed accumulation of vesicles of different sizes and shapes near ER membranes, suggesting that those could have originated from the local ER. In some cases, we observed ER-membrane-bound ribosomes suggesting the presence of rough ER in axons. Together with the previous reports of axon localized ER and Golgi components needed for classical protein synthesis and secretion [135] and the presence of mRNAs for transmembrane and secreted proteins, these findings are suggesting an axon localized mechanism for protein secretion [42]. Thus, we cannot exclude that some of the membranous entities present in our axon branches might actually be Golgi derived or mixed-identity organelles, as proposed by Gonzales at al. [42]. However, more experiments selectively targeting the ER and Golgi components would need to be performed in order to correctly identify the different membrane entities and to provide actual data to this hypothesis.

4. Outlook and future perspectives

Axon branching is a dynamic process that requires local reorganization of axonal architecture to establish new connections with neighboring neurons. The branching process requires a highly coordinated and regulated cooperation of numerous cellular machineries. Our study provides a direct close-up view into the ultrastructure of axon branches with remarkable insight into the spatial architecture of involved cell components and their interactions. The view into the dynamically changing area of the branch presents a contrasting picture to the rather stable arrangement of cell components inside the axon shaft, which has to maintain its stability to support the requirements of axonal transport. Moreover, our intriguing observation of ribosome clusters accumulated at axon branches brings a new perspective on the scope of local protein synthesis used to support dynamic cellular activities.

Future studies will address the mechanisms of how cellular machineries are actively recruited and regulated at axon branches, how the change from filopodia to the mature branch takes place, and what is the full sequence of molecular events from the initiation of branching to the stabilized, matured branch. Understanding the branching process is critical not only for the formation of neural network during the development of the nervous system, but also because it plays a critical role in neural homeostasis throughout the life cycle of the brain, such as axon pruning during the maturation of the brain, and axon regeneration after sustaining brain injuries. Elucidating the mechanisms of axon branching will provide insights into the fundamental neuronal processes and also the underlying mechanism supporting the formation of complex neuronal circuits.

List of Figures

1 **Morphology and ultrastructure of neuron cell.** The scheme represents main neuronal compartments: soma, dendrites with spines, axon shaft and branches, axonal initial segment (AIS), growth cone and synaptic terminal. The cutouts are highlighting the distinct ultrastructure of the given segment. The color code for cell elements is depicted in the legend. 15

2 **Establishment of polarity and stages of neuronal development in hippocampal neurons in culture.** DIV (days in-vitro) refers to a time in culture. 19

3 **Axon binding topology.** A) Collateral branching. New branch emerges along the length of the axon shaft. B) Bifurcation. The tip of the growth cone splits into two equal branches. 20

4 **Axon branching in developing CNS.** A) Sensorimotor cortical axon forms branches into the pons and spinal cord. B) In corpus callosum and thalamocortical axons initially extend past their eventual terminal regions (1). After a delay, branches extend from the axon shaft (2) and the distal axons are eliminated (3). Finally, terminal arbors are formed in target regions (4). C) Retinotectal terminal branching [22]. 22

5 **Signaling pathways promoting axon branching.** A) Signaling promoting actin polymerization. NGF-induced TRKA signaling promotes axon branching by activating PI3K and, in turn, RAC1, which activates actin-associated proteins to increase actin polymerization and the formation of actin patches. Cortactin, recruited by Septin6, promotes the emergence of filopodia from actin patches. B) Signaling promoting microtubule destabilization at early branching stages (top) and microtubule stabilization at later branching stage (bottom). Both pathways promote axon branching each by opposing effects on microtubule stability. BDNF-induced TRKB signaling activates MKP-1 and, in turn, inactivates JNK, resulting in microtubule destabilization caused by increased tyrosination of Stathmin. WNT induced GSK3beta inhibition decreases MAP1B phosphorylation leading to an increase in microtubule stability [22]. 24

6 **Remodeling of the cytoskeleton during axon branching.** A) Extracellular cues activate signaling pathways that locally increase actin remodeling. B) Actin patch is formed by the pressure of accumulated actin on the outer membrane. C) Further extension of plasma membrane under the force of actin-based components leads to the formation of filopodium protrusions. D)-E) Microtubules start invading filopodium to stabilize the new branch and promote its maturation. The color code for cell elements is depicted in the legend. 26

7 **Remodeling of cytoskeleton facilitating the branch growth.** Bundled microtubule arrays in the axon are fragmented with the help of microtubule severing enzymes such as spastin and katanin to increase microtubule mass available for polymerization. Different microtubule-associated proteins (e.g. MAP7 and SSNA1) that promote and stabilize the microtubule growth are reported to localize at the axonal branch. In addition, other cytoskeletal proteins like drebins and septins were suggested to promote the entry of microtubules into the actin-rich filopodia. The color code for cell elements is depicted in the legend. 28

8 **Organelle organization and remodeling of the plasma membrane at the axon branch.** A) Schematic representation of a growing matured branch. At the branching site, mitochondria increase in numbers through fission mediated by mitochondria fission factors. ER is suggested to stabilize microtubules via ER-MT interacting proteins. B) Magnified inset from panel A highlights the various mechanisms taking place to regulate membrane expansion and retraction. Membrane expansion in response to attraction guidance molecules is carried out using the fusion of synaptic vesicles to the plasma membrane or exocytosis using SNARE proteins. Retraction of membrane initiated by repulsion guidance molecules is achieved through endocytosis of membrane material. The color code for cell elements is depicted in the legend. 31

9 **Local translation at axon.** A) Schematic representation of suggested cellular components involved in local translation. mRNA transcripts are transported to distal regions of the axon via mRNA binding proteins. Once at the correct region, mRNA is then translated into new proteins. The translation along the axon is suggested to be performed by single ribosomes (monosomes). B) Locally synthesized beta-actin has been linked to the NGF mediated branching and locally synthesized ribosomal proteins were shown as essential for axon branching. The color code for cell elements is depicted in the legend. 36

References

[1] Barnes, Anthony P. and Polleux, Franck. "Establishment of axon-dendrite polarity in developing neurons". *Annual Review of Neuroscience* 32 (2009), pp. 347–381. ISSN: 1545-4126. DOI: `10.1146/annurev.neuro.31.060407.125536`.

[2] Dent, Erik W. and Gertler, Frank B. "Cytoskeletal dynamics and transport in growth cone motility and axon guidance". *Neuron* 40.2 (2003), pp. 209–227. ISSN: 0896-6273. DOI: `10.1016/s0896-6273(03)00633-0`.

[3] Lowery, Laura Anne and Van Vactor, David. "The trip of the tip: understanding the growth cone machinery". *Nature Reviews. Molecular Cell Biology* 10.5 (2009), pp. 332–343. ISSN: 1471-0080. DOI: `10.1038/nrm2679`.

[4] McCormick, Laura E. and Gupton, Stephanie L. "Mechanistic advances in axon pathfinding". *Current Opinion in Cell Biology* 63 (2020), pp. 11–19. ISSN: 1879-0410. DOI: `10.1016/j.ceb.2019.12.003`.

[5] Vassilopoulos, Stéphane et al. "Ultrastructure of the axonal periodic scaffold reveals a braid-like organization of actin rings". *Nature Communications* 10.1 (2019), p. 5803. ISSN: 2041-1723. DOI: `10.1038/s41467-019-13835-6`.

[6] Xu, Ke, Zhong, Guisheng, and Zhuang, Xiaowei. "Actin, spectrin, and associated proteins form a periodic cytoskeletal structure in axons". *Science* 339.6118 (2013), pp. 452–456. ISSN: 1095-9203. DOI: `10.1126/science.1232251`.

[7] Baas, P. W. et al. "Polarity orientation of microtubules in hippocampal neurons: uniformity in the axon and nonuniformity in the dendrite". *Proceedings of the National Academy of Sciences of the United States of America* 85.21 (1988), pp. 8335–8339. ISSN: 0027-8424. DOI: `10.1073/pnas.85.21.8335`.

[8] Baas, P.W. and Lin, S. "Hooks and comets: The story of microtubule polarity orientation in the neuron". *Developmental Neurobiology* 71.6 (2011), pp. 403–418. DOI: `10.1002/dneu.20818`.

[9] Stepanova, Tatiana et al. "Visualization of microtubule growth in cultured neurons via the use of EB3-GFP (end-binding protein 3-green fluorescent protein)". *The Journal of Neuroscience* 23.7 (2003), pp. 2655–2664. ISSN: 1529-2401.

[10] Beuningen, Sam Fb van and Hoogenraad, Casper C. "Neuronal polarity: remodeling microtubule organization". *Current Opinion in Neurobiology* 39 (2016), pp. 1–7. ISSN: 1873-6882. DOI: `10.1016/j.conb.2016.02.003`.

[11] Dalla Costa, Irene et al. "The functional organization of axonal mRNA transport and translation". *Nature Reviews. Neuroscience* 22.2 (2021), pp. 77–91. ISSN: 1471-0048. DOI: `10.1038/s41583-020-00407-7`.

[12] Goldberg, Jeffrey L. “How does an axon grow?” *Genes & Development* 17.8 (2003), pp. 941–958. ISSN: 0890-9369. DOI: `10.1101/gad.1062303`.

[13] Holt, C. E., Martin, K. C., and Schuman, E. M. “Local translation in neurons: visualization and function”. *Nat Struct Mol Biol* 26.7 (2019), pp. 557–566. ISSN: 1545-9985. DOI: `10.1038/s41594-019-0263-5`.

[14] Stiess, Michael et al. “Axon extension occurs independently of centrosomal microtubule nucleation”. *Science* 327.5966 (2010), pp. 704–707. ISSN: 1095-9203. DOI: `10.1126/science.1182179`.

[15] Cioni, Jean-Michel, Koppers, Max, and Holt, Christine E. “Molecular control of local translation in axon development and maintenance”. *Current Opinion in Neurobiology* 51 (2018), pp. 86–94. ISSN: 1873-6882. DOI: `10.1016/j.conb.2018.02.025`.

[16] Poon, M. M. et al. “Identification of process-localized mRNAs from cultured rodent hippocampal neurons”. *J Neurosci* 26.51 (2006), pp. 13390–9. ISSN: 1529-2401. DOI: `10.1523/JNEUROSCI.3432-06.2006`.

[17] Taylor, A. M. et al. “Axonal mRNA in uninjured and regenerating cortical mammalian axons”. *J Neurosci* 29.15 (2009), pp. 4697–707. ISSN: 1529-2401. DOI: `10.1523/JNEUROSCI.6130-08.2009`.

[18] Biever, Anne et al. “Monosomes actively translate synaptic mRNAs in neuronal processes”. *Science* 367.6477 (2020), eaay4991. ISSN: 1095-9203. DOI: `10.1126/science.aay4991`.

[19] Koenig, E. et al. “Cryptic peripheral ribosomal domains distributed intermittently along mammalian myelinated axons”. *The Journal of Neuroscience* 20.22 (2000), pp. 8390–8400. ISSN: 1529-2401.

[20] Noma, K. et al. “Microtubule-dependent ribosome localization in C. elegans neurons”. *Elife* 6 (2017). ISSN: 2050-084X. DOI: `10.7554/eLife.26376`.

[21] Tcherkezian, Joseph et al. “Transmembrane receptor DCC associates with protein synthesis machinery and regulates translation”. *Cell* 141.4 (2010), pp. 632–644. ISSN: 1097-4172. DOI: `10.1016/j.cell.2010.04.008`.

[22] Kalil, Katherine and Dent, Erik W. “Branch management: mechanisms of axon branching in the developing vertebrate CNS”. *Nature Reviews. Neuroscience* 15.1 (2014), pp. 7–18. ISSN: 1471-0048. DOI: `10.1038/nrn3650`.

[23] Gallo, G. “The cytoskeletal and signaling mechanisms of axon collateral branching”. *Dev Neurobiol* 71.3 (2011), pp. 201–20. ISSN: 1932-846X. DOI: `10.1002/dneu.20852`.

[24] Gibson, Daniel A. and Ma, Le. “Developmental regulation of axon branching in the vertebrate nervous system”. *Development* 138.2 (2011), pp. 183–195. ISSN: 1477-9129. DOI: `10.1242/dev.046441`.

[25] Spillane, M. et al. “Mitochondria coordinate sites of axon branching through localized intra-axonal protein synthesis”. *Cell Rep* 5.6 (2013), pp. 1564–75. ISSN: 2211-1247. DOI: `10.1016/j.celrep.2013.11.022`.

[26] Tang, Fangjun and Kalil, Katherine. “Netrin-1 induces axon branching in developing cortical neurons by frequency-dependent calcium signaling pathways”. *The Journal of Neuroscience* 25.28 (2005), pp. 6702–6715. ISSN: 1529-2401. DOI: `10.1523/JNEUROSCI.0871-05.2005`.

[27] Wang, K. H. et al. “Biochemical purification of a mammalian slit protein as a positive regulator of sensory axon elongation and branching”. *Cell* 96.6 (1999), pp. 771–784. ISSN: 0092-8674. DOI: `10.1016/s0092-8674(00)80588-7`.

[28] Dent, E. W. and Kalil, K. “Axon branching requires interactions between dynamic microtubules and actin filaments”. *The Journal of Neuroscience* 21.24 (2001), pp. 9757–9769. ISSN: 1529-2401.

[29] Gallo, G. “Mechanisms underlying the initiation and dynamics of neuronal filopodia: from neurite formation to synaptogenesis”. *Int Rev Cell Mol Biol* 301 (2013), pp. 95–156. ISSN: 1937-6448. DOI: `10.1016/B978-0-12-407704-1.00003-8`.

[30] Spillane, M. et al. “Nerve growth factor-induced formation of axonal filopodia and collateral branches involves the intra-axonal synthesis of regulators of the actin-nucleating Arp2/3 complex”. *J Neurosci* 32.49 (2012), pp. 17671–89. ISSN: 1529-2401. DOI: `10.1523/JNEUROSCI.1079-12.2012`.

[31] Wong, H. H. et al. “RNA Docking and Local Translation Regulate Site-Specific Axon Remodeling In Vivo”. *Neuron* 95.4 (2017), 852–868 e8. ISSN: 1097-4199. DOI: `10.1016/j.neuron.2017.07.016`.

[32] Donnelly, C. J. et al. “Axonally synthesized beta-actin and GAP-43 proteins support distinct modes of axonal growth”. *J Neurosci* 33.8 (2013), pp. 3311–22. ISSN: 1529-2401. DOI: `10.1523/JNEUROSCI.1722-12.2013`.

[33] Sheng, Zu-Hang. “The Interplay of Axonal Energy Homeostasis and Mitochondrial Trafficking and Anchoring”. *Trends in Cell Biology* 27.6 (2017), pp. 403–416. ISSN: 1879-3088. DOI: `10.1016/j.tcb.2017.01.005`.

[34] Hutchins, B. Ian and Kalil, Katherine. “Differential outgrowth of axons and their branches is regulated by localized calcium transients”. *The Journal of Neuroscience* 28.1 (2008), pp. 143–153. ISSN: 1529-2401. DOI: `10.1523/JNEUROSCI.4548-07.2008`.

[35] Lewis, T. L. et al. “MFF-dependent mitochondrial fission regulates presynaptic release and axon branching by limiting axonal mitochondria size”. *Nat Commun* 9.1 (2018), p. 5008. ISSN: 2041-1723. DOI: `10.1038/s41467-018-07416-2`.

[36] Farías, Ginny G. et al. “Feedback-Driven Mechanisms between Microtubules and the Endoplasmic Reticulum Instruct Neuronal Polarity”. *Neuron* 102.1 (2019), 184–201.e8. ISSN: 0896-6273. DOI: `10.1016/j.neuron.2019.01.030`.

[37] Conde, Cecilia and Cáceres, Alfredo. “Microtubule assembly, organization and dynamics in axons and dendrites”. *Nature Reviews. Neuroscience* 10.5 (2009), pp. 319–332. ISSN: 1471-0048. DOI: `10.1038/nrn2631`.

[38] Kapitein, Lukas C. and Hoogenraad, Casper C. “Building the Neuronal Microtubule Cytoskeleton”. *Neuron* 87.3 (2015), pp. 492–506. ISSN: 1097-4199. DOI: `10.1016/j.neuron.2015.05.046`.

[39] D’Este, Elisa et al. “STED Nanoscopy Reveals the Ubiquity of Subcortical Cytoskeleton Periodicity in Living Neurons”. *Cell Reports* 10.8 (2015). Publisher: Elsevier, pp. 1246–1251. ISSN: 2211-1247. DOI: `10.1016/j.celrep.2015.02.007`.

[40] Leterrier, Christophe. “The Axon Initial Segment: An Updated Viewpoint”. *Journal of Neuroscience* 38.9 (2018), pp. 2135–2145.

[41] Mandal, Amrita and Drerup, Catherine M. "Axonal Transport and Mitochondrial Function in Neurons". *Frontiers in Cellular Neuroscience* 13 (2019). Publisher: Frontiers. ISSN: 1662-5102. DOI: `10.3389/fncel.2019.00373`.

[42] González, Carolina, Cornejo, Víctor Hugo, and Couve, Andrés. "Golgi bypass for local delivery of axonal proteins, fact or fiction?" *Current Opinion in Cell Biology*. Membrane Trafficking 53 (2018), pp. 9–14. ISSN: 0955-0674. DOI: `10.1016/j.ceb.2018.03.010`.

[43] Dotti, C. G., Sullivan, C. A., and Banker, G. A. "The establishment of polarity by hippocampal neurons in culture". *The Journal of Neuroscience* 8.4 (1988), pp. 1454–1468. ISSN: 0270-6474.

[44] Higgins, D. et al. "Mechanisms of neuronal polarity". *Current Opinion in Neurobiology* 7.5 (1997), pp. 599–604. ISSN: 0959-4388. DOI: `10.1016/s0959-4388(97)80078-5`.

[45] Silva, Jorge Santos da and Dotti, Carlos G. "Breaking the neuronal sphere: regulation of the actin cytoskeleton in neuritogenesis". *Nature Reviews. Neuroscience* 3.9 (2002), pp. 694–704. ISSN: 1471-003X. DOI: `10.1038/nrn918`.

[46] Arimura, Nariko et al. "Role of CRMP-2 in neuronal polarity". *Journal of Neurobiology* 58.1 (2004), pp. 34–47. ISSN: 0022-3034. DOI: `10.1002/neu.10269`.

[47] Dickson, Barry J. "Molecular mechanisms of axon guidance". *Science* 298.5600 (2002), pp. 1959–1964. ISSN: 1095-9203. DOI: `10.1126/science.1072165`.

[48] O'Leary, D. D. et al. "Target selection by cortical axons: alternative mechanisms to establish axonal connections in the developing brain". *Cold Spring Harbor Symposia on Quantitative Biology* 55 (1990), pp. 453–468. ISSN: 0091-7451. DOI: `10.1101/sqb.1990.055.01.045`.

[49] Schmidt, Hannes and Rathjen, Fritz G. "Signalling mechanisms regulating axonal branching in vivo". *BioEssays* 32.11 (2010), pp. 977–985. ISSN: 1521-1878. DOI: `https://doi.org/10.1002/bies.201000054`.

[50] Szebenyi, G. et al. "Fibroblast growth factor-2 promotes axon branching of cortical neurons by influencing morphology and behavior of the primary growth cone". *The Journal of Neuroscience* 21.11 (2001), pp. 3932–3941. ISSN: 1529-2401.

[51] Ma, Le and Tessier-Lavigne, Marc. "Dual Branch-Promoting and Branch-Repelling Actions of Slit/Robo Signaling on Peripheral and Central Branches of Developing Sensory Axons". *The Journal of Neuroscience* 27.25 (2007), pp. 6843–6851. ISSN: 0270-6474. DOI: `10.1523/JNEUROSCI.1479-07.2007`.

[52] Schmidt, Hannes et al. "The receptor guanylyl cyclase Npr2 is essential for sensory axon bifurcation within the spinal cord". *The Journal of Cell Biology* 179.2 (2007), pp. 331–340. ISSN: 0021-9525. DOI: `10.1083/jcb.200707176`.

[53] O'Leary, D. D. and Terashima, T. "Cortical axons branch to multiple subcortical targets by interstitial axon budding: implications for target recognition and "waiting periods"". *Neuron* 1.10 (1988), pp. 901–910. ISSN: 0896-6273. DOI: `10.1016/0896-6273(88)90147-x`.

[54] Bastmeyer, M. and O'Leary, D. D. "Dynamics of target recognition by interstitial axon branching along developing cortical axons". *The Journal of Neuroscience* 16.4 (1996), pp. 1450–1459. ISSN: 0270-6474.

[55] Kuang, R. Z. and Kalil, K. "Development of specificity in corticospinal connections by axon collaterals branching selectively into appropriate spinal targets". *The Journal of Comparative Neurology* 344.2 (1994), pp. 270–282. ISSN: 0021-9967. DOI: `10.1002/cne.903440208`.

[56] Luo, Liqun and O'Leary, Dennis D. M. "Axon retraction and degeneration in development and disease". *Annual Review of Neuroscience* 28 (2005), pp. 127–156. ISSN: 0147-006X. DOI: `10.1146/annurev.neuro.28.061604.135632`.

[57] Norris, C. R. and Kalil, K. "Guidance of callosal axons by radial glia in the developing cerebral cortex". *The Journal of Neuroscience* 11.11 (1991), pp. 3481–3492. ISSN: 0270-6474.

[58] Agmon, A. et al. "Organized growth of thalamocortical axons from the deep tier of terminations into layer IV of developing mouse barrel cortex". *The Journal of Neuroscience* 13.12 (1993), pp. 5365–5382. ISSN: 0270-6474.

[59] Yates, P. A. et al. "Topographic-specific axon branching controlled by ephrin-As is the critical event in retinotectal map development". *The Journal of Neuroscience* 21.21 (2001), pp. 8548–8563. ISSN: 1529-2401.

[60] Simon, D. K. and O'Leary, D. D. "Limited topographic specificity in the targeting and branching of mammalian retinal axons". *Developmental Biology* 137.1 (1990), pp. 125–134. ISSN: 0012-1606. DOI: `10.1016/0012-1606(90)90013-9`.

[61] Feldheim, David A. and O'Leary, Dennis D. M. "Visual map development: bidirectional signaling, bifunctional guidance molecules, and competition". *Cold Spring Harbor Perspectives in Biology* 2.11 (2010), a001768. ISSN: 1943-0264. DOI: `10.1101/cshperspect.a001768`.

[62] McLaughlin, Todd and O'Leary, Dennis D. M. "Molecular gradients and development of retinotopic maps". *Annual Review of Neuroscience* 28 (2005), pp. 327–355. ISSN: 0147-006X. DOI: `10.1146/annurev.neuro.28.061604.135714`.

[63] Kaethner, R. J. and Stuermer, C. A. "Dynamics of terminal arbor formation and target approach of retinotectal axons in living zebrafish embryos: a time-lapse study of single axons". *The Journal of Neuroscience* 12.8 (1992), pp. 3257–3271. ISSN: 0270-6474.

[64] Bilimoria, Parizad M. and Bonni, Azad. "Molecular control of axon branching". *The Neuroscientist* 19.1 (2013), pp. 16–24. ISSN: 1089-4098. DOI: `10.1177/1073858411426201`.

[65] Lai Wing Sun, Karen, Correia, James P., and Kennedy, Timothy E. "Netrins: versatile extracellular cues with diverse functions". *Development* 138.11 (2011), pp. 2153–2169. ISSN: 1477-9129. DOI: `10.1242/dev.044529`.

[66] Dent, Erik W. et al. "Netrin-1 and semaphorin 3A promote or inhibit cortical axon branching, respectively, by reorganization of the cytoskeleton". *The Journal of Neuroscience* 24.12 (2004), pp. 3002–3012. ISSN: 1529-2401. DOI: `10.1523/JNEUROSCI.4963-03.2004`.

[67] Lebrand, Cecile et al. "Critical role of Ena/VASP proteins for filopodia formation in neurons and in function downstream of netrin-1". *Neuron* 42.1 (2004), pp. 37–49. ISSN: 0896-6273. DOI: `10.1016/s0896-6273(04)00108-4`.

[68] Manitt, Colleen et al. "Netrin participates in the development of retinotectal synaptic connectivity by modulating axon arborization and synapse formation in the

developing brain". *The Journal of Neuroscience* 29.36 (2009), pp. 11065–11077. ISSN: 1529-2401. DOI: `10.1523/JNEUROSCI.0947-09.2009`.

[69] Palmer, Amparo and Klein, Rudiger. "Multiple roles of ephrins in morphogenesis, neuronal networking, and brain function". *Genes & Development* 17.12 (2003), pp. 1429–1450. ISSN: 0890-9369. DOI: `10.1101/gad.1093703`.

[70] Wilkinson, D. G. "Multiple roles of EPH receptors and ephrins in neural development". *Nature Reviews. Neuroscience* 2.3 (2001), pp. 155–164. ISSN: 1471-003X. DOI: `10.1038/35058515`.

[71] Castellani, V. et al. "Dual action of a ligand for Eph receptor tyrosine kinases on specific populations of axons during the development of cortical circuits". *The Journal of Neuroscience* 18.12 (1998), pp. 4663–4672. ISSN: 0270-6474.

[72] Klein, Rüdiger. "Bidirectional modulation of synaptic functions by Eph/ephrin signaling". *Nature Neuroscience* 12.1 (2009), pp. 15–20. ISSN: 1546-1726. DOI: `10.1038/nn.2231`.

[73] Marler, Katharine et al. "A TrkB/EphrinA interaction controls retinal axon branching and synaptogenesis". *The Journal of Neuroscience* 28.48 (2008), pp. 12700–12712. ISSN: 1529-2401. DOI: `10.1523/JNEUROSCI.1915-08.2008`.

[74] Pasterkamp, R. Jeroen. "Getting neural circuits into shape with semaphorins". *Nature Reviews. Neuroscience* 13.9 (2012), pp. 605–618. ISSN: 1471-0048. DOI: `10.1038/nrn3302`.

[75] Liu, Yan and Halloran, Mary C. "Central and peripheral axon branches from one neuron are guided differentially by Semaphorin3D and transient axonal glycoprotein1". *The Journal of Neuroscience* 25.45 (2005), pp. 10556–10563. ISSN: 1529-2401. DOI: `10.1523/JNEUROSCI.2710-05.2005`.

[76] Cioni, Jean-Michel et al. "SEMA3A signaling controls layer-specific interneuron branching in the cerebellum". *Current biology: CB* 23.10 (2013), pp. 850–861. ISSN: 1879-0445. DOI: `10.1016/j.cub.2013.04.007`.

[77] Campbell, Douglas S. et al. "Slit1a inhibits retinal ganglion cell arborization and synaptogenesis via Robo2-dependent and -independent pathways". *Neuron* 55.2 (2007), pp. 231–245. ISSN: 0896-6273. DOI: `10.1016/j.neuron.2007.06.034`.

[78] Gallo, G. and Letourneau, P. C. "Localized sources of neurotrophins initiate axon collateral sprouting". *The Journal of Neuroscience* 18.14 (1998), pp. 5403–5414. ISSN: 0270-6474.

[79] Gallo, G. and Letourneau, P. C. "Neurotrophins and the dynamic regulation of the neuronal cytoskeleton". *Journal of Neurobiology* 44.2 (2000), pp. 159–173. ISSN: 0022-3034. DOI: `10.1002/1097-4695(200008)44:2<159::aid-neu6>3.0.co;2-h`.

[80] Gibney, Jean and Zheng, James Q. "Cytoskeletal dynamics underlying collateral membrane protrusions induced by neurotrophins in cultured Xenopus embryonic neurons". *Journal of Neurobiology* 54.2 (2003), pp. 393–405. ISSN: 0022-3034. DOI: `10.1002/neu.10149`.

[81] Jeanneteau, Freddy et al. "The MAP kinase phosphatase MKP-1 regulates BDNF-induced axon branching". *Nature Neuroscience* 13.11 (2010), pp. 1373–1379. ISSN: 1546-1726. DOI: `10.1038/nn.2655`.

[82] Alsina, B., Vu, T., and Cohen-Cory, S. “Visualizing synapse formation in arborizing optic axons in vivo: dynamics and modulation by BDNF”. *Nature Neuroscience* 4.11 (2001), pp. 1093–1101. ISSN: 1097-6256. DOI: `10.1038/nn735`.

[83] Ciani, Lorenza and Salinas, Patricia C. “WNTs in the vertebrate nervous system: from patterning to neuronal connectivity”. *Nature Reviews. Neuroscience* 6.5 (2005), pp. 351–362. ISSN: 1471-003X. DOI: `10.1038/nrn1665`.

[84] Salinas, Patricia C. “Modulation of the microtubule cytoskeleton: a role for a divergent canonical Wnt pathway”. *Trends in Cell Biology* 17.7 (2007), pp. 333–342. ISSN: 1879-3088. DOI: `10.1016/j.tcb.2007.07.003`.

[85] Hutchins, B. Ian, Li, Li, and Kalil, Katherine. “Wnt/calcium signaling mediates axon growth and guidance in the developing corpus callosum”. *Developmental Neurobiology* 71.4 (2011), pp. 269–283. ISSN: 1932-846X. DOI: `10.1002/dneu.20846`.

[86] Krylova, Olga et al. “WNT-3, expressed by motoneurons, regulates terminal arborization of neurotrophin-3-responsive spinal sensory neurons”. *Neuron* 35.6 (2002), pp. 1043–1056. ISSN: 0896-6273. DOI: `10.1016/s0896-6273(02)00860-7`.

[87] Purro, Silvia A. et al. “Wnt regulates axon behavior through changes in microtubule growth directionality: a new role for adenomatous polyposis coli”. *The Journal of Neuroscience* 28.34 (2008), pp. 8644–8654. ISSN: 1529-2401. DOI: `10.1523/JNEUROSCI.2320-08.2008`.

[88] Hall, A. C., Lucas, F. R., and Salinas, P. C. “Axonal remodeling and synaptic differentiation in the cerebellum is regulated by WNT-7a signaling”. *Cell* 100.5 (2000), pp. 525–535. ISSN: 0092-8674. DOI: `10.1016/s0092-8674(00)80689-3`.

[89] Liu, Yaobo et al. “Ryk-mediated Wnt repulsion regulates posterior-directed growth of corticospinal tract”. *Nature Neuroscience* 8.9 (2005), pp. 1151–1159. ISSN: 1097-6256. DOI: `10.1038/nn1520`.

[90] Li, Li, Hutchins, B. Ian, and Kalil, Katherine. “Wnt5a induces simultaneous cortical axon outgrowth and repulsive axon guidance through distinct signaling mechanisms”. *The Journal of Neuroscience* 29.18 (2009), pp. 5873–5883. ISSN: 1529-2401. DOI: `10.1523/JNEUROSCI.0183-09.2009`.

[91] Hall, Alan and Lalli, Giovanna. “Rho and Ras GTPases in Axon Growth, Guidance, and Branching”. *Cold Spring Harbor Perspectives in Biology* 2.2 (2010), a001818. ISSN: 1943-0264. DOI: `10.1101/cshperspect.a001818`.

[92] Kim, Woo-Yang et al. “Essential roles for GSK-3s and GSK-3-primed substrates in neurotrophin-induced and hippocampal axon growth”. *Neuron* 52.6 (2006), pp. 981–996. ISSN: 0896-6273. DOI: `10.1016/j.neuron.2006.10.031`.

[93] Ketschek, Andrea and Gallo, Gianluca. “Nerve growth factor induces axonal filopodia through localized microdomains of phosphoinositide 3-kinase activity that drive the formation of cytoskeletal precursors to filopodia”. *The Journal of Neuroscience* 30.36 (2010), pp. 12185–12197. ISSN: 1529-2401. DOI: `10.1523/JNEUROSCI.1740-10.2010`.

[94] Spillane, Mirela et al. “The actin nucleating Arp2/3 complex contributes to the formation of axonal filopodia and branches through the regulation of actin patch

precursors to filopodia". *Developmental Neurobiology* 71.9 (2011), pp. 747–758. ISSN: 1932-846X. DOI: `10.1002/dneu.20907`.

[95] Ren, Gang, Crampton, Matthew S., and Yap, Alpha S. "Cortactin: Coordinating adhesion and the actin cytoskeleton at cellular protrusions". *Cell Motility and the Cytoskeleton* 66.10 (2009), pp. 865–873. ISSN: 1097-0169. DOI: `10.1002/cm.20380`.

[96] Mingorance-Le Meur, Ana and O'Connor, Timothy P. "Neurite consolidation is an active process requiring constant repression of protrusive activity". *The EMBO journal* 28.3 (2009), pp. 248–260. ISSN: 1460-2075. DOI: `10.1038/emboj.2008.265`.

[97] Goold, R. G., Owen, R., and Gordon-Weeks, P. R. "Glycogen synthase kinase 3beta phosphorylation of microtubule-associated protein 1B regulates the stability of microtubules in growth cones". *Journal of Cell Science* 112 (Pt 19) (1999), pp. 3373–3384. ISSN: 0021-9533.

[98] Drinjakovic, Jovana et al. "E3 ligase Nedd4 promotes axon branching by downregulating PTEN". *Neuron* 65.3 (2010), pp. 341–357. ISSN: 1097-4199. DOI: `10.1016/j.neuron.2010.01.017`.

[99] Dwivedy, Asha et al. "Ena/VASP function in retinal axons is required for terminal arborization but not pathway navigation". *Development* 134.11 (2007), pp. 2137–2146. ISSN: 0950-1991. DOI: `10.1242/dev.002345`.

[100] Strasser, Geraldine A. et al. "Arp2/3 is a negative regulator of growth cone translocation". *Neuron* 43.1 (2004), pp. 81–94. ISSN: 0896-6273. DOI: `10.1016/j.neuron.2004.05.015`.

[101] Ketschek, Andrea et al. "Nerve growth factor promotes reorganization of the axonal microtubule array at sites of axon collateral branching". *Developmental Neurobiology* 75.12 (2015), pp. 1441–1461. ISSN: 1932-846X. DOI: `10.1002/dneu.22294`.

[102] Sainath, Rajiv et al. "CSPGs inhibit axon branching by impairing mitochondria-dependent regulation of actin dynamics and axonal translation". *Developmental Neurobiology* 77.4 (2017), pp. 454–473. ISSN: 1932-846X. DOI: `10.1002/dneu.22420`.

[103] Kalil, K., Szebenyi, G., and Dent, E. W. "Common mechanisms underlying growth cone guidance and axon branching". *Journal of Neurobiology* 44.2 (2000), pp. 145–158. ISSN: 0022-3034.

[104] Mitchison, T. and Kirschner, M. "Dynamic instability of microtubule growth". *Nature* 312.5991 (1984), pp. 237–242. ISSN: 0028-0836. DOI: `10.1038/312237a0`.

[105] Mitchison, T. J. "Localization of an exchangeable GTP binding site at the plus end of microtubules". *Science* 261.5124 (1993), pp. 1044–1047. ISSN: 0036-8075. DOI: `10.1126/science.8102497`.

[106] Sainath, Rajiv and Gallo, Gianluca. "Cytoskeletal and signaling mechanisms of neurite formation". *Cell and Tissue Research* 359.1 (2015), pp. 267–278. ISSN: 1432-0878. DOI: `10.1007/s00441-014-1955-0`.

[107] Hu, Jianli et al. "Septin-driven coordination of actin and microtubule remodeling regulates the collateral branching of axons". *Current biology: CB* 22.12 (2012), pp. 1109–1115. ISSN: 1879-0445. DOI: `10.1016/j.cub.2012.04.019`.

[108] Ketschek, Andrea et al. “Drebrin coordinates the actin and microtubule cytoskeleton during the initiation of axon collateral branches”. *Developmental Neurobiology* 76.10 (2016), pp. 1092–1110. ISSN: 1932-846X. DOI: `10.1002/dneu.22377`.

[109] Tymanskyj, Stephen R. et al. “MAP7 Regulates Axon Collateral Branch Development in Dorsal Root Ganglion Neurons”. *The Journal of Neuroscience* 37.6 (2017), pp. 1648–1661. ISSN: 1529-2401. DOI: `10.1523/JNEUROSCI.3260-16.2017`.

[110] Basnet, N. et al. “Direct induction of microtubule branching by microtubule nucleation factor SSNA1”. *Nat Cell Biol* 20.10 (2018), pp. 1172–1180. ISSN: 1476-4679. DOI: `10.1038/s41556-018-0199-8`.

[111] Goyal, Uma et al. “Spastin-Interacting Protein NA14/SSNA1 Functions in Cytokinesis and Axon Development”. *PLoS ONE* 9.11 (2014). ISSN: 1932-6203. DOI: `10.1371/journal.pone.0112428`.

[112] Gallo, G. and Letourneau, P. C. “Different contributions of microtubule dynamics and transport to the growth of axons and collateral sprouts”. *The Journal of Neuroscience* 19.10 (1999), pp. 3860–3873. ISSN: 1529-2401.

[113] Armijo-Weingart, Lorena and Gallo, Gianluca. “It takes a village to raise a branch: Cellular mechanisms of the initiation of axon collateral branches”. *Molecular and Cellular Neuroscience*. Cytoskeleton-dependent regulation of neuronal network formation 84 (2017), pp. 36–47. ISSN: 1044-7431. DOI: `10.1016/j.mcn.2017.03.007`.

[114] Yu, W., Ahmad, F. J., and Baas, P. W. “Microtubule fragmentation and partitioning in the axon during collateral branch formation”. *The Journal of Neuroscience* 14.10 (1994), pp. 5872–5884. ISSN: 0270-6474.

[115] Kuo, Yin-Wei, Trottier, Olivier, and Howard, Jonathon. “Predicted Effects of Severing Enzymes on the Length Distribution and Total Mass of Microtubules”. *Biophysical Journal* 117.11 (2019), pp. 2066–2078. ISSN: 1542-0086. DOI: `10.1016/j.bpj.2019.10.027`.

[116] Kuo, Yin-Wei et al. “Spastin is a dual-function enzyme that severs microtubules and promotes their regrowth to increase the number and mass of microtubules”. *Proceedings of the National Academy of Sciences of the United States of America* 116.12 (2019), pp. 5533–5541. ISSN: 1091-6490. DOI: `10.1073/pnas.1818824116`.

[117] Yu, Wenqian et al. “The microtubule-severing proteins spastin and katanin participate differently in the formation of axonal branches”. *Molecular Biology of the Cell* 19.4 (2008), pp. 1485–1498. ISSN: 1939-4586. DOI: `10.1091/mbc.e07-09-0878`.

[118] Ziv, N. E. and Spira, M. E. “Localized and transient elevations of intracellular Ca2+ induce the dedifferentiation of axonal segments into growth cones”. *The Journal of Neuroscience* 17.10 (1997), pp. 3568–3579. ISSN: 0270-6474.

[119] Janke, Carsten and Magiera, Maria M. “The tubulin code and its role in controlling microtubule properties and functions”. *Nature Reviews. Molecular Cell Biology* 21.6 (2020), pp. 307–326. ISSN: 1471-0080. DOI: `10.1038/s41580-020-0214-3`.

[120] Dan Wei, null et al. “alpha-Tubulin Acetylation Restricts Axon Overbranching by Dampening Microtubule Plus-End Dynamics in Neurons”. *Cerebral Cortex* 28.9 (2018), pp. 3332–3346. ISSN: 1460-2199. DOI: `10.1093/cercor/bhx225`.

[121] Brill, Monika S. et al. “Branch-Specific Microtubule Destabilization Mediates Axon Branch Loss during Neuromuscular Synapse Elimination”. *Neuron* 92.4 (2016), pp. 845–856. ISSN: 1097-4199. DOI: `10.1016/j.neuron.2016.09.049`.

[122] Johri, Ashu and Beal, M. Flint. “Mitochondrial dysfunction in neurodegenerative diseases”. *The Journal of Pharmacology and Experimental Therapeutics* 342.3 (2012), pp. 619–630. ISSN: 1521-0103. DOI: `10.1124/jpet.112.192138`.

[123] Magiera, Maria M. et al. “Tubulin Posttranslational Modifications and Emerging Links to Human Disease”. *Cell* 173.6 (2018), pp. 1323–1327. ISSN: 1097-4172. DOI: `10.1016/j.cell.2018.05.018`.

[124] Guo, Wenting, Stoklund Dittlau, Katarina, and Van Den Bosch, Ludo. “Axonal transport defects and neurodegeneration: Molecular mechanisms and therapeutic implications”. *Seminars in Cell & Developmental Biology* 99 (2020), pp. 133–150. ISSN: 1096-3634. DOI: `10.1016/j.semcdb.2019.07.010`.

[125] Sheng, Zu-Hang and Cai, Qian. “Mitochondrial transport in neurons: impact on synaptic homeostasis and neurodegeneration”. *Nature Reviews. Neuroscience* 13.2 (2012), pp. 77–93. ISSN: 1471-0048. DOI: `10.1038/nrn3156`.

[126] Ruthel, Gordon and Hollenbeck, Peter J. “Response of mitochondrial traffic to axon determination and differential branch growth”. *The Journal of Neuroscience* 23.24 (2003), pp. 8618–8624. ISSN: 1529-2401.

[127] Cai, Qian and Sheng, Zu-Hang. “Mitochondrial transport and docking in axons”. *Experimental Neurology* 218.2 (2009), pp. 257–267. ISSN: 1090-2430. DOI: `10.1016/j.expneurol.2009.03.024`.

[128] Courchet, Julien et al. “Terminal axon branching is regulated by the LKB1-NUAK1 kinase pathway via presynaptic mitochondrial capture”. *Cell* 153.7 (2013), pp. 1510–1525. ISSN: 1097-4172. DOI: `10.1016/j.cell.2013.05.021`.

[129] Tao, Kentaro, Matsuki, Norio, and Koyama, Ryuta. “AMP-activated protein kinase mediates activity-dependent axon branching by recruiting mitochondria to axon”. *Developmental Neurobiology* 74.6 (2014), pp. 557–573. ISSN: 1932-846X. DOI: `10.1002/dneu.22149`.

[130] Spronsen, Myrrhe van et al. “TRAK/Milton motor-adaptor proteins steer mitochondrial trafficking to axons and dendrites”. *Neuron* 77.3 (2013), pp. 485–502. ISSN: 1097-4199. DOI: `10.1016/j.neuron.2012.11.027`.

[131] Armijo-Weingart, Lorena et al. “Neurotrophins induce fission of mitochondria along embryonic sensory axons”. *eLife* 8 (2019). ISSN: 2050-084X. DOI: `10.7554/eLife.49494`.

[132] Nixon-Abell, Jonathon et al. “Increased spatiotemporal resolution reveals highly dynamic dense tubular matrices in the peripheral ER”. *Science* 354.6311 (2016). Publisher: American Association for the Advancement of Science Section: Research Articles. ISSN: 0036-8075, 1095-9203. DOI: `10.1126/science.aaf3928`.

[133] Wu, Y. et al. “Contacts between the endoplasmic reticulum and other membranes in neurons”. *Proc Natl Acad Sci U S A* 114.24 (2017), E4859–E4867. ISSN: 1091-6490. DOI: `10.1073/pnas.1701078114`.

[134] Willis, Dianna E. et al. “Extracellular stimuli specifically regulate localized levels of individual neuronal mRNAs”. *The Journal of Cell Biology* 178.6 (2007), pp. 965–980. ISSN: 0021-9525. DOI: `10.1083/jcb.200703209`.

[135] Merianda, Tanuja T. et al. “A functional equivalent of endoplasmic reticulum and Golgi in axons for secretion of locally synthesized proteins”. *Molecular and Cellular Neurosciences* 40.2 (2009), pp. 128–142. ISSN: 1095-9327. DOI: `10.1016/j.mcn.2008.09.008`.

[136] Jin, Li-Qing et al. “Protein synthetic machinery and mRNA in regenerating tips of spinal cord axons in lamprey”. *The Journal of Comparative Neurology* 524.17 (2016), pp. 3614–3640. ISSN: 1096-9861. DOI: `10.1002/cne.24020`.

[137] Schwarz, Dianne S. and Blower, Michael D. “The endoplasmic reticulum: structure, function and response to cellular signaling”. *Cellular and molecular life sciences: CMLS* 73.1 (2016), pp. 79–94. ISSN: 1420-9071. DOI: `10.1007/s00018-015-2052-6`.

[138] Renvoisé, Benoît and Blackstone, Craig. “Emerging themes of ER organization in the development and maintenance of axons”. *Current Opinion in Neurobiology* 20.5 (2010), pp. 531–537. ISSN: 1873-6882. DOI: `10.1016/j.conb.2010.07.001`.

[139] Shibata, Yoko et al. “Mechanisms determining the morphology of the peripheral ER”. *Cell* 143.5 (2010), pp. 774–788. ISSN: 1097-4172. DOI: `10.1016/j.cell.2010.11.007`.

[140] Zhu, Peng-Peng et al. “SPG3A protein atlastin-1 is enriched in growth cones and promotes axon elongation during neuronal development”. *Human Molecular Genetics* 15.8 (2006), pp. 1343–1353. ISSN: 0964-6906. DOI: `10.1093/hmg/ddl054`.

[141] Liu, Xianzhuang et al. “Atlastin-1 regulates morphology and function of endoplasmic reticulum in dendrites”. *Nature Communications* 10.1 (2019), p. 568. ISSN: 2041-1723. DOI: `10.1038/s41467-019-08478-6`.

[142] Friedman, Jonathan R. et al. “ER tubules mark sites of mitochondrial division”. *Science* 334.6054 (2011), pp. 358–362. ISSN: 1095-9203. DOI: `10.1126/science.1207385`.

[143] Korobova, Farida, Ramabhadran, Vinay, and Higgs, Henry N. “An actin-dependent step in mitochondrial fission mediated by the ER-associated formin INF2”. *Science* 339.6118 (2013), pp. 464–467. ISSN: 1095-9203. DOI: `10.1126/science.1228360`.

[144] Thayer, Desiree A., Jan, Yuh Nung, and Jan, Lily Yeh. “Increased neuronal activity fragments the Golgi complex”. *Proceedings of the National Academy of Sciences of the United States of America* 110.4 (2013), pp. 1482–1487. ISSN: 0027-8424. DOI: `10.1073/pnas.1220978110`.

[145] Chen, Xiao et al. “Simultaneous acquisition of neuronal morphology and cytoarchitecture in the same Golgi-stained brain”. *Biomedical Optics Express* 9.1 (2018), pp. 230–244. ISSN: 2156-7085. DOI: `10.1364/BOE.9.000230`.

[146] Lowe, Martin. “Structural organization of the Golgi apparatus”. *Current Opinion in Cell Biology* 23.1 (2011), pp. 85–93. ISSN: 1879-0410. DOI: `10.1016/j.ceb.2010.10.004`.

[147] Guo, Yusong, Sirkis, Daniel W., and Schekman, Randy. “Protein sorting at the trans-Golgi network”. *Annual Review of Cell and Developmental Biology* 30 (2014), pp. 169–206. ISSN: 1530-8995. DOI: `10.1146/annurev-cellbio-100913-013012`.

[148] Hanus, Cyril et al. “Unconventional secretory processing diversifies neuronal ion channel properties”. *eLife* 5 (2016), e20609. ISSN: 2050-084X. DOI: `10.7554/eLife.20609`.

[149] Ramírez, Omar A. and Couve, Andrés. “The endoplasmic reticulum and protein trafficking in dendrites and axons”. *Trends in Cell Biology* 21.4 (2011), pp. 219–227. ISSN: 1879-3088. DOI: `10.1016/j.tcb.2010.12.003`.

[150] Mikhaylova, Marina et al. “A Dendritic Golgi Satellite between ERGIC and Retromer”. *Cell Reports* 14.2 (2016). Publisher: Elsevier, pp. 189–199. ISSN: 2211-1247. DOI: `10.1016/j.celrep.2015.12.024`.

[151] Horton, April C. and Ehlers, Michael D. “Dual modes of endoplasmic reticulum-to-Golgi transport in dendrites revealed by live-cell imaging”. *The Journal of Neuroscience* 23.15 (2003), pp. 6188–6199. ISSN: 1529-2401.

[152] Ye, Bing et al. “Growing dendrites and axons differ in their reliance on the secretory pathway”. *Cell* 130.4 (2007), pp. 717–729. ISSN: 0092-8674. DOI: `10.1016/j.cell.2007.06.032`.

[153] Raiborg, Camilla et al. “Repeated ER-endosome contacts promote endosome translocation and neurite outgrowth”. *Nature* 520.7546 (2015), pp. 234–238. ISSN: 1476-4687. DOI: `10.1038/nature14359`.

[154] Winkle, Cortney Chelise and Gupton, Stephanie L. “Membrane Trafficking in Neuronal Development: Ins and Outs of Neural Connectivity”. *International review of cell and molecular biology* 322 (2016), pp. 247–280. ISSN: 1937-6448. DOI: `10.1016/bs.ircmb.2015.10.003`.

[155] Söllner, T. et al. “SNAP receptors implicated in vesicle targeting and fusion”. *Nature* 362.6418 (1993), pp. 318–324. ISSN: 0028-0836. DOI: `10.1038/362318a0`.

[156] Kraszewski, K. et al. “Synaptic vesicle dynamics in living cultured hippocampal neurons visualized with CY3-conjugated antibodies directed against the lumenal domain of synaptotagmin”. *The Journal of Neuroscience* 15.6 (1995), pp. 4328–4342. ISSN: 0270-6474.

[157] Verderio, C. et al. “Tetanus toxin blocks the exocytosis of synaptic vesicles clustered at synapses but not of synaptic vesicles in isolated axons”. *The Journal of Neuroscience* 19.16 (1999), pp. 6723–6732. ISSN: 1529-2401.

[158] Perin, M. S. et al. “Phospholipid binding by a synaptic vesicle protein homologous to the regulatory region of protein kinase C”. *Nature* 345.6272 (1990), pp. 260–263. ISSN: 0028-0836. DOI: `10.1038/345260a0`.

[159] Greif, K. F. et al. “Synaptotagmin-1 promotes the formation of axonal filopodia and branches along the developing axons of forebrain neurons”. *Dev Neurobiol* 73.1 (2013), pp. 27–44. ISSN: 1932-846X. DOI: `10.1002/dneu.22033`.

[160] Hu, Bing, Nikolakopoulou, Angeliki Maria, and Cohen-Cory, Susana. “BDNF stabilizes synapses and maintains the structural complexity of optic axons in vivo”. *Development* 132.19 (2005), pp. 4285–4298. ISSN: 0950-1991. DOI: `10.1242/dev.02017`.

[161] Winkle, Cortney C. et al. “A novel Netrin-1-sensitive mechanism promotes local SNARE-mediated exocytosis during axon branching”. *The Journal of Cell Biology* 205.2 (2014), pp. 217–232. ISSN: 1540-8140. DOI: `10.1083/jcb.201311003`.

[162] Ruthazer, Edward S., Li, Jianli, and Cline, Hollis T. “Stabilization of axon branch dynamics by synaptic maturation”. *The Journal of Neuroscience* 26.13 (2006), pp. 3594–3603. ISSN: 1529-2401. DOI: `10.1523/JNEUROSCI.0069-06.2006`.

[163] Meyer, Martin P. and Smith, Stephen J. “Evidence from in vivo imaging that synaptogenesis guides the growth and branching of axonal arbors by two distinct mechanisms”. *The Journal of Neuroscience* 26.13 (2006), pp. 3604–3614. ISSN: 1529-2401. DOI: `10.1523/JNEUROSCI.0223-06.2006`.

[164] Jahn, R. “Sec1/Munc18 proteins: mediators of membrane fusion moving to center stage”. *Neuron* 27.2 (2000), pp. 201–204. ISSN: 0896-6273. DOI: `10.1016/s0896-6273(00)00029-5`.

[165] Waters, M. G. and Hughson, F. M. “Membrane tethering and fusion in the secretory and endocytic pathways”. *Traffic* 1.8 (2000), pp. 588–597. ISSN: 1398-9219. DOI: `10.1034/j.1600-0854.2000.010802.x`.

[166] Steiner, P. et al. “Overexpression of neuronal Sec1 enhances axonal branching in hippocampal neurons”. *Neuroscience* 113.4 (2002), pp. 893–905. ISSN: 0306-4522. DOI: `10.1016/s0306-4522(02)00225-7`.

[167] Fowler, Philippa C. et al. “NeurodegenERation: The Central Role for ER Contacts in Neuronal Function and Axonopathy, Lessons From Hereditary Spastic Paraplegias and Related Diseases”. *Frontiers in Neuroscience* 13 (2019), p. 1051. ISSN: 1662-4548. DOI: `10.3389/fnins.2019.01051`.

[168] De Gregorio, Cristian et al. “Drosophila Atlastin in motor neurons is required for locomotion and presynaptic function”. *Journal of Cell Science* 130.20 (2017), pp. 3507–3516. ISSN: 1477-9137. DOI: `10.1242/jcs.201657`.

[169] Shirane, Michiko and Nakayama, Keiichi I. “Protrudin induces neurite formation by directional membrane trafficking”. *Science* 314.5800 (2006), pp. 818–821. ISSN: 1095-9203. DOI: `10.1126/science.1134027`.

[170] Matsuzaki, Fumiko et al. “Protrudin serves as an adaptor molecule that connects KIF5 and its cargoes in vesicular transport during process formation”. *Molecular Biology of the Cell* 22.23 (2011), pp. 4602–4620. ISSN: 1939-4586. DOI: `10.1091/mbc.E11-01-0068`.

[171] Petrova, Veselina et al. “Protrudin functions from the endoplasmic reticulum to support axon regeneration in the adult CNS”. *Nature Communications* 11.1 (2020), p. 5614. ISSN: 2041-1723. DOI: `10.1038/s41467-020-19436-y`.

[172] Shirane, Michiko. “Lipid Transfer-Dependent Endosome Maturation Mediated by Protrudin and PDZD8 in Neurons”. *Frontiers in Cell and Developmental Biology* 8 (2020), p. 615600. ISSN: 2296-634X. DOI: `10.3389/fcell.2020.615600`.

[173] Zhou, Xiang et al. “Unc-51-like kinase 1/2-mediated endocytic processes regulate filopodia extension and branching of sensory axons”. *Proceedings of the National Academy of Sciences of the United States of America* 104.14 (2007), pp. 5842–5847. ISSN: 0027-8424. DOI: `10.1073/pnas.0701402104`.

[174] Hausott, B. et al. “Inhibition of fibroblast growth factor receptor 1 endocytosis promotes axonal branching of adult sensory neurons”. *Neuroscience* 188 (2011), pp. 13–22. ISSN: 1873-7544. DOI: `10.1016/j.neuroscience.2011.04.064`.

[175] Kanamori, Takahiro et al. “Local endocytosis triggers dendritic thinning and pruning in Drosophila sensory neurons”. *Nature Communications* 6 (2015), p. 6515. ISSN: 2041-1723. DOI: `10.1038/ncomms7515`.

[176] Ponomareva, Olga Y. et al. “Calsyntenin-1 regulates axon branching and endosomal trafficking during sensory neuron development in vivo”. *The Journal of Neuroscience* 34.28 (2014), pp. 9235–9248. ISSN: 1529-2401. DOI: `10.1523/JNEUROSCI.0561-14.2014`.

[177] Bishop, Derron L. et al. “Axon branch removal at developing synapses by axosome shedding”. *Neuron* 44.4 (2004), pp. 651–661. ISSN: 0896-6273. DOI: `10.1016/j.neuron.2004.10.026`.

[178] Cajigas, I. J. et al. “The local transcriptome in the synaptic neuropil revealed by deep sequencing and high-resolution imaging”. *Neuron* 74.3 (2012), pp. 453–66. ISSN: 1097-4199. DOI: `10.1016/j.neuron.2012.02.036`.

[179] Hafner, A. S. et al. “Local protein synthesis is a ubiquitous feature of neuronal pre- and postsynaptic compartments”. *Science* 364.6441 (2019). ISSN: 1095-9203. DOI: `10.1126/science.aau3644`.

[180] Bassell, G. J. et al. “Sorting of beta-actin mRNA and protein to neurites and growth cones in culture”. *The Journal of Neuroscience* 18.1 (1998), pp. 251–265. ISSN: 0270-6474.

[181] Zivraj, K. H. et al. “Subcellular profiling reveals distinct and developmentally regulated repertoire of growth cone mRNAs”. *J Neurosci* 30.46 (2010), pp. 15464–78. ISSN: 1529-2401. DOI: `10.1523/JNEUROSCI.1800-10.2010`.

[182] Gumy, Laura F., Tan, Chin Lik, and Fawcett, James W. “The role of local protein synthesis and degradation in axon regeneration”. *Experimental Neurology* 223.1 (2010), pp. 28–37. ISSN: 1090-2430. DOI: `10.1016/j.expneurol.2009.06.004`.

[183] Cioni, J. M. et al. “Late Endosomes Act as mRNA Translation Platforms and Sustain Mitochondria in Axons”. *Cell* 176.1-2 (2019), 56–72 e15. ISSN: 1097-4172. DOI: `10.1016/j.cell.2018.11.030`.

[184] Bodian, D. “A SUGGESTIVE RELATIONSHIP OF NERVE CELL RNA WITH SPECIFIC SYNAPTIC SITES”. *Proceedings of the National Academy of Sciences of the United States of America* 53 (1965), pp. 418–425. ISSN: 0027-8424. DOI: `10.1073/pnas.53.2.418`.

[185] Steward, O. and Levy, W. B. “Preferential localization of polyribosomes under the base of dendritic spines in granule cells of the dentate gyrus”. *The Journal of Neuroscience* 2.3 (1982), pp. 284–291. ISSN: 0270-6474.

[186] Shigeoka, T. et al. “Dynamic Axonal Translation in Developing and Mature Visual Circuits”. *Cell* 166.1 (2016), pp. 181–92. ISSN: 1097-4172. DOI: `10.1016/j.cell.2016.05.029`.

[187] Ostroff, L. E. et al. “Polyribosomes redistribute from dendritic shafts into spines with enlarged synapses during LTP in developing rat hippocampal slices”. *Neuron* 35.3 (2002), pp. 535–45. ISSN: 0896-6273. DOI: `10.1016/s0896-6273(02)00785-7`.

[188] Walker, B. A. et al. “Reprogramming axonal behavior by axon-specific viral transduction”. *Gene Therapy* 19.9 (2012), pp. 947–955. ISSN: 1476-5462. DOI: `10.1038/gt.2011.217`.

[189] Heyer, E. E. and Moore, M. J. “Redefining the Translational Status of 80S Monosomes”. *Cell* 164.4 (2016), pp. 757–69. ISSN: 1097-4172. DOI: `10.1016/j.cell.2016.01.003`.

[190] Shigeoka, T. et al. “On-Site Ribosome Remodeling by Locally Synthesized Ribosomal Proteins in Axons”. *Cell Rep* 29.11 (2019), 3605–3619 e10. ISSN: 2211-1247. DOI: `10.1016/j.celrep.2019.11.025`.

[191] Vassilopoulos, Stéphane et al. “Ultrastructure of the axonal periodic scaffold reveals a braid-like organization of actin rings”. *Nature Communications* 10.1 (2019). Number: 1 Publisher: Nature Publishing Group, p. 5803. ISSN: 2041-1723. DOI: `10.1038/s41467-019-13835-6`.

[192] Baas, Peter W. et al. “Stability properties of neuronal microtubules”. *Cytoskeleton* 73.9 (2016), pp. 442–460. ISSN: 1949-3592. DOI: `10.1002/cm.21286`.

[193] Chen, J. et al. “Projection domains of MAP2 and tau determine spacings between microtubules in dendrites and axons”. *Nature* 360.6405 (1992), pp. 674–677. ISSN: 0028-0836. DOI: `10.1038/360674a0`.

[194] Moores, Carolyn et al. “Mechanism of microtubule stabilization by doublecortin”. *Molecular Cell* 14.6 (2004), pp. 833–839. ISSN: 1097-2765. DOI: `10.1016/j.molcel.2004.06.009`.

[195] Tymanskyj, Stephen R. and Ma, Le. “MAP7 Prevents Axonal Branch Retraction by Creating a Stable Microtubule Boundary to Rescue Polymerization”. *The Journal of Neuroscience* 39.36 (2019), pp. 7118–7131. ISSN: 1529-2401. DOI: `10.1523/JNEUROSCI.0775-19.2019`.

Acknowledgment

First, I want to thank my PhD supervisor Naoko Mizuno for giving me the opportunity to explore and learn about neurons and cryo-ET. I greatly appreciate the support and guidance not only in my science career but also in difficult lifetimes. I am grateful for her understanding. I also want to thank Christian Biertümpfel for his advice, help, and support especially during challenging situations and adapting to the new environment.

I would like to thank my thesis advisor Elena Conti for providing a great research environment to work in the department at Max Planck Institute of Biochemistry. I also want to express my extended thanks to my thesis advisory committee members.

I would also like to thank the Graduate Partnership Program of the National Health Institute and the National Heart Lung and Blood Institute, USA, for giving me the opportunity for the valuable experience abroad.

I want to thank my colleagues Nirakar, Iosune, Satish, Keni and Chris for their great help with my project, valuable discussions, and suggestions. I also thank all my lab members and friends, from NIH and from MPI for making my time in the lab a nice experience.

I want to thank all members of the cryo-EM core facility at Max Planck Institute of Biochemistry, Mike Strauss, Daniel Bollschweiler and Tillman Schäfer, and Giovanni Cardone, and at MICEF at the National Institutes of Health, USA, for all the support and technical help.

I want to thank all the people who helped me to learn the skills needed to conduct my research. I appreciate all their valuable expertise and advice. I want to thank Daniel del Toro Ruiz and Rüdiger Klein (Max Planck Institute of Neurobiology), and Carsten Janke (Institut Curie, Orsay, Paris), for giving me advice for neuronal cultures. I also want to thank the lab of Wolfgang Baumeister (Max Planck Institut of Biochemistry), particularly, Juergen Plitzko, Ben Engel, Marion Jasnin and Will Wan for their advice and help in the initial stage of the project, and Philipp Erdmann, Christos Papantoiou, and Vladan Lucic, for sharing their laboratory facilities and experience with the preparation of cryo-ET samples.

Finally, I would like to thank my partner and my family for their love and support on my adventurous journey.